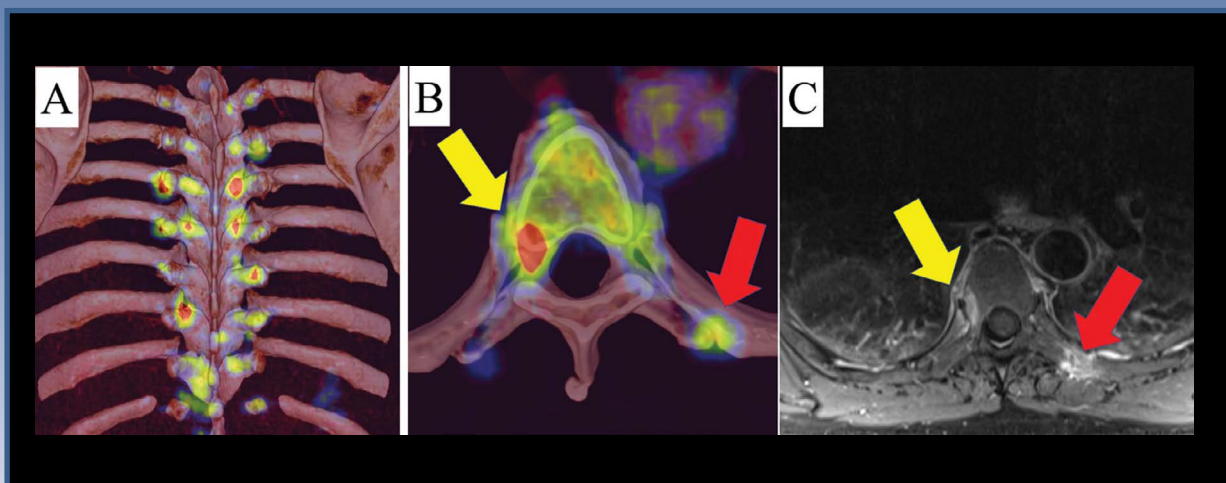


Nuclear Medicine

R · E · V · I · E · W

merged with Problems of Nuclear Medicine

MEiN: 40 pkt.



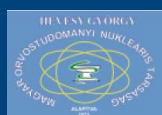
See page 69

ISSN 1506–9680

2022, Volume 25, Number 1

e-ISSN 1644–4345

Journal of Polish, Serbian, Hungarian, Bulgarian
and Macedonian Societies of Nuclear Medicine



Nuclear Medicine

R · E · V · I · E · W

merged with *Problems of Nuclear Medicine**

Editor-in-Chief

G. Kamiński (Warszawa, Poland)

Deputy Editor-in-Chief

M. Dziuk (Warszawa, Poland)

J. Kunikowska (Warszawa, Poland)

National Editors

I. Garai (Debrecen, Hungary)

D. Huić (Zagreb, Croatia)

D. Sobic Saranovic (Belgrade, Serbia)

Board of Editors:

V. Artiko (Belgrade, Serbia)

R.P. Baum (Bad Berka, Germany)

O. Belohlavek (Prague, Czech Republic)

B. Birkenfeld (Szczecin, Poland)

K. Borbély (Budapest, Hungary)

J. Braziewicz (Kielce, Poland)

J. Buscombe (London, United Kingdom)

J.M. Carrill (Santander, Spain)

I. Carrio (Barcelona, Spain)

A. Celler (Vancouver, Canada)

A. Chiti (Rozzano, Italy)

B. Chrapko (Lublin, Poland)

A. Cuocolo (Naples, Italy)

C.S. Cutler (Columbia, United States)

G. De Vincentis (Rome, Italy)

E. Dziuk (Warszawa, Poland)

R. Howman-Giles (Sydney, Australia)

A. Hubalewska-Dydejczyk (Kraków, Poland)

B. Jarzab (Gliwice, Poland)

W. Kloc (Gdańsk, Poland)

W. Knapp (Hannover, Germany)

V.N. Korsunsky (Moscow, Russia)

M. Kostkiewicz (Kraków, Poland)

I. Kozłowicz-Gudzińska (Warszawa, Poland)

O. Kraft (Ostrava, Czech Republic)

L. Królicki (Warszawa, Poland)

J. Kuśmierek (Łódź, Poland)

J. Lepej (Banska Bystrica, Slovak Republic)

A. Lewiński (Łódź, Poland)

T. Maina (Athens, Greece)

B. Małkowski (Bydgoszcz, Poland)

R. Mikołajczak (Otwock-Świerk, Poland)

M. Myslivecek (Olomuc, Czech Republic)

V. Obradović (Belgrade, Serbia)

A.K. Padhy (Singapore)

E. Piperkova (Sofia, Bulgaria)

A. Płachcińska (Łódź, Poland)

Z. Rajkova (Banja Luka, Bosnia & Herzegovina)

F. Rogowski (Białystok, Poland)

D. Rubello (Rovigo, Italy)

M. Ruchala (Poznań, Poland)

M.M. Saw (Singapore)

A. Signore (Rome, Italy)

H. Sinzinger (Vienna, Austria)

A. Soricelli (Italy)

A. Sowa-Staszczak (Kraków, Poland)

D.A. Stanescu (Bucharest, Romania)

M. Studniarek (Gdańsk, Poland)

A. Syrenicz (Szczecin, Poland)

I. Szilvasi (Budapest, Hungary)

J.H. Turner (Fremantle, Australia)

I. Velikyan (Uppsala, Sweden)

M. Vljakovic (Nis, Serbia)

P. Vlcek (Praha, Czech Republic)

The Scientific Committee of the journal is being created and the list of the scientific council members contains the persons who have declared willingness to collaborate.

Secretary

A. Krajewska (Warszawa, Poland)

Editorial Office

Wojskowy Instytut Medyczny

ul. Szaserów 128, 04–141 Warszawa

e-mail: nmr@viamedica.pl

Managing Editor

M. Nehrebecka (Gdańsk, Poland)

*Following the agreement concluded on 23 February 2011 between the Polish Society of Nuclear Medicine and Via Medica Sp. z o.o. the journal „Nuclear Medicine Review” has merged with „Problemy Medycyny Nuklearnej”, a journal published since 1987.

Nuclear Medicine Review (ISSN 1506-9680, e-ISSN 1644-4345) is published twice a year by VM Media sp. z o.o., VM Group sp. k., Grupa Via Medica

ul. Świętokrzyska 73, 80–180 Gdańsk, Poland

tel: (+48 58) 320 94 94, fax: (+48 58) 320 94 60; e-mail: redakcja@viamedica.pl, marketing@viamedica.pl

http://www.viamedica.pl

Advertising: For details on media opportunities within this journal please contact the advertising sales department, ul. Świętokrzyska 73, 80–180 Gdańsk, Poland

tel: (+48 58) 320 94 94, e-mail: marketing@viamedica.pl

The Editors accept no responsibility for the advertisement contents.

Single issues requests should be send to e-mail: prenumerata@viamedica.pl. Electronic orders option available at: www.nmr.viamedica.pl



© Via Medica 2022

All rights reserved, including translation into foreign languages. No part of this periodical, either text or illustration, may be used in any form whatsoever. It is particularly forbidden for any part of this material to be copied or translated into a mechanical or electronic language and also to be recorded in whatever form, stored in any kind of retrieval system or transmitted, whether in an electronic or mechanical form or with the aid of photocopying, microfilm, recording, scanning or in any other form, without the prior written permission of the publisher. The rights of the publisher are protected by national copyright laws and by international conventions, and their violation will be punishable by penal sanctions.

Indexation: Crossref, DOAJ (Directory of Open Access Journals), EMBASE, ESCI (Emerging Sources Citation Index), Index Copernicus (100.00), MEDLINE, Polish Medical Bibliography, Ministry of Science and Higher Education (40), Scopus, Ulrich's Periodicals Directory.

Editorial policies and author guidelines are published on journal website: www.journals.viamedica.pl/nuclear_medicine_review



21-0531.001.001

Nuclear Medicine

R · E · V · I · E · W

merged with *Problems of Nuclear Medicine**

2022, Volume 25, Number 1

Editorial V

Original articles

Hasan Ikbal Atilgan, Hulya Yalcin

Sensitivity of [¹⁸F]FDG PET/CT and classification of the primary tumor site in patients with carcinoma of unknown primary 1

Ismet Sarikaya, Ali Sarikaya, Ahmed N. Albatineh, Ebru Tastekin, Yavuz Atakan Sezer

Assessing the correlation between FDG PET findings of IDC breast carcinoma and histopathology of coexisting ductal carcinoma in-situ 6

Elyas Aditya, Yunia Irawati, Benny Zulkarnaen, Joedo Prihartono

Degree of agreement between dacryoscintigraphy and dacryocystography examinations results in primary acquired nasolacrimal duct obstruction 12

Yukinori Okada, Makoto Shiraishi, Koji Hori, Keiichiro Yamaguchi, Yasuhiro Hasegawa

Relationship between cerebral blood flow reduction patterns on scintigraphy and nonmotor symptoms in new-onset Lewy body disease 18

Paulina Cegla, Katarzyna Scibisz-Dziedzic, Kamila Witkowska, Anna Kubiak, Ewa Wierchoslawska,

Witold Kycler, Beata Chrapko, Rafal Czepczynski

Detection of a second primary cancer in a ¹⁸F-fluorocholine PET/CT – multicentre retrospective analysis on a group of 1345 prostate cancer patients 25

Soudabe Alidadi, Ali Shabestani Monfared, Mehrangiz Amiri, Ebrahim Zabih, Ehsan Assadollahi, Amir Gholami,

Zolekha Moazezi, Zeinab Abedian

The efficacy of melatonin against radiotoxicity of iodine-131 and its response to treatment in hyperthyroid patients: a randomized controlled trial 31

Hanna Piwowska-Bilska, Sara Kurkowska, Bozena Birkenfeld

Optimized method for normal range estimation of standardized uptake values (SUVmax, SUVmean) in liver SPECT/CT images with somatostatin analog [^{99m}Tc]-HYNIC-TOC (Tekrotyd) 37

Mirosław Dziuk, Ewa Witkowska-Patena, Agnieszka Gizewska, Andrzej Mazurek, Anna Pieczonka, Magdalena Koza,

Marina Gerszewska, Zbigniew Podgajny, Marta Chojnowska

Optimal activity of [¹⁸F]FDG for Hodgkin lymphoma imaging performed on PET/CT camera with BGO crystals 47

Barbara Bober, Marek Saracyn, Arkadiusz Lubas, Maciej Kolodziej, Dorota Brodowska-Kania, Waldemar Kapusta, Grzegorz Kaminski

Hepatic complications of peptide receptor radionuclide therapy with Lutetium-177 and Yttrium-90 in patients with neuroendocrine neoplasm 54

Clinical vignettes

Vlatka Jozanovic, Sanja Kusacic Kuna, Marija Despot, Tatjana Samardzic, Drazen Huic

Efficacy of long-term ultrasonography in follow-up of patients with papillary thyroid carcinoma: a case of neck metastasis developed 19 years following primary treatment 62

Pietro Bellini, Domenico Albano, Francesco Dondi, Francesco Bertagna, Raffaele Giubbini

Different glucose metabolism behavior relating to histotypes in synchronous breast cancers evaluated by [¹⁸F]FDG PET-CT 64

Vlatka Jozanovic, Drazen Huic

Incidental detection of breast cancer by ¹⁸F-fluorocholine PET/CT performed for primary hyperparathyroidism 66

Jan-Henning Schierz, Anke McLeod, Farzana Ali

Rare osteoarticular complications on [¹⁸F]FDG-PET/CT — following intravesical BCG immunotherapy for bladder cancer 68

Konstantinos Sakellariou, Sofia Charalampidou, Andreas Fotopoulos, Chrissa Sioka

Hybrid bone SPECT/CT reveals spleen calcification in sickle cell mutation and beta-thalassemia 70



Dear Sirs and Madams,

I would like to announce the first issue of "Nuclear Medicine Review" in 2022, the period when Omikron variant of SARS-CoV-2 dominates in the world's population. It seems that there is the end of horrible pandemia hopefully. The chapter "Original articles" consists of nine interesting papers. It opens two articles written by Turkish colleagues who concluded that PET/CT should be the first-line diagnostic tool for carcinoma of unknown primary. In the second one: primary tumor grade is correlated with the nuclear grade of the coexisting ductal carcinoma in-situ (DCIS). It seems that SUV of primary tumor does not correlate with the histopathological features of coexisting DCIS.

The next paper from Indonesia shows that both dacryocystography and dacryoscintigraphy has high convenience level for patients. These methods has a good agreement in detecting and locating in primary acquired nasolacrimal duct obstruction.

Japanese scientists concluded in their paper that the cerebral blood flow is reduced in several areas of the cerebral cortex and suggest an association between reduced blood flow in the frontal lobe and the appearance of visual hallucinations in patients with new-onset dementia with Lewy bodies.

An article considering prostate cancer patients by Polish authors shows that incidental detection of a second primary cancer using [¹⁸F]FCH PET/CT is not very common and that lung cancer and hematologic malignancies are most frequently detected. In the next paper Iranian colleagues conclude that melatonin has a non-significant positive impact on reducing the rate of chromosomal damages in hyperthyroid patients treated with iodine-131 but the outcome of treatment was significantly higher by melatonin compared to the placebo group. Three articles — again — by Polish scientists: 1. Shows how to optimise the method and estimate normal ranges for standardized uptake values of Tekrotyd in healthy livers. 2. Proves that [¹⁸F]FDG activity can be reduced by up to 25% when using a camera with bismuth germanate crystals in patients with Hodgkin lymphoma. 3. It seems that there is no liver damage after Radionuclid Therapy with [¹⁷⁷Lu]Lu-DOTATATE with an activity of 7.4 GBq or tandem [⁹⁰Y]Y-DOTATATE + [¹⁷⁷Lu]Lu-DOTATATE with equal activity of 3.7 GBq in patients with neuroendocrine neoplasms.

Clinical Vignette consists of five very interesting cases from Croatia, Italy, Germany and Greece.

Dear colleagues, I wish you to be strong and healthy. Enjoy your reading!

Yours,

Grzegorz Kamiński

G. Kamiński

Editor-in-Chief

Nuclear Medicine Review

Sensitivity of [¹⁸F]FDG PET/CT and classification of the primary tumor site in patients with carcinoma of unknown primary

Hasan Ikbal Atilgan[✉], Hulya Yalcin

Hatay Mustafa Kemal University, Faculty of Medicine, Department of Nuclear Medicine, Hatay, Turkey

[Received 17 VII 2020; Accepted 27 X 2021]

Abstract

Background: The aim of this study is to find the sensitivity of the [¹⁸F]FDG PET/CT and the classification of the primary sites of carcinoma of unknown primary (CUP) as a single-center experience.

Material and methods: Sixty-eight patients with a mean age of 62.43 ± 12.78 years were included in this study retrospectively. Sixty-five patients had biopsy or surgery after PET/CT, which revealed pathological diagnoses of malign primary tumors, while primary tumor site could not be detected in three patients with histopathological examination. We evaluated the primary site of CUP with [¹⁸F]FDG PET/CT.

Results: Primary sites of three patients were not determined by histopathological examination. Malign lesions indicating the primary site of tumor were identified in 52 of 68 patients with PET/CT correctly. The primary tumor was lung cancer in 14 patients, cholangiocellular cancer in 9 patients, lymphoma in 9 patients, pancreas cancer in 6 patients, gastric cancer in 4 patients, ovary cancer in 4 patients, colon cancer in 4 patients, breast cancer in 3 patients, hepatocellular cancer in 2 patients, rectal cancer in 2 patients, sarcoma in 2 patients, esophagus, renal cell cancer, squamous cell cancer, endometrium cancer, malign melanoma, and multiple myeloma in 1 patient with histopathological examination. PET/CT was false positive in one patient. There were 13 patients in whom primary tumor could not be localized by PET/CT, but was diagnosed by histopathological evaluation.

Conclusions: PET/CT should be the first-line diagnostic tool for CUP, other diagnostic imaging tools should be applied after a negative whole-body PET/CT.

KEY words: positron emission tomography-computed tomography; unknown primary tumors; ¹⁸F-fluorodeoxyglucose

Nucl Med Rev 2022; 25, 1: 1–5

Introduction

Cancer of unknown primary (CUP) presents with metastasis and the original site of malignancy cannot be identified with a properly standardized diagnostic work-up. CUP is a separate entity because

of its different biological properties from other known primary tumors [1]. CUP is one of the ten most frequent cancers and the fourth most common cancer-related death cause [2]. Identification of the primary tumor influences the patient management positively because specific chemotherapy regimens and targeted therapy develop continuously [3].

Detection of the primary tumor in CUP is a diagnostic challenge. Despite many investigations, the primary tumor cannot be identified. The detection rate of the primary tumor varies in a range of 22–73% [2, 4]. Whole-body scanning with fluorodeoxyglucose (FDG) positron emission tomography/computed tomography (PET/CT) may detect the primary tumor. FDG PET/CT

Correspondence to: Hasan Ikbal Atilgan
Hatay Mustafa Kemal University, Faculty of Medicine,
Department of Nuclear Medicine,
31060 Hatay, Turkey
e-mail: h_i_atilgan@yahoo.com

provides functional and anatomical imaging [4]. The therapeutic impact of PET/CT is not only the localization of the primary tumor but also the result of the identification of additional metastases [5, 6]. FDG PET/CT contributes to patient management by determining the extent of the disease [7]. Despite the identification of the primary tumor, optimal staging, and an opportunity for prognosis, monitoring of chemotherapy response can be evaluated by FDG PET/CT [8].

In this study, we aimed to find the sensitivity of the [^{18}F]FDG PET/CT and the classification of the primary sites of CUP as a single-center experience.

Material and methods

Sixty-eight patients (31 female and 37 male) with a mean age of 62.43 ± 12.78 years (min.: 29, max.: 88) were enrolled in this study retrospectively. Sixty-five patients had biopsy or surgery after PET/CT, which revealed malign pathological diagnoses of the primary tumor, while primary tumor sites of three patients could not be found with histopathological examination. We evaluated the primary site of CUP with [^{18}F]FDG PET/CT. An ethical approval was obtained from Mustafa Kemal University Local Ethics Committee.

[^{18}F]FDG PET/CT imaging

All patients underwent [^{18}F]FDG PET/CT imaging after 6 hours of fasting. Before [^{18}F]FDG injection, the blood glucose of all patients was evaluated and a blood sugar level less than 180 mg/dL was accepted. Oral contrast was given to all patients without intravenous (iv) contrast. After iv injection of F-18 FDG in a dose of $\sim 300\text{--}450$ mBq according to body weight. Approximately 60 minutes after injection, whole-body scan from vertex to feet was acquired by a PET/CT scanner (Siemens, BioGraph mCT, Germany) with 1–2 minute acquisition for each 6–8 bed positions. The CT scan was used for attenuation correction and anatomical localization. The images were evaluated by two experienced nuclear medicine specialists both visually and semiquantitatively. A lesion with a SUVmax value equal to or greater than 2.5 other than metastatic lesions was considered as the primary site of the tumor.

Data analysis

Age which is a quantitative parameter was represented as mean \pm standard deviation. Qualitative parameters such as gender and primary sites of CUP were expressed as frequency. Sensitivity, specificity, and accuracy of PET/CT were calculated as the histopathological results accepted as gold standard.

Results

Locations of the metastatic foci were as liver in 29, bone in 13, lymphadenopathy in 10, peritoneal carcinomatosis or omental cake in 5, brain in 6, adrenal in 2, lung in 1, ascites in 1, and pelvic mass in 1 patient. Sixty-five patients had malignancy with histopathological evaluation. The primary sites of three patients were not determined by histopathological examination. Malign lesions indicating the primary site of tumor were identified in 52 of 68 patients with PET/CT correctly. Fifty-two patients detected with PET/CT had malign histopathological results. The primary tumor was lung cancer in 14 patients, cholangiocellular cancer in 9 patients, lymphoma in

9 patients, pancreas cancer in 6 patients, gastric cancer in 4 patients, ovarian cancer in 4 patients, colon cancer in 4 patients, breast cancer in 3 patients, hepatocellular cancer in 2 patients, rectal cancer in 2 patients, sarcoma in 2 patients, esophagus, renal cell cancer, squamous cell cancer, endometrium cancer, malign melanoma and multiple myeloma in 1 patient with histopathological examination. PET/CT could not detect the primary tumor site in 16 patients correctly. PET/CT was false positive in one patient. There were 13 patients that primary tumor could not be localized by PET/CT, but was diagnosed by histopathological evaluation. The diagnosis was lymphoma in four patients, ovary cancer in three patients, lung cancer in three patients, malign melanoma in one patient, sarcoma in one patient, squamous cell cancer in one patient. Sensitivity, specificity, and accuracy values were 80%, 66.7%, and 79.4% respectively (Fig. 1 and 2).

Discussion

CUP is an aggressive disease with early dissemination, accounting for 3–5% of all malignant epithelial tumors [9]. Accurate localization of the primary tumor provides the targeted therapy and maintains better locoregional treatment and survival [10]. The primary site of cancer can be identified as antemortem in less than 20% of patients with CUP despite extensive workup and 70% of cases remained undiagnosed in autopsy series. Half of the patients with CUP are diagnosed as well to moderately differentiated adenocarcinoma, 30% with poorly differentiated or undifferentiated carcinomas, 15% with squamous cell carcinomas, and 5% with undifferentiated carcinomas [11].

FDG PET/CT is a noninvasive and sensitive whole-body imaging modality both allowing for the detection of the primary tumor and tumor staging. FDG PET/CT should be used as a first-line imaging modality rather than using after other imaging procedures that failed to detect primary tumors [12]. If PET/CT is used as an initial workup, it may reduce the cost, save time and guide the other examinations and biopsies [13]. PET/CT-directed biopsy is also more accurate than random biopsies for the detection of the occult primary tumor [14]. High glucose metabolism in cancer cells is exploited in PET/CT scans [15]. FDG PET/CT is not a specific for malign tumors. [^{18}F]FDG is also accumulated in inflammatory or benign tumors and causes false-positive results [7]. Tumors with low or no FDG uptake may be missed with PET/CT [2]. FDG PET/CT also guides biopsy of probable sites of the primary tumor. Intravenous contrast enhancement improves the detection of non-FDG avid tumors like hepatocellular carcinoma, neuroendocrine tumors, and bronchoalveolar carcinoma [16].

Kaya et al. [17] evaluated the primary tumor site with metastatic carcinoma of unknown origin. FDG PET/CT detected the primary tumor in 24 of 43 patients (55.8%), with one false positive benign inflammatory lung lesion. Positive predictive value (PPV) of PET/CT was 96%, whereas in 18 patients (41.8%) scan was negative. Most of the primary (54.2%) tumors were in the lung. In our study, there was only one false-positive result too. In this false positive patient, the primary site was thought ovary with PET/CT, but hypermetabolism in the ovary was physiological as seen in other imaging methods. In another study, the primary tumor was correctly identified in 24% of patients. 31% of patients had metastatic spread without clear identification of a primary tumor. In 4% of patients had a potential

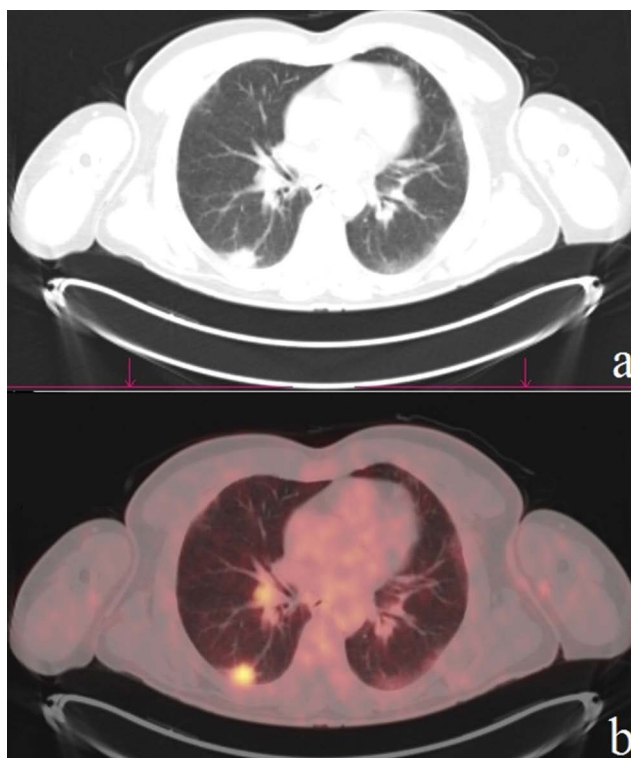


Figure 1. Multiple metastatic lesions on pelvic bones were incidentally detected with bone scintigraphy in a 55-year-old male patient. A lung lesion compatible with the primary tumor was detected in the superior segment of the inferior lobe of the right lung with positron emission tomography/computed tomography

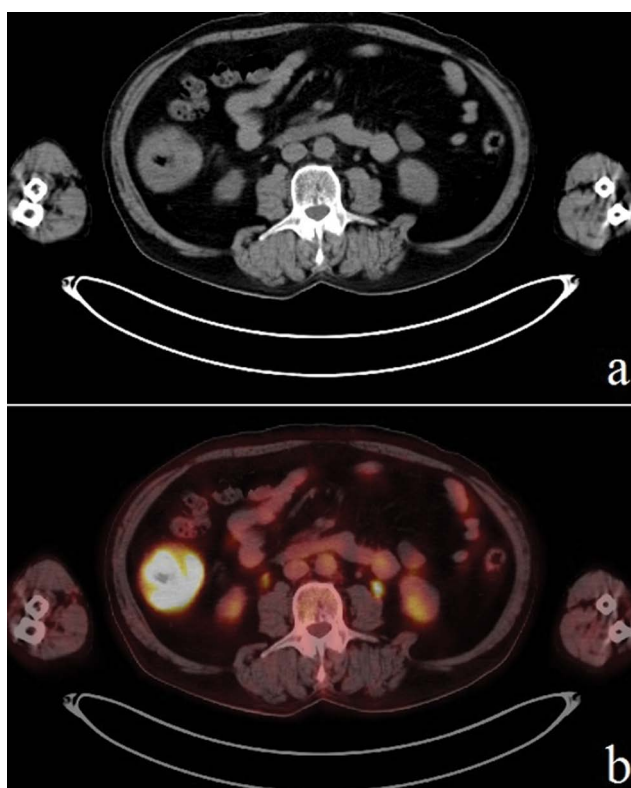


Figure 2. Positron emission tomography/computed tomography was performed for the metastatic lesion in the cerebellum in 62-year-old male patients. The primary tumor was detected in the hepatic flexure of the colon

primary tumor identified turned out to be false positive. The sensitivity, specificity, PPV, and negative predictive value (NPV) were found at 96%, 80%, 95% and 86% when the presence or absence of malignant lesions anywhere in the body were considered [18]. In a study of Deonarine et al. [19], the overall detection rate of primary tumor locations with FDG PET/CT and additional investigations and procedures was 49% with the detection rate of FDG PET/CT being 37.3% and the sensitivity was 79.2%. Lung was the most common primary tumor site and they mentioned that FDG PET/CT should be an early method to improve the accuracy of tumor staging. As in these studies, the most common primary tumor was in the lung. Fencel et al. [20] found the sensitivity and specificity 62.0% and 81.9% for the primary search, 93.6%, and 85.7% for the presence of malignancy search. In our study, the most common primary tumor site was the lung as in these previous studies. In a study of Tamam et al. [21] FDG PET/CT findings correctly diagnosed lesions as the site of the primary true positive in 75% (238 of 316 patients) with the most common was lung cancer (42.4%). Fifty-six cases were false negative with PET/CT. The sensitivity, specificity, accuracy, PPV and NPV of PET/CT were 81%, 45%, 78%, 95% and 15%, respectively [21]. In our study, the sensitivity (80%) and accuracy (79.4%) were similar to the study of Tamam et al. [21].

In some studies identification of the primary tumor was studied in specific metastatic locations. Koç et al. [22] studied the primary tumor which has been admitted with brain metastases. Twenty of 26 patients had positive PET/CT for the primary tumor, 6 lung cancer, 9 primary brain tumor, 2 renal cell carcinoma, 1 skin, 1 breast, and 1 neuroendocrine tumor. They mentioned that PET/CT must be performed in patients with brain metastases to find the primary tumor. Dandekar et al. [23] studied the utility of PET in an unknown primary with cervical metastases. They found the sensitivity and specificity of conventional imaging 92.3% and 50% whereas FDG PET showed 92.8% and 71.4%, respectively. PET had an additional benefit over CT because PET aids in screening infraclavicular primaries and distant metastases. Fan et al. [24] observed patients with malignant ascites of unknown primary sites after conventional imaging methods. 23 of 28 cases had elevated FDG with 20 patients were confirmed by pathology, but 3 were found to be falsely positive due to tuberculosis. In patients with bone metastasis of unknown origin, the primary tumor was identified in 92% of patients, with the most common cause being adenocarcinoma. The most common primary tumor was lung carcinoma (52%) [25].

In a study, the performance of FDG PET/CT was compared with conventional imaging methods, including CT, magnetic resonance imaging, and mammography in cancer of unknown primary. FDG PET/CT detected the primary tumor more than conventional imaging, but not statistically significant. It was considered that FDG PET/CT can be performed as a first-line imaging tool and then adding radiodiagnostic imaging in selective cases [5]. Jain et al. [16] mentioned that tumors that cannot be identified with PET/CT should be subjected to further extensive workup. All patients do not require PET/CT to identify the primary tumor. The decision of PET/CT scan should be made multidisciplinary [14]. But in a few studies, it was found that FDG PET/CT did not have or might be less diagnostic advantage than expected over CT or extensive conventional diagnostic workups for the detection of primary tumor site in CUP patients [26, 27]. Invasive diagnostic procedures or

additional imaging were reduced after PET/CT. Additional imaging of selected organs was needed in individual cases after PET/CT [28]. As a limitation, FDG PET/CT had a very low detection rate in locating the primary site in metastatic melanoma and metastatic location in the axilla [29]. We have only one patient diagnosed with malign melanoma, and in this patient PET/CT could not detect the primary tumor site.

As in our study, PET/CT should be the first-line diagnostic tool for CUP, because almost four of five patients' primary tumor sites can be determined with PET/CT. Other diagnostic imaging tools should be applied after a negative whole-body PET/CT.

References

1. Losa F, Iglesias L, Pané M, et al. 2018 consensus statement by the Spanish Society of Pathology and the Spanish Society of Medical Oncology on the diagnosis and treatment of cancer of unknown primary. *Clin Transl Oncol*. 2018; 20(11): 1361–1372, doi: [10.1007/s12094-018-1899-z](https://doi.org/10.1007/s12094-018-1899-z), indexed in Pubmed: [29808414](https://pubmed.ncbi.nlm.nih.gov/29808414/).
2. Kwee TC, Kwee RM. Combined FDG-PET/CT for the detection of unknown primary tumors: systematic review and meta-analysis. *Eur Radiol*. 2009; 19(3): 731–744, doi: [10.1007/s00330-008-1194-4](https://doi.org/10.1007/s00330-008-1194-4), indexed in Pubmed: [18925401](https://pubmed.ncbi.nlm.nih.gov/18925401/).
3. Moller AK, Loft A, Berthelsen AK, et al. 18F-FDG PET/CT as a diagnostic tool in patients with extracervical carcinoma of unknown primary site: a literature review. *Oncologist*. 2011; 16(4): 445–451, doi: [10.1634/theoncologist.2010-0189](https://doi.org/10.1634/theoncologist.2010-0189), indexed in Pubmed: [21427201](https://pubmed.ncbi.nlm.nih.gov/21427201/).
4. Riaz S, Nawaz MK, Faruqi ZS, et al. Diagnostic accuracy of 18F-fluorodeoxyglucose positron emission tomography-computed tomography in the evaluation of carcinoma of unknown primary. *Mol Imaging Radionucl Ther*. 2016; 25(1): 11–18, doi: [10.4274/mirt.05706](https://doi.org/10.4274/mirt.05706), indexed in Pubmed: [27299283](https://pubmed.ncbi.nlm.nih.gov/27299283/).
5. Cetin Avci N, Hatipoglu F, Alacacioglu A, et al. FDG PET/CT and conventional imaging methods in cancer of unknown primary: an approach to overscanning. *Nucl Med Mol Imaging*. 2018; 52(6): 438–444, doi: [10.1007/s13139-018-0544-7](https://doi.org/10.1007/s13139-018-0544-7), indexed in Pubmed: [30538775](https://pubmed.ncbi.nlm.nih.gov/30538775/).
6. Garin E, Prigent-Lejeune F, Lesimple T, et al. Impact of PET-FDG in the diagnosis and therapeutic care of patients presenting with metastases of unknown primary. *Cancer Invest*. 2007; 25(4): 232–239, doi: [10.1080/07357900701206331](https://doi.org/10.1080/07357900701206331), indexed in Pubmed: [17612933](https://pubmed.ncbi.nlm.nih.gov/17612933/).
7. Cengiz A, Göksel S, Yürekli Y. Diagnostic value of 18F-FDG PET/CT in patients with carcinoma of unknown primary. *Mol Imaging Radionucl Ther*. 2018; 27(3): 126–132, doi: [10.4274/mirt.64426](https://doi.org/10.4274/mirt.64426), indexed in Pubmed: [30317849](https://pubmed.ncbi.nlm.nih.gov/30317849/).
8. Yapar Z, Kibar M, Yapar AF, et al. The value of 18F-fluorodeoxyglucose positron emission tomography/computed tomography in carcinoma of an unknown primary: diagnosis and follow-up. *Nucl Med Commun*. 2010; 31(1): 59–66, doi: [10.1097/MNM.0b013e328332b340](https://doi.org/10.1097/MNM.0b013e328332b340), indexed in Pubmed: [19952921](https://pubmed.ncbi.nlm.nih.gov/19952921/).
9. Pavlidis N, Pentheroudakis G. Cancer of unknown primary site. *Lancet*. 2012; 379(9824): 1428–1435, doi: [10.1016/s0140-6736\(11\)61178-1](https://doi.org/10.1016/s0140-6736(11)61178-1), indexed in Pubmed: [22414598](https://pubmed.ncbi.nlm.nih.gov/22414598/).
10. Liu Y. FDG PET/CT for metastatic squamous cell carcinoma of unknown primary of the head and neck. *Oral Oncol*. 2019; 92: 46–51, doi: [10.1016/j.oraloncology.2019.03.014](https://doi.org/10.1016/j.oraloncology.2019.03.014), indexed in Pubmed: [31010622](https://pubmed.ncbi.nlm.nih.gov/31010622/).
11. Pavlidis N, Fizazi K. Carcinoma of unknown primary (CUP). *Crit Rev Oncol Hematol*. 2009; 69(3): 271–278, doi: [10.1016/j.critrevonc.2008.09.005](https://doi.org/10.1016/j.critrevonc.2008.09.005), indexed in Pubmed: [18977667](https://pubmed.ncbi.nlm.nih.gov/18977667/).
12. Han A, Xue J, Hu M, et al. Clinical value of 18F-FDG PET-CT in detecting primary tumor for patients with carcinoma of unknown primary. *Cancer Epidemiol*. 2012; 36(5): 470–475, doi: [10.1016/j.canep.2012.03.002](https://doi.org/10.1016/j.canep.2012.03.002), indexed in Pubmed: [22504050](https://pubmed.ncbi.nlm.nih.gov/22504050/).

13. Pak K, Kim SJ, Kim IJ, et al. Clinical implication of (18)F-FDG PET/CT in carcinoma of unknown primary. *Neoplasma*. 2011; 58(2): 135–139, doi: [10.4149/neo_2011_02_135](https://doi.org/10.4149/neo_2011_02_135), indexed in Pubmed: [21275463](https://pubmed.ncbi.nlm.nih.gov/21275463/).
14. Kinder KJ, Lavertu P, Yao M. Positron emission tomography in head and neck squamous cell carcinoma of unknown primary. *PET Clin*. 2012; 7(4): 443–452, doi: [10.1016/j.cpet.2012.06.007](https://doi.org/10.1016/j.cpet.2012.06.007), indexed in Pubmed: [27157650](https://pubmed.ncbi.nlm.nih.gov/27157650/).
15. Burglin SA, Hess S, Høilund-Carlsen PF, et al. 18F-FDG PET/CT for detection of the primary tumor in adults with extracervical metastases from cancer of unknown primary: a systematic review and meta-analysis. *Medicine (Baltimore)*. 2017; 96(16): e6713, doi: [10.1097/MD.00000000000006713](https://doi.org/10.1097/MD.00000000000006713), indexed in Pubmed: [28422888](https://pubmed.ncbi.nlm.nih.gov/28422888/).
16. Jain A, Srivastava MK, Pawaskar AS, et al. Contrast-enhanced [18F] fluorodeoxyglucose-positron emission tomography-computed tomography as an initial imaging modality in patients presenting with metastatic malignancy of undefined primary origin. *Indian J Nucl Med*. 2015; 30(3): 213–220, doi: [10.4103/0972-3919.158529](https://doi.org/10.4103/0972-3919.158529), indexed in Pubmed: [26170563](https://pubmed.ncbi.nlm.nih.gov/26170563/).
17. Kaya AO, Coskun U, Unlu M, et al. Whole body 18F-FDG PET/CT imaging in the detection of primary tumours in patients with a metastatic carcinoma of unknown origin. *Asian Pac J Cancer Prev*. 2008; 9(4): 683–686, indexed in Pubmed: [19256759](https://pubmed.ncbi.nlm.nih.gov/19256759/).
18. Breuer N, Behrendt FF, Heinzl A, et al. Prognostic relevance of (18)F-FDG PET/CT in carcinoma of unknown primary. *Clin Nucl Med*. 2014; 39(2): 131–135, doi: [10.1097/RLU.0000000000000304](https://doi.org/10.1097/RLU.0000000000000304), indexed in Pubmed: [24368527](https://pubmed.ncbi.nlm.nih.gov/24368527/).
19. Deonarine P, Han S, Poon FW, et al. The role of 18F-fluoro-2-deoxyglucose positron emission tomography/computed tomography in the management of patients with carcinoma of unknown primary. *Scott Med J*. 2013; 58(3): 154–162, doi: [10.1177/0036933013496958](https://doi.org/10.1177/0036933013496958), indexed in Pubmed: [23960054](https://pubmed.ncbi.nlm.nih.gov/23960054/).
20. Fencil P, Belohlavek O, Skopalova M, et al. Prognostic and diagnostic accuracy of [18F]FDG-PET/CT in 190 patients with carcinoma of unknown primary. *Eur J Nucl Med Mol Imaging*. 2007; 34(11): 1783–1792, doi: [10.1007/s00259-007-0456-8](https://doi.org/10.1007/s00259-007-0456-8), indexed in Pubmed: [17541584](https://pubmed.ncbi.nlm.nih.gov/17541584/).
21. Tamam MO, Mulazimoglu M, Guveli TK, et al. Prediction of survival and evaluation of diagnostic accuracy whole body 18F-fluoro-2-deoxyglucose positron emission tomography/computed tomography in the detection of carcinoma of unknown primary origin. *Eur Rev Med Pharmacol Sci*. 2012; 16(15): 2120–2130, indexed in Pubmed: [23280029](https://pubmed.ncbi.nlm.nih.gov/23280029/).
22. Koç ZP, Kara PÖ, Dağtekin A. Detection of unknown primary tumor in patients presented with brain metastasis by F-18 fluorodeoxyglucose positron emission tomography/computed tomography. *CNS Oncol*. 2018; 7(2): CNS12, doi: [10.2217/cns-2017-0018](https://doi.org/10.2217/cns-2017-0018), indexed in Pubmed: [29708403](https://pubmed.ncbi.nlm.nih.gov/29708403/).
23. Dandekar MR, Kannan S, Rangarajan V, et al. Utility of PET in unknown primary with cervical metastasis: a retrospective study. *Indian J Cancer*. 2011; 48(2): 181–186, doi: [10.4103/0019-509X.82882](https://doi.org/10.4103/0019-509X.82882), indexed in Pubmed: [21768663](https://pubmed.ncbi.nlm.nih.gov/21768663/).
24. Fan HB, Wang AJ, Yang DL, et al. Use of 18F-FDG PET/CT to locate primary malignancies in patients with hepatic cirrhosis and malignant ascites. *Chin J Cancer Res*. 2013; 25(5): 500–504, doi: [10.3978/j.issn.1000-9604.2013.09.01](https://doi.org/10.3978/j.issn.1000-9604.2013.09.01), indexed in Pubmed: [24255572](https://pubmed.ncbi.nlm.nih.gov/24255572/).
25. Budak E, Yanarateş A. Role of F-FDG PET/CT in the detection of primary malignancy in patients with bone metastasis of unknown origin. *Rev Esp Med Nucl Imagen Mol (Engl Ed)*. 2020; 39(1): 14–19, doi: [10.1016/j.remnm.2019.06.002](https://doi.org/10.1016/j.remnm.2019.06.002), indexed in Pubmed: [31744788](https://pubmed.ncbi.nlm.nih.gov/31744788/).
26. Møller AK, Loft A, Berthelsen AK, et al. A prospective comparison of 18F-FDG PET/CT and CT as diagnostic tools to identify the primary tumor site in patients with extracervical carcinoma of unknown primary site. *Oncologist*. 2012; 17(9): 1146–1154, doi: [10.1634/theoncologist.2011-0449](https://doi.org/10.1634/theoncologist.2011-0449), indexed in Pubmed: [22711751](https://pubmed.ncbi.nlm.nih.gov/22711751/).
27. Park JS, Yim JJ, Kang WJ, et al. Detection of primary sites in unknown primary tumors using FDG-PET or FDG-PET/CT. *BMC Res Notes*. 2011; 4: 56, doi: [10.1186/1756-0500-4-56](https://doi.org/10.1186/1756-0500-4-56), indexed in Pubmed: [21385465](https://pubmed.ncbi.nlm.nih.gov/21385465/).
28. Reinert CP, Sekler J, la Fougère C, et al. Impact of PET/CT on clinical management in patients with cancer of unknown primary—a PET/CT registry study. *Eur Radiol*. 2020; 30(3): 1325–1333, doi: [10.1007/s00330-019-06518-9](https://doi.org/10.1007/s00330-019-06518-9), indexed in Pubmed: [31728688](https://pubmed.ncbi.nlm.nih.gov/31728688/).
29. Yu X, Li X, Song X, et al. Advantages and disadvantages of F-18 fluorodeoxyglucose positron emission tomography/computed tomography in carcinoma of unknown primary. *Oncol Lett*. 2016; 12(5): 3785–3792, doi: [10.3892/ol.2016.5203](https://doi.org/10.3892/ol.2016.5203), indexed in Pubmed: [27895731](https://pubmed.ncbi.nlm.nih.gov/27895731/).

Assessing the correlation between FDG PET findings of IDC breast carcinoma and histopathology of coexisting ductal carcinoma in-situ

Ismet Sarikaya¹, Ali Sarikaya², Ahmed N. Albatineh³, Ebru Tastekin⁴, Yavuz Atakan Sezer⁵

¹Faculty of Medicine, Department of Nuclear Medicine, Kuwait University, Kuwait

²Faculty of Medicine, Department of Nuclear Medicine, Trakya University, Edirne, Turkey

³Faculty of Medicine, Department of Community Medicine and Behavioral Sciences, Kuwait University, Kuwait

⁴Faculty of Medicine, Department of Pathology, Trakya University, Edirne, Turkey

⁵Faculty of Medicine, Department of Surgery, Trakya University, Edirne, Turkey

[Received 2 XI 2020; Accepted 15 III 2021]

Abstract

Background: Ductal carcinoma in-situ (DCIS) often coexists with invasive ductal carcinoma (IDC) of the breast. DCIS is considered as a non-obligate precursor of IDC when both coexist. ¹⁸F-fluorodeoxyglucose positron emission tomography/computed tomography (¹⁸F]FDG PET/CT) imaging is commonly used in the staging and follow-up assessment of breast cancer. In this study, we aimed to assess if there is any correlation between primary tumor PET and histopathology findings and histopathological features of the coexisting DCIS.

Material and methods: FDG PET/CT images and histopathology results of the patients with newly diagnosed breast cancer (IDC) with coexisting DCIS were analyzed in this retrospective study. The grade and size of the primary tumor and histopathological features of the coexisting DCIS (nuclear grade and architectural pattern) were obtained from the postoperative histopathology results. Maximum standardized uptake values (SUV: SUV_{max} and SUL_{max}) of the primary tumor normalized by weight and lean body mass were measured. Statistical analysis was performed to assess the correlation between various parameters of IDC and DCIS.

Results: This study included sixty-two (62) patients with IDC-DCIS. Primary tumor grade was significantly correlated and associated with the nuclear grade of the coexisting DCIS (polychoric correlation $r = 0.736$, and Fisher exact test, $PV < 0.001$, respectively). Primary tumor SUV was not correlated with the nuclear grade and architectural pattern of the coexisting DCIS (polyserial correlation $r = 0.172$, $PV = 0.155$, and Point Bi-Serial correlation $r = -0.009$, $PV = 0.955$, respectively). Median primary tumor size was marginally significantly different among DCIS nuclear grades but it was not significantly different in comedo and non-comedo cases (Kruskal-Wallis test $PV = 0.053$, and Mann-Whitney U test $PV = 0.890$, respectively).

Conclusions: Primary tumor grade is correlated with the nuclear grade of the coexisting DCIS. SUV of primary tumor does not seem to be correlated with the histopathological features of coexisting DCIS (nuclear grade and architectural pattern) but this may be further studied in a larger number of patients.

KEY words: breast carcinoma; invasive ductal carcinoma; coexisting DCIS; FDG PET; nuclear grade; architectural pattern

Nucl Med Rev 2022; 25, 1: 6–11

Correspondence to: Ismet Sarikaya,
Department of Nuclear Medicine, Faculty of Medicine,
Kuwait University, PO Box 24923
Safat, Kuwait 13110, tel.: (965) 25319592/6414, fax: (965) 25338936
e-mail: isarikaya99@yahoo.com

This article is available in open access under Creative Common Attribution-Non-Commercial-No Derivatives 4.0 International (CC BY-NC-ND 4.0) license, allowing to download articles and share them with others as long as they credit the authors and the publisher, but without permission to change them in any way or use them commercially.

Introduction

Ductal carcinoma in situ (DCIS) is a pre-invasive (non-invasive) type of breast cancer. In DCIS, malignant ductal epithelial cell proliferations remain confined within the intact breast ducts [1]. DCIS often coexists with invasive ductal carcinoma (IDC) of the breast [2, 3]. DCIS is recognized as the non-obligate precursor of IDC when both of them coexist [4, 5]. In tumors with no coexisting DCIS (pure IDC), it is assumed that IDC arises de novo [6, 7].

^{18}F -fluorodeoxyglucose (^{18}F FDG) positron emission tomography/computed tomography (PET/CT) is widely used for initial staging/detecting distant metastases of high-risk locally advanced invasive and inflammatory breast cancers, particularly where standard staging studies show equivocal or suspicious results [8–10]. FDG uptake is usually higher in IDC and inflammatory breast cancer and lower in invasive lobular carcinoma of the breast [8, 11]. DCIS lesions usually show a low degree of FDG uptake [12]. FDG uptake (metabolic activity of the tumor) is positively correlated with the tumor grade and proliferation (Ki-67 expression) and negatively correlated with the hormonal receptor status of breast cancer [8, 13]. Estrogen and progesterone receptor (ER and PR) negative tumors demonstrate higher metabolic activity than receptor-positive tumors [11, 14]. Triple-negative breast cancer (negative for ER, PR, and HER2) usually shows high FDG uptake (high metabolic activity) and is associated with poor prognosis [14, 15].

In a recently published study, we have compared FDG PET/CT findings of IDC-DCIS and pure IDC cases [16]. In the current study, our aim was to assess if there is any correlation between primary tumor's (IDC) PET and histopathology findings and histopathological features of the coexisting DCIS. We wanted to understand if FDG PET findings can support the hypothesis of DCIS as the precursor of IDC when they coexist.

Material and methods

Histopathology results of the newly diagnosed breast cancer patients who had FDG PET/CT imaging for initial staging and prior to any treatment were reviewed. Patients with IDC and coexisting DCIS (IDC-DCIS) were selected for further analysis.

This retrospective study was approved by two institutes (Kuwait Ministry of Health and Trakya University Faculty of Medicine Health and Ethics Committee).

FDG PET/CT images were obtained approximately 60 min following intravenous injection of 222–296 MBq (6–8 mCi) of ^{18}F FDG using Philips Gemini Time of Flight (Philips Medical Systems, Best, Netherlands) and GE discovery 8 (General Electric Medical Systems, Milwaukee, WI, USA) PET/CT cameras. First, a low-dose CT was obtained (for attenuation correction and anatomic localization). PET image acquisition was 2–3 min/bed from vertex to mid-thigh levels. PET images were corrected for attenuation using the CT data. PET images were reconstructed using a standard iterative algorithm and reformatted into transaxial, coronal, and sagittal planes. A maximum intensity projection image was generated.

FDG PET/CT images were evaluated by 2 board-certified Nuclear Medicine physicians with over 30 years of experience. Weight and lean body mass normalized maximum standardized uptake values (SUV_{max} and SUL_{max}) of the primary tumors were measured. PET/CT images were reviewed to assess the primary tumor, regional

and distant metastases, and additional findings but those were not included in the analysis.

Histopathology results were reviewed to collect information for the features of the primary tumor (grade and size) and coexisting DCIS (nuclear grade and architectural subtype).

Statistical analysis

The statistical analysis was conducted using the SPSS statistical software (Version 24) and R statistical software. Counts and percentages were reported for categorical variables and means (SD) were reported for continuous variables. Two sample t-test or Mann-Whitney U tests were used to compare two continuous variables depending on the data normality condition. Analysis of variance (ANOVA) or Kruska-Wallis test was used to compare a continuous outcome and a three or more levels categorical covariate. The strength of the associations was measured by correlation coefficients of either Spearman rank correlation, point biserial correlation, polyserial correlation, or polychoric correlations depending on the type of variables under investigation. All tests were two-tailed, and p-values < 0.05 were considered statistically significant.

Results

Sixty-two (62) female patients with newly diagnosed IDC-DCIS from 2 institutes (Mubarak Al-Kabeer hospital: 26 patients and Trakya University hospital: 36 patients) were included in this study (mean age 55.2 ± 9.5 years).

Patients underwent various surgeries such as mastectomy, wide local excision, or breast preservation surgery (lumpectomy or segmental mastectomy). All of the patients also had sentinel lymph node biopsy and/or axillary dissection. Some of the patients received neoadjuvant chemotherapy before the surgery (after PET imaging). TNM staging of the tumors is available in our data but not provided in this article.

Primary tumor grade was grade-3 in 28 patients, grade-2 in 27, and grade-1 in 7 patients. The nuclear grade of the coexisting DCIS was grade-3 in 38 patients, grade-2 in 13, and grade-1 in 8 patients. Nuclear grade of the DCIS in 3 patients and the size of the primary tumor in 5 patients were not available in the pathology report. The architectural pattern of the coexisting DCIS was mainly mixed (combination of at least 2 of the following patterns; solid, papillary, micropapillary, cribriform, and comedo, 49 patients) and the rest of the patients showed only solid pattern (13 patients). For statistical comparison, we further classified the architectural pattern as comedo (37 patients) and non-comedo (25 patients) based on the presence of comedo necrosis. Figure 1 and 2 shows primary tumor grade versus a nuclear grade of coexisting DCIS and nuclear grade versus architectural subtype of DCIS, respectively.

Statistical results

Primary tumor SUVs (SUV_{max} and SUL_{max}) were not significantly correlated with the nuclear grade of the coexisting DCIS (Polyserial correlation, $r = 0.172$; $PV = 0.155$ and $r = 0.158$, and $PV = 0.211$, respectively). Median primary tumor SUVs (SUV_{max} and SUL_{max}) were higher in nuclear grade-3 than nuclear grade-2 and -1 cases but according to the Kruskal-Wallis test, they were

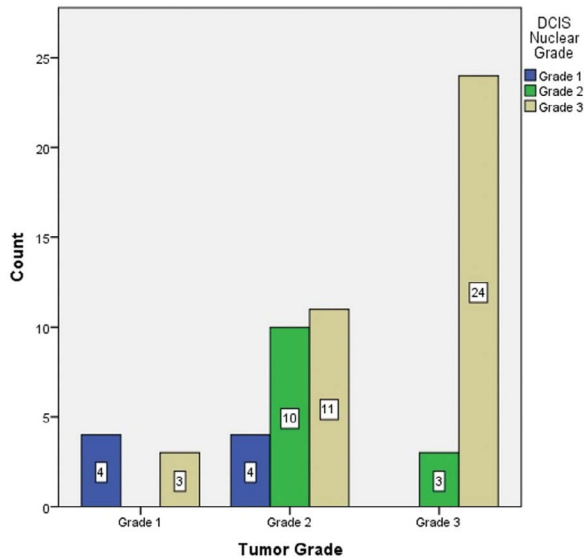


Figure 1. Primary tumor grade versus nuclear grade of the coexisting DCIS; count — number of patients)

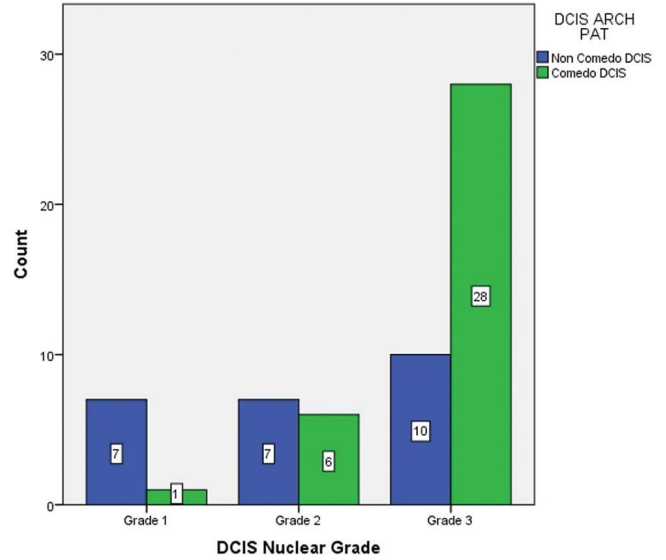


Figure 2. Nuclear grade versus the architectural pattern of coexisting ductal carcinoma in-situ (DCIS); Count — number of patients)

not significantly different ($PV = 0.288$, and 0.340 , respectively) (Fig. 3, Tab. 1).

Primary tumor SUVs (SUV_{max} and SUL_{max}) were not correlated with the architectural pattern of the coexisting DCIS (Point Bi-Serial correlation, $r = -0.009$, $PV = 0.955$ and $r = -0.017$, $PV = 0.919$, respectively). Median primary tumor SUVs (SUV_{max} and SUL_{max}) were higher in comedo than non-comedo coexisting DCIS, but according to the Mann-Whitney U test, they were not significantly different ($PV = 0.966$, and 0.886 , respectively) (Fig. 3, Tab. 2).

Primary tumor grade was correlated with the nuclear grade (Polychoric correlation, $r = 0.736$, $PV < 0.001$) but not with the architectural pattern (Polychoric correlation, $r = 0.265$, $PV = 0.157$)

of the coexisting DCIS. There was a significant association between the primary tumor grade and nuclear grade of the coexisting DCIS (Fisher exact test, $PV < 0.001$), but no significant association between primary tumor grade and architectural pattern of the coexisting DCIS (comedo versus non-comedo) (Fisher exact test, $PV = 0.233$).

According to the Kruskal-Wallis test, there was marginally significant evidence that the median primary tumor size among DCIS nuclear grade was different ($PV = 0.053$) but according to the Mann-Whitney U test, the median primary tumor size in comedo and non-comedo cases were not significantly different ($PV = 0.890$) (Tab. 1 and 2, Fig. 4).

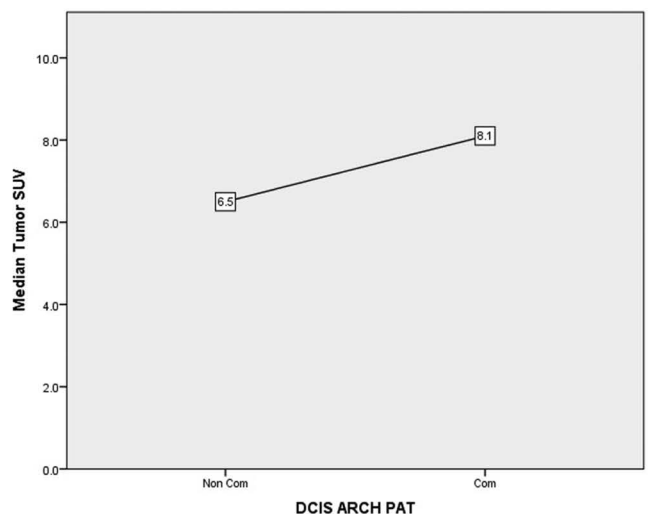
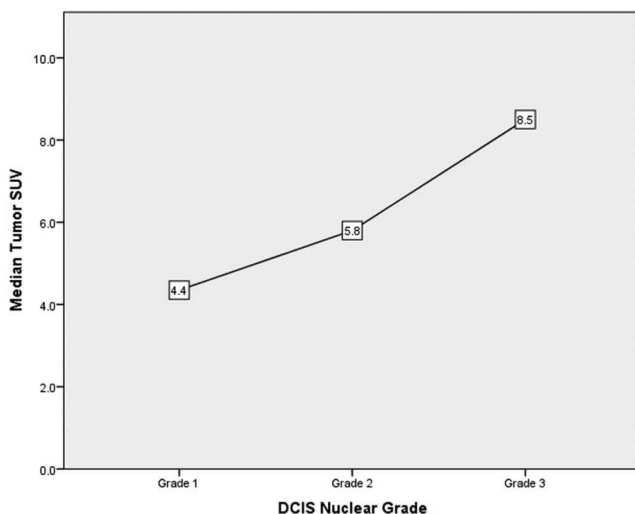
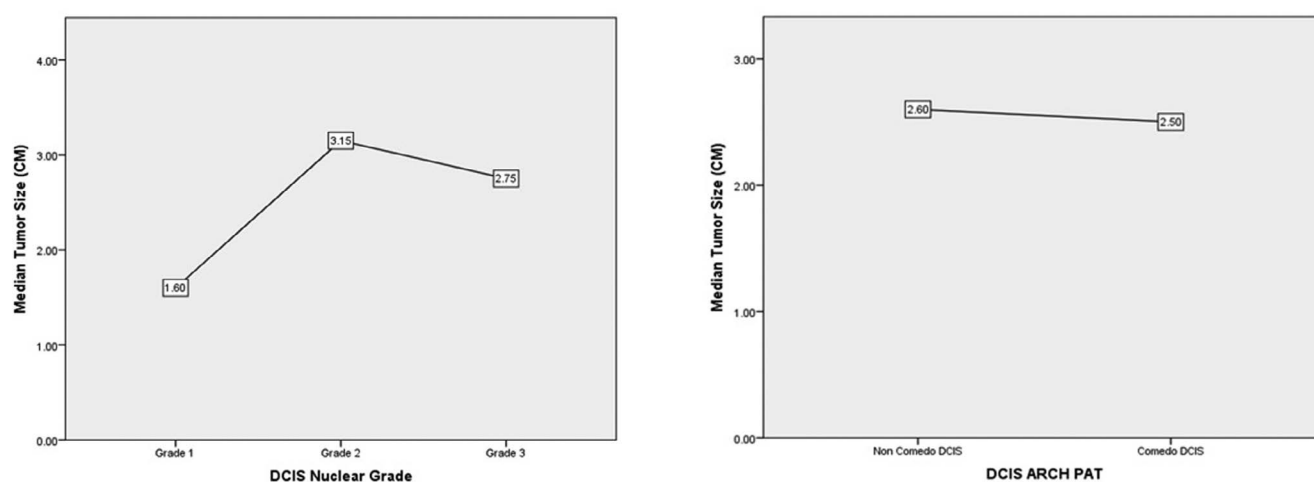


Figure 3. Graphs of median primary tumor SUV versus nuclear grade and architectural pattern (comedo and non-comedo) of coexisting ductal carcinoma in-situ (DCIS). Median SUVs are shown in boxes

Table 1. Tests of differences in primary tumor (IDC) size, primary tumor SUV_{max} and primary tumor SUL_{max} according to primary tumor grade and nuclear grade of coexisting ductal carcinoma in-situ (DCIS)

Covariate	Primary Tumor Size (cm)		Primary Tumor SUV _{max}		Primary Tumor SUL _{max}	
	median	p-value	median	p-value	(n)(median)	p-value
Primary Tumor Grade		0.001 [†]		0.013 [†]		0.010 [†]
Grade 1	1.05		3.8		2.75	
Grade 2	2.40		6.25		3.40	
Grade 3	3.10		8.70		5.60	
Nuclear Grade of Coexisting DCIS		0.053 [†]		0.288 [†]		0.340 [†]
Grade 1	1.6		4.35		2.70	
Grade 2	3.15		5.75		3.40	
Grade 3	2.75		8.5		4.70	

[†]p-value calculated using Kruskal-Wallis test

**Figure 4.** Graphs of median primary tumor size versus nuclear grade and architectural pattern (comedo and non-comedo) of coexisting ductal carcinoma in-situ (DCIS). Median sizes are shown in boxes

As expected, primary tumor grade was significantly correlated with the primary tumor SUVs (SUV_{max} and SUL_{max}) (Polyserial correlation, $r = 0.312$, $PV = 0.023$, and $r = 0.303$, $PV = 0.024$, respectively). According to the Kruskal-Wallis test, there was evidence of a significant difference in median primary tumor SUVs (SUV_{max} and SUL_{max}) across primary tumor grades ($PV = 0.013$, and 0.010 , respectively) (Tab. 1). Primary tumor grade was significantly correlated with the primary tumor size (Polyserial correlation, $r = 0.545$, $PV < 0.001$) (Tab. 1). Also, the nuclear grade of the DCIS was significantly correlated with the architectural pattern of the DCIS (Polychoric correlation, $r = 0.614$, $PV < 0.001$).

Discussion

DCIS often coexists with IDC (32% and 63.1% of the cases) [2, 3]. DCIS is recognized as the non-obligate precursor of IDC when they coexist [4, 5]. It was suggested that up to 50% of patients with

microscopic foci of DCIS develop invasive carcinomas of the breast [4]. The invasive lesion occurs in the same region as the original DCIS lesion which indicates a precursor process [4, 17]. Other studies have also supported the hypothesis of transition from DCIS to IDC based on the concordant expression of immunohistochemical markers, biomarkers, and genomic data [18–26]. Progression from DCIS to invasive breast cancer may follow a Darwinian evolutionary model [5].

Histologic parameters of the clinical significance of DCIS include architectural subtypes/patterns, nuclear grade, size and extent of the lesion, status of microcalcifications, necrosis, and margins [27]. The nuclear grade of the DCIS lesions is classified as low grade (grade-1), intermediate grade (grade-2), and high grade (grade-3). Grade-3 DCIS is composed of pleomorphic large cells and abundant mitoses. High nuclear grade DCIS is an aggressive subtype of DCIS with an overall poorer prognosis as compared to low and intermediate nuclear grade DCIS [28]. DCIS with low-nuclear grade

Table 2. Testing median differences of primary tumor size, primary tumor SUV_{max}¹ and primary tumor SUL_{max} by architectural subtype of coexisting ductal carcinoma in-situ (DCIS)

Covariate	Architectural Subtype of Coexisting DCIS		p-value [†]
	Comedo	Non-Comedo	
Primary Tumor Size (cm, median)	2.50	2.60	0.890
Primary Tumor SUV _{max} (median)	8.1	6.5	0.966
Primary Tumor SUL _{max} (median)	4.50	3.70	0.886

[†]p-value was obtained according to Mann-Whitney U test

is composed of uniform cells with small size and low-mitotic rate. In intermediate nuclear grade DCIS, neoplastic nuclei show pleomorphism (between high- and low- nuclear grade DCIS).

The architectural patterns of DCIS are classified as solid, comedo necrosis (comedo), cribriform, micropapillary, and papillary. DCIS commonly demonstrates a mixed pattern. DCIS is usually categorized as comedo and non-comedo. The comedo subtype of DCIS is defined by high-grade cells, prominent necrosis in the center of the ducts, and a high proliferation rate [29, 30]. Non-comedo subtypes of DCIS are composed of low-grade cells, and a low proliferation rate [27]. Angiogenesis and foci of microinvasion are common around comedo lesions and low in non-comedo lesions [31–33]. Ketcham et al. have indicated there is more often and more rapid progression into invasive carcinoma from high-grade DCIS as compared to low-grade [34].

In the current study, there was a significant correlation and association between the grade of the primary tumor and the nuclear grade of the coexisting DCIS. Median primary tumor SUV was higher in nuclear grade-3 cases and comedo pattern as compared to cases with nuclear grade-1 and-2 and non-comedo pattern but it was not statistically significant. This result may be affected by the relatively small number of nuclear grade-1 (n = 8) and -2 (n = 12) cases in our study. In a recently published study, we did not find a significant difference in primary tumor SUV in IDC-DCIS and pure IDC cases but multifocal tumor and multifocal uptake were more common in IDC-DCIS cases [16]. As expected, in the current study primary tumor grade was significantly correlated with the primary tumor's metabolic activity and nuclear grade of the DCIS was significantly correlated with the architectural pattern of the DCIS [8, 13, 29, 30].

Studies have also reported that IDC-DCIS show lower metastatic potential and recurrence and better overall survival as compared to pure IDC but some other studies show controversial results [6, 7, 23, 35, 36]. In our recent study, axillary metastases appeared to be more common in pure IDC than IDC-DCIS cases [16].

A limitation of this study could be the relatively small number of patients, particularly patients with nuclear grade-1 and -2 coexisting DCIS. Assessing primary tumor metabolic activity alone is not adequate to understand if DCIS could be the precursor of IDC in IDC-DCIS cases but it may be supportive if primary tumor SUV correlates with the nuclear grade of coexisting DCIS. This preliminary study also serves as the only available data in

the literature investigating the correlation between PET findings of the primary tumor (IDC) with the histopathological findings of the coexisting DCIS.

Conclusions

Primary tumor grade is significantly correlated with the nuclear grade of the coexisting DCIS. SUV of primary tumor does not seem to be significantly correlated with the histopathological features of the coexisting DCIS (nuclear grade and architectural pattern) but this may be studied in a larger number of patients.

Conflict of interest

There is no potential conflict of interest relevant to this article.

Acknowledgments

Dr. Ahmed N. Albatineh and Dr. Ebru Tastekin contributed to the manuscript equally both as 3rd authors.

References

- Barnes NLP, Ooi JL, Yarnold JR, et al. Ductal carcinoma in situ of the breast. *BMJ*. 2012; 344: e797, doi: [10.1136/bmj.e797](https://doi.org/10.1136/bmj.e797), indexed in Pubmed: [22378935](https://pubmed.ncbi.nlm.nih.gov/22378935/).
- Jo BH, Chun YK. Heterogeneity of invasive ductal carcinoma: proposal for a hypothetical classification. *J Korean Med Sci*. 2006; 21(3): 460–468, doi: [10.3346/jkms.2006.21.3.460](https://doi.org/10.3346/jkms.2006.21.3.460), indexed in Pubmed: [16778390](https://pubmed.ncbi.nlm.nih.gov/16778390/).
- Logullo AF, Godoy AB, Mourão-Neto M, et al. Presence of ductal carcinoma in situ confers an improved prognosis for patients with T1N0M0 invasive breast carcinoma. *Braz J Med Biol Res*. 2002; 35(8): 913–919, doi: [10.1590/s0100-879x2002000800008](https://doi.org/10.1590/s0100-879x2002000800008), indexed in Pubmed: [12185383](https://pubmed.ncbi.nlm.nih.gov/12185383/).
- Pinder SE, Ellis IO. The diagnosis and management of pre-invasive breast disease: ductal carcinoma in situ (DCIS) and atypical ductal hyperplasia (ADH)—current definitions and classification. *Breast Cancer Res*. 2003; 5(5): 254–257, doi: [10.1186/bcr623](https://doi.org/10.1186/bcr623), indexed in Pubmed: [12927035](https://pubmed.ncbi.nlm.nih.gov/12927035/).
- Cowell CF, Weigelt B, Sakr RA, et al. Progression from ductal carcinoma in situ to invasive breast cancer: revisited. *Mol Oncol*. 2013; 7(5): 859–869, doi: [10.1016/j.molonc.2013.07.005](https://doi.org/10.1016/j.molonc.2013.07.005), indexed in Pubmed: [23890733](https://pubmed.ncbi.nlm.nih.gov/23890733/).
- Dieterich M, Hartwig F, Stubert J, et al. Accompanying DCIS in breast cancer patients with invasive ductal carcinoma is predictive of improved local recurrence-free survival. *Breast*. 2014; 23(4): 346–351, doi: [10.1016/j.breast.2014.01.015](https://doi.org/10.1016/j.breast.2014.01.015), indexed in Pubmed: [24559611](https://pubmed.ncbi.nlm.nih.gov/24559611/).
- Wong H, Lau S, Yau T, et al. Presence of an in situ component is associated with reduced biological aggressiveness of size-matched invasive breast cancer. *Br J Cancer*. 2010; 102(9): 1391–1396, doi: [10.1038/sj.bjc.6605655](https://doi.org/10.1038/sj.bjc.6605655), indexed in Pubmed: [20424617](https://pubmed.ncbi.nlm.nih.gov/20424617/).
- Groheux D, Cochet A, Humbert O, et al. ¹⁸F-FDG PET/CT for Staging and Restaging of Breast Cancer. *J Nucl Med*. 2016; 57 Suppl 1: 17S–26S, doi: [10.2967/jnumed.115.157859](https://doi.org/10.2967/jnumed.115.157859), indexed in Pubmed: [26834096](https://pubmed.ncbi.nlm.nih.gov/26834096/).
- Edge SB, Compton CC. The American Joint Committee on Cancer: the 7th edition of the AJCC cancer staging manual and the future of TNM. *Ann Surg Oncol*. 2010; 17(6): 1471–1474, doi: [10.1245/s10434-010-0985-4](https://doi.org/10.1245/s10434-010-0985-4), indexed in Pubmed: [20180029](https://pubmed.ncbi.nlm.nih.gov/20180029/).
- NCCN Clinical Practice Guidelines in Oncology (NCCN Guidelines). National Comprehensive Cancer Network. Version 4.2017-February 7, 2018.
- Groheux D, Giacchetti S, Moretti JL, et al. Correlation of high ¹⁸F-FDG uptake to clinical, pathological and biological prognostic factors in breast cancer. *Eur J Nucl Med Mol Imaging*. 2011; 38(3): 426–435, doi: [10.1007/s00259-010-1640-9](https://doi.org/10.1007/s00259-010-1640-9), indexed in Pubmed: [21057787](https://pubmed.ncbi.nlm.nih.gov/21057787/).

12. Avril N, Menzel M, Dose J, et al. Glucose metabolism of breast cancer assessed by 18F-FDG PET: histologic and immunohistochemical tissue analysis. *J Nucl Med*. 2001; 42(1): 9–16, indexed in Pubmed: [11197987](#).
13. Gil-Rendo A, Martínez-Regueira F, Zornoza G, et al. Association between [18F]fluorodeoxyglucose uptake and prognostic parameters in breast cancer. *Br J Surg*. 2009; 96(2): 166–170, doi: [10.1002/bjs.6459](#), indexed in Pubmed: [19160365](#).
14. Yoon HJ, Kang KW, Chun InK, et al. Correlation of breast cancer subtypes, based on estrogen receptor, progesterone receptor, and HER2, with functional imaging parameters from ⁶⁷Ga-RGD PET/CT and ¹⁸F-FDG PET/CT. *Eur J Nucl Med Mol Imaging*. 2014; 41(8): 1534–1543, doi: [10.1007/s00259-014-2744-4](#), indexed in Pubmed: [24652232](#).
15. Gonçalves H, Guerra MR, Duarte Cintra JR, et al. Survival Study of Triple-Negative and Non-Triple-Negative Breast Cancer in a Brazilian Cohort. *Clin Med Insights Oncol*. 2018; 12: 1179554918790563, doi: [10.1177/1179554918790563](#), indexed in Pubmed: [30083066](#).
16. Sarikaya I, Sarikaya A, Albatineh AN, et al. Is there a difference in FDG PET findings of invasive ductal carcinoma of the breast with and without coexisting DCIS? *Asia Ocean J Nucl Med Biol*. 2020; 8: 27–35.
17. Betsill WL, Rosen PP, Lieberman PH, et al. Intraductal carcinoma. Long-term follow-up after treatment by biopsy alone. *JAMA*. 1978; 239(18): 1863–1867, doi: [10.1001/jama.239.18.1863](#), indexed in Pubmed: [205686](#).
18. Steinman S, Wang J, Bourne P, et al. Expression of cytokeratin markers, ER-alpha, PR, HER-2/neu, and EGFR in pure ductal carcinoma in situ (DCIS) and DCIS with co-existing invasive ductal carcinoma (IDC) of the breast. *Ann Clin Lab Sci*. 2007; 37(2): 127–134, indexed in Pubmed: [17522367](#).
19. Alexe G, Dalgin GS, Ganesan S, et al. Analysis of breast cancer progression using principal component analysis and clustering. *J Biosci*. 2007; 32(5): 1027–1039, doi: [10.1007/s12038-007-0102-4](#), indexed in Pubmed: [17914245](#).
20. Aubele M, Mattis A, Zitzelsberger H, et al. Extensive ductal carcinoma In situ with small foci of invasive ductal carcinoma: evidence of genetic resemblance by CGH. *Int J Cancer*. 2000; 85(1): 82–86, doi: [10.1002/\(sici\)1097-0215\(20000101\)85:1<82::aid-ijc15>3.0.co;2-s](#), indexed in Pubmed: [10585588](#).
21. Iakovlev VV, Arneson NCR, Wong V, et al. Genomic differences between pure ductal carcinoma in situ of the breast and that associated with invasive disease: a calibrated aCGH study. *Clin Cancer Res*. 2008; 14(14): 4446–4454, doi: [10.1158/1078-0432.CCR-07-4960](#), indexed in Pubmed: [18628458](#).
22. Castro NP, Osório CA, Torres C, et al. Evidence that molecular changes in cells occur before morphological alterations during the progression of breast ductal carcinoma. *Breast Cancer Res*. 2008; 10(5): R87, doi: [10.1186/bcr2157](#), indexed in Pubmed: [18928525](#).
23. Schuetz CS, Bonin M, Clare SE, et al. Progression-specific genes identified by expression profiling of matched ductal carcinomas in situ and invasive breast tumors, combining laser capture microdissection and oligonucleotide microarray analysis. *Cancer Res*. 2006; 66(10): 5278–5286, doi: [10.1158/0008-5472.CAN-05-4610](#), indexed in Pubmed: [16707453](#).
24. Wong H, Lau S, Leung R, et al. Coexisting ductal carcinoma in situ independently predicts lower tumor aggressiveness in node-positive luminal breast cancer. *Med Oncol*. 2012; 29(3): 1536–1542, doi: [10.1007/s12032-011-0082-y](#), indexed in Pubmed: [21983862](#).
25. Buerger H, Otterbach F, Simon R, et al. Comparative genomic hybridization of ductal carcinoma in situ of the breast-evidence of multiple genetic pathways. *J Pathol*. 1999; 187(4): 396–402, doi: [10.1002/\(SICI\)1096-9896\(199903\)187:4<396::AID-PATH286>3.0.CO;2-L](#), indexed in Pubmed: [10398097](#).
26. Burkhardt L, Grob TJ, Hermann I, et al. Gene amplification in ductal carcinoma in situ of the breast. *Breast Cancer Res Treat*. 2010; 123(3): 757–765, doi: [10.1007/s10549-009-0675-8](#), indexed in Pubmed: [20033484](#).
27. Siziopikou KP. Ductal carcinoma in situ of the breast: current concepts and future directions. *Arch Pathol Lab Med*. 2013; 137(4): 462–466, doi: [10.5858/arpa.2012-0078-RA](#), indexed in Pubmed: [23544935](#).
28. Ballard LJ, Ballard GV. High-grade ductal carcinoma in situ: An overview for the radiologist. *J Am Osteopath Coll Rad*. 2013; 2: 18–25.
29. Fitzgibbons PL, Henson DE, Hutter RV. Benign breast changes and the risk for subsequent breast cancer: an update of the 1985 consensus statement. Cancer Committee of the College of American Pathologists. *Arch Pathol Lab Med*. 1998; 122(12): 1053–1055, indexed in Pubmed: [9870852](#).
30. Consensus Conference on the classification of ductal carcinoma in situ. The Consensus Conference Committee. *Cancer*. 1997; 80(9): 1798–1802, doi: [10.1002/\(sici\)1097-0142\(19971101\)80:9<1798::aid-cnrcr15>3.0.co;2-0](#), indexed in Pubmed: [9351550](#).
31. Guidi AJ, Schnitt SJ, Fischer L, et al. Microvessel density and distribution in ductal carcinoma in situ of the breast. *J Natl Cancer Inst*. 1994; 86(8): 614–619, doi: [10.1093/jnci/86.8.614](#), indexed in Pubmed: [7511693](#).
32. Engels K, Fox SB, Whitehouse RM, et al. Distinct angiogenic patterns are associated with high-grade in situ ductal carcinomas of the breast. *J Pathol*. 1997; 181(2): 207–212, doi: [10.1002/\(SICI\)1096-9896\(199702\)181:2<207::AID-PATH758>3.0.CO;2-4](#), indexed in Pubmed: [9120727](#).
33. Lagios M, Westdahl P, Margolin F, et al. Duct carcinoma in situ. Relationship of extent of noninvasive disease to the frequency of occult invasion, multicentricity, lymph node metastases, and short-term treatment failures. *Cancer*. 1982; 50(7): 1309–1314, doi: [10.1002/1097-0142\(19821001\)50:7<1309::aid-cnrcr2820500716>3.0.co;2-#](#).
34. Ketcham A, Moffat F. Vexed surgeons, perplexed patients, and breast cancers which may not be cancer. *Cancer*. 1990; 65(3): 387–393, doi: [10.1002/1097-0142\(19900201\)65:3<387::aid-cnrcr2820650302>3.0.co;2-y](#).
35. Chagpar AB, McMasters KM, Sahoo S, et al. Does ductal carcinoma in situ accompanying invasive carcinoma affect prognosis? *Surgery*. 2009; 146(4): 561–7; discussion 567, doi: [10.1016/j.surg.2009.06.039](#), indexed in Pubmed: [19789013](#).
36. Mylonas I, Makovitzky J, Jeschke U, et al. Expression of Her2/neu, steroid receptors (ER and PR), Ki67 and p53 in invasive mammary ductal carcinoma associated with ductal carcinoma In Situ (DCIS) Versus invasive breast cancer alone. *Anticancer Res*. 2005; 25(3A): 1719–1723, indexed in Pubmed: [16033090](#).

Degree of agreement between dacryoscintigraphy and dacryocystography examinations results in primary acquired nasolacrimal duct obstruction

Elyas Aditya¹, Yunia Irawati², Benny Zulkarnaen³, Joedo Prihartono⁴

¹Department of Ophthalmology, Faculty of Medicine Universitas Indonesia, Dr. Cipto Mangunkusumo Hospital, Jakarta, Indonesia

²Division of Plastic and Reconstructive Surgery, Department of Ophthalmology, Faculty of Medicine Universitas Indonesia, Jakarta, Indonesia

³Division of Nuclear Medicine, Department of Radiology, Faculty of Medicine Universitas Indonesia, Dr. Cipto Mangunkusumo Hospital, Jakarta, Indonesia

⁴Department of Community Medicine, Faculty of Medicine Universitas Indonesia, Dr. Cipto Mangunkusumo Hospital, Jakarta, Indonesia

[Received 17 I 2021; Accepted 30 XI 2021]

Abstract

Background: This diagnostic study aimed to assess degree of agreement between dacryoscintigraphy and dacryocystography as supporting examinations in patients with primary acquired nasolacrimal duct obstruction (PANDO). Patients with PANDO who complained of epiphora and visited our outpatient clinic were subsequently sent for dacryoscintigraphy and dacryocystography examinations. Side effects and convenience of both examinations were assessed by observation and questionnaire.

Material and methods: Through irrigation and probing, there were 47 out of 62 eyes were found with PANDO. As much as 87.1% subjects were female, with mostly (74.2%) aged > 40 years old. With dacryoscintigraphy, time needed to reach sac was 0 minutes, 5 minutes (duct), and 12.5 minutes (nasal cavity).

Results: Degree of agreement between both examinations was 83.8% to determine obstruction and 70.9% to locate obstruction. There were 22 subjects complained about pain in dacryocystography examination while none with dacryoscintigraphy ($p < 0.005$). Sixteen subjects feel dacryoscintigraphy examination was more convenient, eleven subjects feel dacryocystography was more convenient, while 4 subjects feel the two examinations were similar.

Conclusions: Even though dacryocystography examination was considered more painful than dacryoscintigraphy, both examinations had high convenience level for patients. Dacryoscintigraphy and dacryocystography also had a good agreement in detecting and locating obstruction in PANDO.

KEY words: nasolacrimal duct obstruction; dacryocystography; dacryoscintigraphy

Nucl Med Rev 2022; 25, 1: 12–17

Correspondence to: Yunia Irawati, Division of Plastic and Reconstructive Surgery, Department of Ophthalmology, Faculty of Medicine Universitas Indonesia, Dr. Cipto Mangunkusumo Hospital, Jalan Kimia No. 8, 10320 Jakarta, Indonesia, phone: +68816789595, e-mail: yunia_irawati@yahoo.com

This article is available in open access under Creative Common Attribution-Non-Commercial-No Derivatives 4.0 International (CC BY-NC-ND 4.0) license, allowing to download articles and share them with others as long as they credit the authors and the publisher, but without permission to change them in any way or use them commercially.

Introduction

Epiphora is an abnormal condition when patients experience watery eyes due to chronic tears overflow. Epiphora induced by nasolacrimal duct obstruction (NLDO) was considered often and accounted for one-third of the total number of epiphora cases [1]. Dacryocystography (DCG) is a form of radiology modality most commonly used to assess the lacrimal drainage system [1]. DCG is a very useful anatomy examination to determine the location of obstruction and stenosis by administering contrast using irrigation cannula through the lacrimal punctum. However, this modality also has some disadvantages. Examination by DCG is invasive because we put instruments into the canaliculus. Moreover, this examination can raise a false positive result in partial obstruction cases [2,3].

Besides DCG, dacryoscintigraphy is another radiology modality used to assess tear drainage systems more physiologically. It uses radioactive (^{99m}Tc) to mark off the tear and record the flow with a gamma camera [1]. Generally, dacryoscintigraphy is used to assess tear flow in patients with lacrimal pump dysfunction [1]. In mechanical obstruction cases, the obstructed parts of the lacrimal drainage system will be visualized by the contrast [4].

Even though dacryoscintigraphy is a good lacrimal drainage system obstruction examination modality, this examination is still rarely used by ophthalmologists [1]. This may be due to a lack of tools or facilities to do dacryoscintigraphy [5]. Therefore, this study aimed to determine the degree of agreement of dacryoscintigraphy and DCG as additional examination in patients with primary acquired nasolacrimal duct obstruction (PANDO). Additionally, we also assessed side effects and patient convenience of both dacryoscintigraphy and DCG examination that have not been published in the previous studies.

Material and methods

Our study was classified as a diagnostic test study. We included patients with PANDO aged ≥ 18 years old with epiphora and negative irrigation test (Anel test). The exclusion criteria were patients with the acute inflammatory process, NLDO caused by tumor/abscess, history of allergy to radioactive contrast, and patients who were in pregnancy or breastfeeding. The participants were selected by the consecutive sampling method. Thirty-one subjects were included in this study. The study protocol was approved by the Ethics Committee of Faculty of Medicine Universitas Indonesia, number KET.142/UN2.F1/ETIK/PPM.00.02/2019.

In the outpatient settings, we conducted an irrigation test on both eyes by injecting saline solution into the lacrimal punctum followed by probe insertion to the canaliculus through the punctum to determine whether there was a hard stop or soft stop. A hard stop was originated from the lower system (nasolacrimal duct) while the latter was originated from the upper system (canaliculus). Subjects with obstruction located in the canaliculus would be excluded.

Dacryoscintigraphy was performed by dripping ^{99m}Tc -Pertechnetate solution into both eyes. Afterward, the picture was taken with a gamma camera at the dynamic phase (first 5 minutes), and then at 10, 15, 20, 25, and 30 minutes. DCG examination was performed by positioning the patient in a supine position. Topical anesthesia was instilled into both eyes. Each punctum was injected with contrast using a blunt needle and a 3 cc syringe. Fluoroscopy was used

to observe contrast flow dynamically. Dacryoscintigraphy and DCG results were analyzed without knowing previous ophthalmology conditions. Side effects and the convenience level of DCG and dacryoscintigraphy examinations were assessed with observation and questionnaires.

We measured both primary and secondary outcomes. The primary outcome was defined as the degree of agreement in deciding the presence and the location of the obstruction, analyzed by concordance rate and Kohens Kappa through SPSS Statistics 20.0. Secondary outcome in this study was the tracer transit time of unobstructed eye in dacryoscintigraphy examination that would be described in minutes when the tracer reaches lacrimal sac, nasolacrimal duct, and nasal cavum.

Results

We recruited 62 eyes from 31 subjects whose characteristics were described in Table 1. Forty-seven out of 62 eyes tested negative in the irrigation test, hence, fulfilled the inclusion criteria as patients with PANDO.

Table 2 showed the degree of agreement between dacryoscintigraphy and DCG in the determination of obstruction in the lacrimal drainage system. There were 45 obstructed eyes (72%) found with a DCG examination whereas a higher percentage (85%) was found in a dacryoscintigraphy examination. Dacryoscintigraphy examination revealed nine eyes without obstruction in the lacrimal drainage system but there was one eye with an obstruction found with irrigation test and DCG examination. The degree of agreement between the two examinations was 83.8%. The concordance rate value was 83.8% showing a strong agreement between the two examinations.

Table 1. Subject characteristics

Subject Characteristics	n	Percentage (%)
Gender		
Male	4	12.9
Female	27	87.1
Age group		
18–40 years	8	25.8
> 40 years	23	74.2
Mean \pm SD age (years)	50.8	15.2
Negative irrigation test		
Unilateral	15	48.4
Bilateral	16	51.6

Table 2. Dacryoscintigraphy and dacryocystography conformity of obstruction presence results (n = 62 eyes)

	Dacryocystography (n)		Total
	Obstruction	No obstruction	
Dacryoscintigraphy			
Obstruction	44	9	53
No obstruction	1	8	9
Total	45	17	62

Mc Nemar $p = 0.021$; degree of agreement = 52/62 (83.8%); p value < 0.005

Table 3. Dacryoscintigraphy and dacryocystography conformity of obstruction height (n = 62 eyes)

	Dacryocystography (n)			Total
	Sac-duct junction	Duct	No obstruction	
Dacryoscintigraphy				
Sac-duct junction	35	7	6	48
Duct	1	1	3	5
No obstruction	1	0	8	9
Total	37	8	17	62

Mc Nemar $p = 0.011$; degree of agreement = 44/62 (70.9%); p value < 0.005

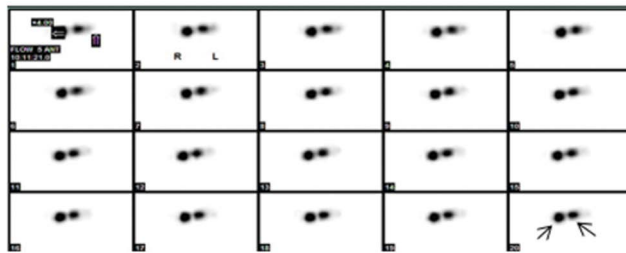
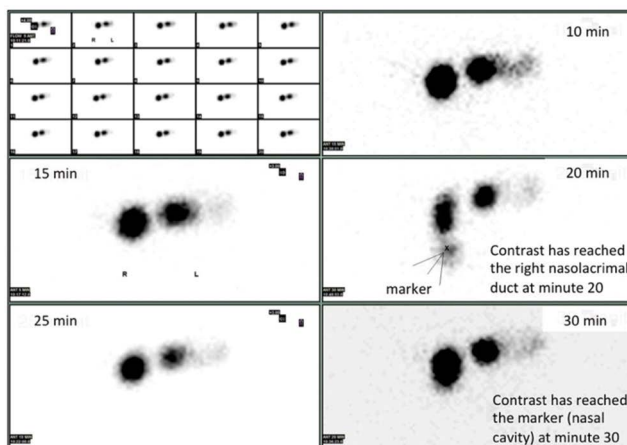
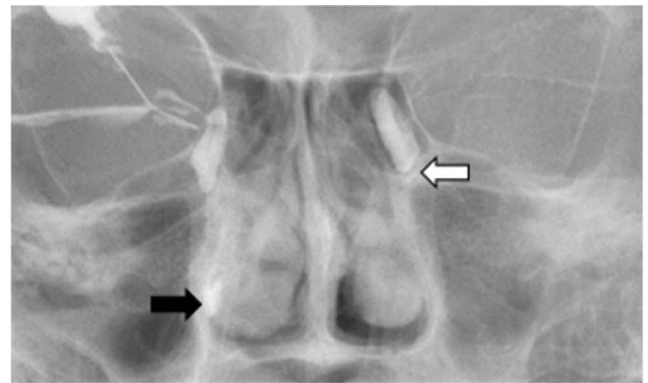
**Figure 1.** The dynamic phase of dacryoscintigraphy (first 5 minutes). The contrast reached both lacrimal sacs (black arrows)**Figure 2.** Dacryoscintigraphy in obstruction at left sac-duct (S/D) junction level at dynamic phase, minute 10–30

Table 3 demonstrated the degree of agreement between dacryoscintigraphy and DCG in determining the location of the obstruction. The degree of agreement between the two examinations was 70.9% (44/62). A percentage of 70% to 79% was considered an agreement. In sac-duct (S/D) junction, dacryoscintigraphy could detect more eyes with obstruction (11 eyes, 17.7%). On the other hand, DCG was able to detect more eyes with obstruction located in the nasolacrimal duct (3 eyes, 4.8%).

Figures 1 and 2 showed dacryoscintigraphy examination results of obstruction in the left S/D junction. Figure 1 depicted the examination at the dynamic phase (first 5 minutes). The contrast reached the lacrimal sac right after the recording started. Figure 2 showed dacryoscintigraphy examination from minute 10 to 30.

**Figure 3.** Dacryocystography examination result of obstruction at the left lacrimal sac-duct (S/D) junction level

At minute 20, contrast reached the right nasolacrimal duct but on the fellow eye, the contrast was still in the lacrimal sac (S/D junction). At minute 30, contrast reached the right nasal cavity but on the right eye, contrast stayed in the left S/D junction suggesting an obstruction. Figure 3 showed the DCG result of obstruction at the left lacrimal sac (S/D junction) level. The black arrow points out contrast flow to the right inferior meatus of the nasal cavity. The white arrow indicates that contrast flow stayed in the left S/D junction suggesting an obstruction in the left lacrimal drainage system at the left S/D junction level. However, obstruction in both systems was shown through dacryoscintigraphy (Fig. 4).

Out of 62 eyes, eight asymptomatic eyes with no lacrimal drainage obstruction were found by irrigation test and dacryoscintigraphy. In these eight eyes, not only positive results were found on irrigation test and dacryoscintigraphy but also no contrast blockage seen on dacryoscintigraphy and contrast reached nasal cavity. Tracer transit time of these 8 eyes was determined as the normal value of eyes without lacrimal drainage system obstruction. Table 4 evaluates the tracer transit time needed to reach the lacrimal sac (0 minutes), nasolacrimal duct (median 5 minutes), and nasal cavity (median 12.5 minutes).

According to the side effect and convenience level checklist in the observation section, there were no side effects found on the dacryoscintigraphy examination. However, there were two subjects who experienced hyperemic conjunctiva immediately after DCG and it quickly disappeared in 15 minutes after the procedure (Tab. 5).

On DCG examination, there was one subject who felt inconvenient when being examined due to pain. There was a significant difference ($p < 0.005$) of painful feeling between dacryoscintigraphy and DCG examination.

We included one additional question about which examination the subject would prefer since all of them underwent both examinations. Sixteen patients felt that dacryoscintigraphy was more comfortable than DCG because the procedure did not use any instrumentation into the punctum. Other 11 patients felt more comfortable with DCG in comparison to dacryoscintigraphy because of the shorter examination time and the other four patients said both examinations were similarly convenient.

In this study, the selected subjects were all adults because irrigation tests would be more difficult to be performed in

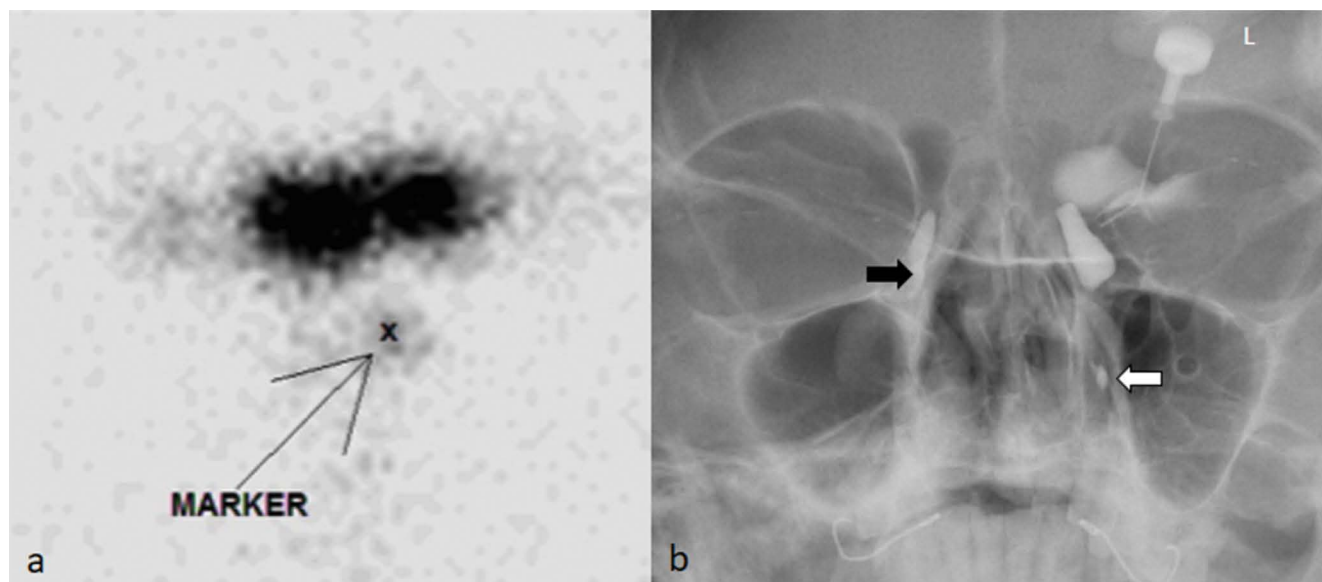


Figure 4. a) Dacryoscintigraphy showed obstruction in both systems; **b)** dacryocystography showed obstruction only in the right lacrimal drainage system (black arrow). The contrast flowed through the inferior meatus of the left lacrimal drainage system (white arrow)

Table 4. Tracer transit time of dacryoscintigraphy examination (n = 8 eyes)

	n	%
Duration to reach sac		
Immediate (0 min)	8	100.0
Duration to reach duct		
Immediate (0 min)	2	25.0
5 min	4	50.0
10 min	1	12.5
20 min	1	12.5
Duration to reach nasal cavum		
Immediate (0 min)	1	12.5
10 min	3	37.5
15 min	3	37.5
30 min	1	12.5

non-sedated pediatric patients. About 74.2% of subjects aged more than 40 years old with a mean value of 50.8 years old. Subjects were mostly female (87.1%). Kashkouli et al. reported that patients with PANDO were mostly female (78.2%) with a mean age value of

61.9 years old [6]. The possible reason is that female nasolacrimal duct anatomy is longer and tighter than male so obstruction is more prone to occur.

The grade of agreement between dacryoscintigraphy and DCG in deciding the presence of obstruction was 83.8%. Both examinations had a strong agreement in determining an obstruction. This result was in accordance with Al-Ghamdi et al. that stated the degree of agreement between dacryoscintigraphy and DCG in epiphora patients with lacrimal drainage system obstruction was 77.9% [7].

Dacryoscintigraphy was carried out in a more physiological process using contrast dripped into the eye. When the eyes blink, eyelids were closed, hence, preseptal orbicularis muscle would be contracted and pulled lacrimal sac to make negative pressure which then pulled the contrast into the lacrimal sac. When the eyes open, orbicularis muscles would be relaxed and elastic force would create positive pressure inside the lacrimal sac and pull contrast down to the nasolacrimal duct [8]. Dacryoscintigraphy has the ability to detect more abnormalities than DCG because dacryoscintigraphy was done with a more physiological process. Through DCG examination in our study, there were 45 (72%) lacrimal drainage system obstructions found while dacryoscintigraphy

Table 5. Percentage of patients who answered yes in the questionnaire section (n = 31 subjects)

Questions	Dacryoscintigraphy	Dacryocystography	p value
Comfortable eye	31 (100%)	31 (100%)	No value
Dry eye	2 (6.5%)	2 (6.5%)	1.000
Gritty sensation	0 (0.0%)	1 (3.2%)	0.313
Burning sensation	8 (25.8%)	6 (19.4)	0.544
Fatigue eye	4 (12.9%)	3 (9.7%)	0.688
Painful eye	0 (0.0%)	22 (71.0%)	< 0.005*
Scratchy sensation	0 (0.0%)	2 (6.5%)	0.492
Blurred vision	0 (0.0%)	0 (0.0%)	No value
Convenient examination	31 (100%)	30 (96.8%)	0.313

found 53 obstructions (85%). This data is in accordance with a study by Wearne et al. [9] that found dacryoscintigraphy could detect more abnormality (95%) compared to DCG (93%) in patients with functional nasolacrimal duct obstruction. A study by Rose et al. [10] performed dacryoscintigraphy and DCG in patients with epiphora. In this study, dacryoscintigraphy detected more obstruction (77%) than DCG (51%). Amanat et al. [11] also reported irrigation tests could detect obstruction as much as 44% while DCG detected 55.7% and dacryoscintigraphy detected 76.6%. This might be due to the DCG examination that created positive pressure into the lacrimal drainage system that could lead to false-positive results in partial obstruction [12]. In addition, dacryoscintigraphy could detect abnormality in patients with lacrimal pump dysfunction or functional epiphora [13]. On DCG examination, patients with lacrimal pump dysfunction and functional epiphora showed a normal result because these conditions were not caused by lacrimal drainage system obstruction.

Our study included one subject with facial nerve paresis abnormality in the unobstructed eye group that caused contrast flow disturbance. Even though we performed a DCG examination, there was no obstruction found. In patients with facial nerve paresis, orbicularis muscles weakness would create lacrimal pump dysfunction [13]. Therefore, tear flow would be obstructed and demonstrate an abnormality on dacryoscintigraphy but no obstruction on irrigation test and DCG (Fig. 4).

The degree of agreement between dacryoscintigraphy and DCG in detecting location or the level of obstruction was 70.9%. The degree of agreement found in this study was higher than the study by Al-Ghamdi et al. [7] and Wearne et al. [9] that found a degree of agreement in detecting obstruction location between dacryoscintigraphy and DCG of 58.3% and 59%. This difference might be affected due to the division of obstruction location. Previous studies divided the location of obstruction into 3 categories (pre sac delay, sac delay, dan duct delay). However, our study divided the location into the sac or sac-duct junction; and duct due to the limited resolution of the imaging modality. Dacryoscintigraphy in our hospital did not have a pinhole collimator to increase resolution. Based on this division, the chance of agreement became greater. Therefore, this study has a higher degree of agreement than previous studies. On S/D junction, dacryoscintigraphy could detect more obstruction than DCG. On the other hand, DCG is superior for the detection in the nasolacrimal duct. These results were in accordance with a study by Wearne et al. [9] that found dacryoscintigraphy detected more proximal locations of obstruction (33%) than DCG. A study by Denffer et al. [14] showed a degree of agreement between DCG and dacryoscintigraphy in detecting the location of obstruction was 85%, and in 15% dacryoscintigraphy, locations of obstruction were found more proximal than in DCG. This may be due to positive pressure that DCG created using contrast into the lacrimal system so that it dilates proximal obstruction and creates it more distal.

In this study, only 8 asymptomatic eyes were assessed normal with irrigation test and dacryoscintigraphy. Table 4 described the contrast transit time needed to reach the lacrimal sac, nasolacrimal sac, nasolacrimal duct, and nasal cavum in minutes. These 8 eyes had contrast transit time to reach the lacrimal sac within

0 minutes (immediate). This result is in accordance to a study by Brizel et al. [15] that found transit time to reach lacrimal sac within 0–120 seconds. This study, however, might have a biased result due to the variety of duration between the start of contrast administration and the start of recording.

In this study, from the 8 lacrimal systems that were assessed normal with irrigation test and dacryoscintigraphy, median values for tracer transit time in nasolacrimal duct were 5 minutes and 12.5 minutes to reach nasal cavum. These results were in accordance with a study by MacDonald et al. [4] that stated that in normal dacryoscintigraphy, there would be contrast visualization through a nasolacrimal duct to nasal cavum in 5 minutes [4]. This result may be various. Consequently, contrast visualization in nasal cavum at minute — 10 to 15 was still considered as a normal variation [4]. There was a great variety of tracer transit time in dacryoscintigraphy in previous studies. Variety was affected by frequency and intensity of blinking, gravitation, tear volume production changes, tear flow variation, lacrimal drainage valve resistance, and other factors, such as emotion, conjunctiva irritation, and contrast volume.

According to the checklist of side effects and convenience level in the observation section, there were no side effects found in dacryoscintigraphy. Meanwhile, in DCG, there were 2 subjects (6.2%) showing conjunctival hyperemia immediately after the procedure. Conjunctival hyperemia might present due to the contrast cleaning process at the end of the DCG procedure using the saline solution on the eyes. This result was similar to a study by Shweel et al. [16] that found only 1 patient (4.7%) experiencing minimal irritation on the eye after DCG.

There was a significant difference between pain during dacryoscintigraphy and DCG ($p < 0.005$). Twenty-two subjects complained of painful sensations during DCG due to instrumentation into the lacrimal punctum. However, 11 subjects felt DCG was more comfortable than dacryoscintigraphy due to shorter examination time while 16 subjects felt both examinations were convenient. This result is similar to a study by Reddy et al. [12] that claimed no uncomfortable complaint found in dacryoscintigraphy examination due to its more invasive procedure.

Conclusions

Dacryoscintigraphy had a good agreement grade with DCG in assessing the presence of obstruction and detecting its location or level in patients with PANDO. There was no side effect found on the dacryoscintigraphy examination. Dacryoscintigraphy and DCG examinations had a similar convenience level although DCG was considered more painful during the examination.

Conflict of interest

The authors declare that they have no conflict of interest.

Acknowledgement

We thank the staff of the Ophthalmology, Radiology and Community Medicine Department, Faculty of Medicine Universitas Indonesia for their support and cooperation in this study.

References

1. Lin LK, Gokoffski KK. Epiphora. In: Cornea 4th ed. Elsevier 2016: 403–409.
2. Nixon J, Birchall IW, Virjee J. The role of dacryocystography in the management of patients with epiphora. *Br J Radiol.* 1990; 63(749): 337–339, doi: [10.1259/0007-1285-63-749-337](https://doi.org/10.1259/0007-1285-63-749-337), indexed in Pubmed: [2379059](https://pubmed.ncbi.nlm.nih.gov/2379059/).
3. Hurwitz JJ. The lacrimal drainage system. In: Ophthalmology. 3rd ed. Elsevier, London 2009: 1482–1487.
4. MacDonald A, Burrell S. Infrequently performed studies in nuclear medicine: Part 1. *J Nucl Med Technol.* 2008; 36(3): 132–43; quiz 145, doi: [10.2967/jnmt.108.051383](https://doi.org/10.2967/jnmt.108.051383), indexed in Pubmed: [18703616](https://pubmed.ncbi.nlm.nih.gov/18703616/).
5. Cuthbertson FM, Webber S. Assessment of functional nasolacrimal duct obstruction--a survey of ophthalmologists in the southwest. *Eye (Lond).* 2004; 18(1): 20–23, doi: [10.1038/sj.eye.6700522](https://doi.org/10.1038/sj.eye.6700522), indexed in Pubmed: [14707959](https://pubmed.ncbi.nlm.nih.gov/14707959/).
6. Kashkouli MB, Sadeghipour A, Kaghazkanani R, et al. Pathogenesis of primary acquired nasolacrimal duct obstruction. *Orbit.* 2010; 29(1): 11–15, doi: [10.3109/01676830903207828](https://doi.org/10.3109/01676830903207828), indexed in Pubmed: [20302403](https://pubmed.ncbi.nlm.nih.gov/20302403/).
7. Al-Ghamdi AH, El-Saban K. Clinical Values of The Lacrimal Scintigraphic Parameters In Diagnosis Of Epiphora: Comparison To Dacryocystography. *Med J Cairo Univ.* 2011; 79(2): 13–22.
8. Foster J, Carter K, Durairaj V, et al. Section 7. Orbits, Eyelids, and Lacrimal System. In: American Academy of Ophthalmology. LEO, Singapore 2015: 284–290.
9. Wearne MJ, Pitts J, Frank J, et al. Comparison of dacryocystography and lacrimal scintigraphy in the diagnosis of functional nasolacrimal duct obstruction. *Br J Ophthalmol.* 1999; 83(9): 1032–1035, doi: [10.1136/bjo.83.9.1032](https://doi.org/10.1136/bjo.83.9.1032), indexed in Pubmed: [10460770](https://pubmed.ncbi.nlm.nih.gov/10460770/).
10. Rose JD, Clayton CB. Scintigraphy and contrast radiography for epiphora. *Br J Radiol.* 1985; 58(696): 1183–1186, doi: [10.1259/0007-1285-58-696-1183](https://doi.org/10.1259/0007-1285-58-696-1183), indexed in Pubmed: [3842629](https://pubmed.ncbi.nlm.nih.gov/3842629/).
11. Amanat LA, Wraight EP, Watson PG, et al. Role of lacrimal scintigraphy and subtraction macrodacryocystography in the management of epiphora. *Br J Ophthalmol.* 1979; 63(7): 511–519, doi: [10.1136/bjo.63.7.511](https://doi.org/10.1136/bjo.63.7.511), indexed in Pubmed: [380636](https://pubmed.ncbi.nlm.nih.gov/380636/).
12. Reddy SC, Zakaria A, Bhavaraju VM. Evaluation of lacrimal drainage system by radionuclide dacryoscintigraphy in patients with epiphora. *Iran J Nucl Med.* 2016; 24(2): 98–105.
13. Chan W, Malhotra R, Kakizaki H, et al. Perspective: what does the term functional mean in the context of epiphora? *Clin Exp Ophthalmol.* 2012; 40(7): 749–754, doi: [10.1111/j.1442-9071.2012.02791.x](https://doi.org/10.1111/j.1442-9071.2012.02791.x), indexed in Pubmed: [22429759](https://pubmed.ncbi.nlm.nih.gov/22429759/).
14. Denffer H, Dressler J, Pabst HW. Lacrimal dacryoscintigraphy. *Seminars in Nuclear Medicine.* 1984; 14(1): 8–15, doi: [10.1016/s0001-2998\(84\)80050-1](https://doi.org/10.1016/s0001-2998(84)80050-1).
15. Brizel HE, Sheils WC, Brown M. The effects of radiotherapy on the nasolacrimal system as evaluated by dacryoscintigraphy. *Radiology.* 1975; 116(02): 373–381, doi: [10.1148/116.2.373](https://doi.org/10.1148/116.2.373), indexed in Pubmed: [807946](https://pubmed.ncbi.nlm.nih.gov/807946/).
16. Shweel M, Elshafei A, AbdelRahman RD, et al. Evaluation of lacrimal drainage system obstruction using combined multidetector CT and instillation dacryocystography. *Egypt J Radiol Nucl Med.* 2012; 43(3): 413–420, doi: [10.1016/j.ejrnm.2012.04.005](https://doi.org/10.1016/j.ejrnm.2012.04.005).

Relationship between cerebral blood flow reduction patterns on scintigraphy and nonmotor symptoms in new-onset Lewy body disease

Yukinori Okada¹, Makoto Shiraishi², Koji Hori³, Keiichiro Yamaguchi⁴, Yasuhiro Hasegawa²

¹Department of Medical Radiology, St. Marianna University School of Medicine, Kawasaki, Japan

²Department of Internal Medicine and Brain Neurology, St. Marianna University School of Medicine, Kawasaki, Japan

³Department of Neuropsychiatry, St. Marianna University School of Medicine, Kawasaki, Japan

⁴Department of Proton Therapy and Tumor Imaging, St. Marianna University School of Medicine, Kawasaki, Japan

[Received 27 VI 2021; Accepted 31 XII 2021]

Abstract

Background: This study aimed to investigate the relationship between patterns of reduced cerebral blood flow (CBF) evaluated by means of ¹²³I-N-isopropyl-p-iodoamphetamine ([¹²³I]IMP) scintigraphy and nonmotor symptoms in new-onset Lewy body disease (Parkinson's disease and dementia with Lewy bodies [DLB]).

Material and methods: Twenty-four patients diagnosed with new-onset Parkinson's disease or DLB underwent [¹²³I]IMP CBF scintigraphy at St. Marianna Medical University Hospital between January 1, 2010, and March 30, 2018. The reductions in CBF in various brain regions were analyzed using the three-dimensional stereotactic surface projection method and were compared to standard database values, yielding extent values (%). The extent values were evaluated in relation to the presence/absence of motor or nonmotor symptoms such as visual hallucinations, auditory hallucinations, delirium, depression, delusions, and dementia.

Results: The extent value was 100% in the angular, supramarginal, and lingual gyri; 95% in the orbital gyri; and 92.6% in the fusiform gyri. The extent value in patients without hallucinations and those with visual hallucinations was 41.2% and 54.3%, respectively, in the frontal lobe ($p = 0.02$) and 33.3% and 51.0%, respectively, in the medial prefrontal gyri ($p = 0.02$). Age-adjusted multivariate analysis showed that extent values in the frontal lobe were associated with visual hallucinations (odds ratio: 1.09, 95% confidence interval 1.00–1.18, $p = 0.04$).

Conclusions: The above results show that the CBF is reduced in several areas of the cerebral cortex and suggest an association between reduced blood flow in the frontal lobe and the appearance of visual hallucinations in patients with new-onset DLB.

KEY words: hallucinations; dementia with Lewy bodies; radionuclide imaging

Nucl Med Rev 2022; 25, 1: 18–24

Introduction

Lewy body disease, an umbrella term encompassing Parkinson's disease (PD) and dementia with Lewy bodies (DLB), is reported to occur in about 1 in 1000 adults [1]. This disease

develops owing to the deposition of alpha-synuclein aggregates, called Lewy bodies, in the brain, resulting in neuronal damage. In PD, Lewy body deposits are limited to the brain stem, whereas in DLB, the deposits extend to the cerebral cortex, subcortex, and peripheral neurons [2,3]. Between 8% and 40% of patients with PD experience visual hallucinations during the course of the disease [4].

¹⁸Fluorine-labeled fluorodeoxyglucose positron emission tomography (¹⁸F]FDG PET) is widely used to diagnose functional cognitive impairment and has been reported to be useful for the diagnosis of visual hallucinations associated with DLB [5]. However,

Correspondence to: Yukinori Okada, Department of Medical Radiology, St. Marianna University School of Medicine, 2-16-1 Sugao, Kawasaki City, Japan, phone: +81 449778111; e-mail: igaueno512@yahoo.co.jp

in Japan, [^{18}F]FDG PET is not routinely used to diagnose Lewy body disease or Alzheimer's disease. Instead, these are commonly diagnosed by means of cerebral blood flow (CBF) scintigraphy [6]. The extent of CBF reduction associated with PD has been shown to differ between Hoehn and Yahr (H&Y) stages [7]. In addition, both patients with Alzheimer's disease and those with DLB exhibit reduced [^{18}F]FDG metabolism in the temporoparietal junction, posterior cingulate gyri, precuneus, and medial occipital lobe [8]. The cingulate island sign is useful for distinguishing DLB from Alzheimer's disease on [^{18}F]FDG PET [6] and has been shown to be an excellent discriminator between Alzheimer's disease and DLB when assessed using $^{99\text{m}}\text{Tc}$ -L-ethyl cysteinate dimer CBF scintigraphy and the easy Z-score imaging system (eZIS; FUJIFILM Toyama Chemical Co., Ltd, Tokyo) analysis software [9].

[^{123}I]IMP scintigraphy is used for CBF evaluation. Three-dimensional stereotactic surface projection (3D-SSP) is commonly used to improve the diagnostic accuracy of PET and single-photon emission computed tomography (SPECT) [10]. In a previous study incorporating 3D-SSP, CBF values obtained from [^{123}I]IMP scintigraphy were compared statistically to those from a normal database and those from a CT-based attenuation correction normal database [11]. The cerebral metabolic changes associated with PD and those associated with Alzheimer's disease can be distinguished by means of 3D-SSP [12]. However, few studies have examined the relationship between nonmotor symptoms and CBF in patients with new-onset Lewy body disease. In addition, reports on CBF reductions related to dementia associated with PD and DLB are scarce. Moreover, there have been few attempts to quantify CBF in patients with PD dementia and in those with DLB.

In this study, we examined the patterns of CBF reduction in patients with new-onset Lewy body disease by using [^{123}I]IMP scintigraphy and compared the findings based on the presence or absence of motor and nonmotor symptoms.

Material and methods

Ethical considerations

This retrospective study was approved by the Ethics Committee of St. Marianna Medical University Hospital, Kawasaki, Japan (approval no. 4019). Patients were given the opportunity to opt out through the hospital website and in the hospital.

Patients

Image interpretation terminals and electronic medical records were searched for patients diagnosed with new-onset PD or new-onset DLB who underwent [^{123}I]IMP CBF scintigraphy at St. Marianna Medical University Hospital between January 1, 2010, and March 30, 2018.

All patients were evaluated by neurologists and psychiatrists. PD was diagnosed on the basis of the UK Parkinson's Disease Society's Brain Bank diagnostic criteria [13], and DLB was diagnosed according to the clinical diagnostic criteria proposed by McKeith et al. [14]. Nonmotor symptoms were diagnosed on the basis of the Unified Parkinson's Disease Rating Scale, Part 1, items 1, 2, and 3 (with a score above 1 indicating the presence of symptoms) [15].

At the time of [^{123}I]IMP CBF scintigraphy, 16 of the 24 patients included in the study were being treated with levodopa

and carbidopa hydrate in combination ($n = 9$), levodopa ($n = 2$), ropinirole hydrochloride ($n = 2$), selegiline ($n = 1$), or donepezil hydrochloride ($n = 2$).

CBF scintigraphy and 3D-SSP imaging

Immediately after injection of 111 MBq [^{123}I]IMP (Nihon Med-Physics Co., Tokyo, Japan), SPECT was performed with a triple detector system (GCA-9300, Canon Medical Systems, Ohtawara, Japan) equipped with a fan-beam collimator. Image reconstruction was performed with a ramp filter and Fourier back projection. The [^{123}I]IMP scintigraphy CBF values were compared to normal CBF values derived from 3D-SSP images. The 3D-SSP database was derived from 34 volunteers (17 men and 17 women, aged 61.7 ± 8.0 years).

We calculated the CBF reductions in various brain regions by comparing CBF values obtained in our patients against normal reference values. The CBF reduction was calculated as follows: number of pixels exceeding the threshold number in a region/number of pixels in that region. The threshold values were considered abnormal when the Z-score ($Z\text{-score} = [\text{normal group mean voxel} - \text{case voxel}] / [\text{normal group standard deviation}]$) was greater than 2, which is quite close to the commonly used threshold value of 1.96 [16]. When differences were observed between the left and right cerebral hemispheres, the larger value was selected for analysis.

Data and statistical analyses

For the purpose of the study, we compared the extent values of each brain region between patients with PD and those with DLB. We also compared the extent values within each brain region in relation to the presence vs absence of nonmotor symptoms, such as visual hallucinations, auditory hallucinations, delirium, depression, delusions, and dementia, and in relation to the presence vs absence of motor symptoms, such as rigidity, tremors, abnormal postural reflex, hypokinesia, mask-like facies, and short-stepped gait.

Median values were calculated, and between-group differences were analyzed by means of a Mann-Whitney U test. Univariate and multivariate analyses were conducted to identify factors associated with visual hallucinations. All analyses were performed with EZR, a statistical analysis software program developed at Jichi Medical University's Saitama Medical Center (Jichi Medical University's Omiya Hospital). P-values < 0.05 were considered statistically significant.

Results

Clinical characteristics of the study patients are summarized in Table 1. The total group comprised 14 men and 10 women, aged 41–86 years (median, 75 years), with new-onset PD ($n = 15$) or new-onset DLB ($n = 9$). Patient distribution according to the H&Y stages was as follows: stage I, $n = 3$; stage II, $n = 6$; stage III, $n = 11$; and stage IV, $n = 4$. Motor symptoms were noted in the following proportions of the study cohort: rigidity, 58.8%; tremors, 50.0%; abnormal postural reflex, 12.5%; hypokinesia, 8.3%; mask-like facies, 54.1%; and short-stepped gait, 45.8%. Nonmotor symptoms were noted in the following proportions of the study cohort: visual hallucination, 25%; auditory hallucinations, 4.1%; delirium, 12.3%; depression, 16.4% 1 patient had a past history and received therapy; delusions, 8.2%; and dementia, 71%.

Table 1. Patient clinical characteristics (n = 24)

Age (median [range]; years)	75 [41–86]
Sex ratio (male/female)	14/10
Parkinson disease/Lewy body dementia	15/9
Hoehn and Yahr stage I/II/III/IV	3/6/11/4
Motor symptoms	
Rigidity (%)	58.8
Tremors (%)	50.0
Abnormal postural reflex (%)	12.5
Hypokinesia (%)	8.3
Mask-like facies (%)	54.1
Short-stepped gait (%)	45.8
Nonmotor symptoms	
Visual hallucinations (%)	25
Auditory hallucinations (%)	4.1
Delirium (%)	12.3
Depression (%) (1 patient had a history of depression)	16.4
Delusions (%)	8.2
Dementia (%)	71

Data are presented as numbers or percentages, unless otherwise indicated

The extent values per lobe and per respective gyri for the total patient group are summarized in Table 2. Of the four cerebral lobes, the occipital lobe showed the greatest CBF reduction (at $89.6 \pm 18.1\%$). Among the cerebral gyri, the angular ($98.9 \pm 4.23\%$), supramarginal ($98.8 \pm 4.00\%$), and lingual gyri ($91.9 \pm 15\%$) showed the greatest extent values, with all three values reflective of a mean decrease in the extent values of 90% or more. The distribution of notable extent values in the occipital lobe in patients with PD and those with DLB is shown in Figure 1. The extent value in the occipital lobe was significantly greater in patients with DLB than in those with PD (99.9% vs 91.5%; $p = 0.01$; Figure 1 — left panel). Additionally, compared to patients with PD, patients with DLB had significantly greater extent values in the posterior cingulate cortex (77.3% vs 32.7%; $p < 0.01$; Figure 1 — middle panel) and precuneus (74.8% vs 59.5%; $p = 0.03$; Figure 1 — right panel).

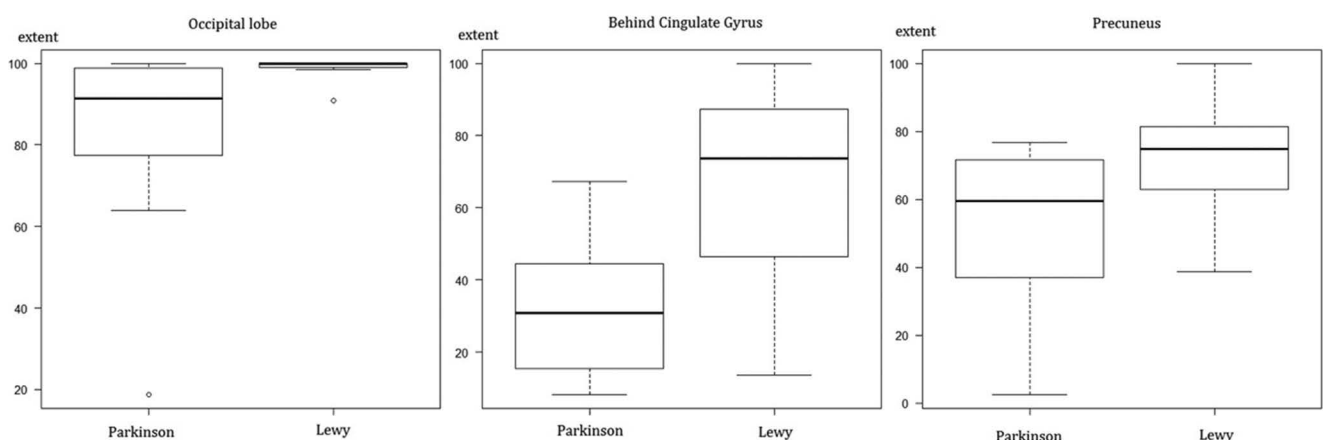
There were no significant differences in the extent values in other brain regions according to the presence or absence of the following nonmotor symptoms: auditory hallucinations, delirium, depression, delusions, and dementia.

The distribution of notable extent values in patients with and without visual hallucinations is shown in Figure 2. The prevalence of visual hallucinations was 0% among patients with PD (0/15) and 66.7% among those with DLB (6/9). In the frontal lobe, the extent value was 41.2% in patients without visual hallucinations and 54.3% in patients with visual hallucinations ($p = 0.02$; Figure 2 — left panel). In the medial frontal gyrus, the extent value was 33.3% in patients without visual hallucinations and 51.0% in patients with visual hallucinations ($p = 0.02$; Figure 2 — right panel). More specifically, in the right medial frontal gyrus, the extent value was 27.2% and 48.4% in patients without and with visual hallucinations, respectively ($p = 0.01$); in the left medial frontal gyrus, the extent value was 28.1% and 51.0% in patients without and with visual hallucinations, respectively ($p = 0.01$). No significant difference in the extent values in any other brain region was found between patients without and with visual hallucinations.

In quantifying the relationship between extent values and visual hallucinations, both univariate and age-adjusted multivariate analyses (stepwise regression) showed reduced CBF in the frontal lobe to be statistically significant (odds ratio [OR]: 1.09, 95% confidence interval [CI] 1.00–1.18; $p = 0.04$; Table 3). Age, sex, H&Y stage, presence of PD vs that of DLB, and use of cholinesterase inhibitors or anti-Parkinson agents were not associated with visual hallucinations. Moreover, both univariate and age-adjusted multivariate analyses (stepwise regression) showed reduced CBF in the right, left, or both frontal lobes specifically and in the medial frontal gyri (right, left, or both specifically), with that in the right frontal lobe being statistically significant (OR: 1.09, 95% CI 1.01–1.18, $p = 0.04$; Table 4).

Discussion

In this study, we examined the patterns of CBF reduction in patients with new-onset Lewy body disease and compared the findings based on the presence or absence of motor and nonmotor

**Figure 1.** Box and whisker plots of the extent values for patients with Parkinson disease and patients with Lewy body disease

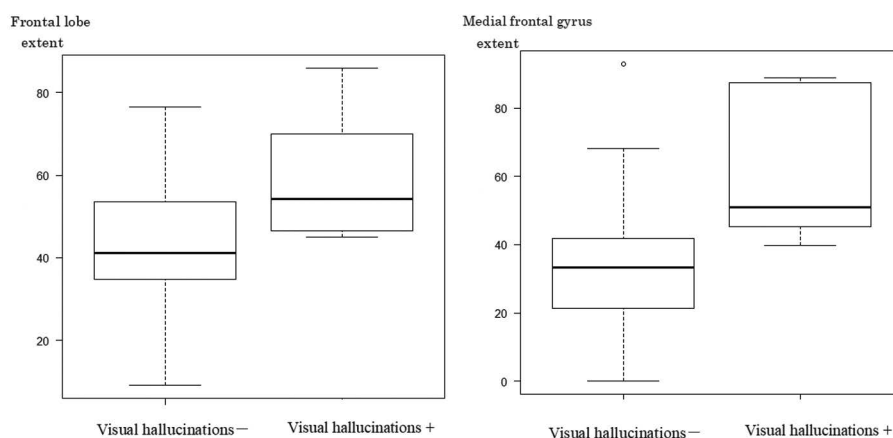


Figure 2. Box and whisker plots of the extent values in the frontal lobe and medial frontal lobe for patients with and without visual hallucinations

Table 2. Extent values per lobe and respective gyri

	Extent Value (%)
Frontal lobe	45.4 ± 18.1
Orbital gyri	71.8 ± 39.1
Gyri recti	51.9 ± 33.3
Parietal lobe	64.3 ± 17.4
Angular gyri	98.9 ± 4.23
Precuneus	58.6 ± 25.6
Supramarginal gyri	98.8 ± 4.00
Temporal lobe	80.2 ± 18.0
Fusiform gyri	84.5 ± 16.0
Occipital lobe	89.6 ± 18.1
Lingual gyri	91.9 ± 15.1
Anterior cingulate gyri	35.2 ± 29.6
Posterior cingulate gyri	47.1 ± 26.8

Data are presented as mean ± standard deviation

symptoms. Our results showed that the CBF is reduced in several areas of the cerebral cortex in these patients. Furthermore, our findings suggest an association between reduced blood flow in the frontal lobe and the appearance of visual hallucinations in patients with new-onset Lewy body disease.

There have been several reports on CBF scintigraphy in patients with PD and those with DLB. Patients with H&Y stages I–II disease were found to exhibit reduced CBF in the gray matter (reduced diffusion), hippocampus, and right temporal lobe inferior horn, whereas those with H&Y stages III–IV disease were found to exhibit reduced CBF in the cerebrum overall and relatively increased CBF in the left and right thalamus, globus pallidus, hippocampus, dentate nucleus, and right insular cortex [7]. DLB has been shown to be characterized by reduced [¹⁸F]FDG metabolism in the temporoparietooccipital lobe [8]. Patients with DLB, compared to patients with Alzheimer's disease, exhibit more prominently reduced CBF in the two occipital lobes and in the left temporal lobe [17]. Patients with DLB exhibit what appears to be decreased CBF in the

Table 3. Results of univariate and multivariate analyses (stepwise regression) for identification of factors associated with visual hallucinations

Factor	Univariate Analysis			Multivariate Analysis		
	OR	95% CI	p value	OR	95% CI	p value
Age	1.32	1.02–1.72	0.03	1.47	0.99–2.19	0.06
Sex	1.57	0.25–10.1	0.63			
H&Y stage (0–II vs III–IV)	0.50	0.08–3.27	0.47			
Use of a cholinesterase inhibitor or anti-Parkinson agent	0.14	0.02–1.09	0.06			
PD or DLB	NA	NA	NA			
Frontal lobe	1.07	0.99–1.15	0.06	1.09	1.00–1.18	0.04
Parietal lobe	1.07	0.99–1.16	0.08			
Temporal lobe	0.97	0.93–1.02	0.27			
Occipital lobe	1.68	0.68–4.13	0.26			

CI — confidence interval; H&Y — Hoehn and Yahr; LBD — Lewy body disease; NA — not available; OR — odds ratio; PD — Parkinson's disease

Table 4. Results of the univariate and multivariate analyses (stepwise regression) for visual hallucinations related to the frontal lobe (right, left, both) and medial frontal gyri (right, left, both)

Factor	Univariate analysis			Multivariate analysis		
	OR	95% CI	p value	OR	95% CI	p value
Age				1.52	0.98–2.32	0.05
Frontal lobe (right)	1.06	1.00–1.13	0.07	1.09	1.01–1.18	0.04
Age				1.41	0.95–2.05	0.08
Frontal lobe (left)	1.11	1.00–1.22	0.05	1.11	0.99–1.26	0.07
Age				1.48	1.01–2.15	0.04
Medial frontal gyri	1.05	1.00–1.09	0.05	1.07	0.99–1.15	0.06

CI — confidence interval; OR — odds ratio

occipital lobe [18] and reduced CBF in the occipital lobe, along with a relative increase in CBF in the deep white matter [19]. However, the actual CBF varies from reduced to normal in the frontal, parietal, temporal, and occipital lobes and in the basal ganglia [20]. In this study, we found reduced CBF in the orbital gyri, an area where reduced CBF has been found to correlate with the severity of Alzheimer's disease [21], which is thought to be related to Yakovlev's circuit involving the amygdala-thalamus-orbital gyri-anterior temporal lobe areas [21, 22]. In addition, there is some supporting evidence that the volume of the medial temporal lobe is better maintained in patients with Lewy body disease than in those with Alzheimer's disease [14]. A statistical parametric mapping analysis found reduced CBF in the supplementary motor area and showed that the CBF in the dorsolateral premotor cortex decreases as the severity of the disease [20]. The differences between these studies are thought to be due to non-uniform areas of functional decline, owing to differing assessment methods and differing disease-progression patterns in the selected cases. Although various tracers have been developed for PD and DLB, tracers that specifically bind to alpha-synuclein protein aggregates could help clarify the pathologies of these conditions and provide data for assessing treatments and prognosis.

A greater distribution of Lewy bodies in the temporal lobes is associated with a higher frequency of visual hallucinations [23]. Pathological examination of the brains of deceased patients with PD or DLB and of those who experienced visual hallucinations has shown the presence of large numbers of Lewy bodies in areas of the temporal lobe, such as the amygdala and parahippocampal gyri [23]. Furthermore, the presence of many Lewy bodies has been noted in the middle frontal, middle temporal gyri, transentorhinal, and anterior cingulate cortices of patients with visual hallucinations [24].

Moreover, visual hallucinations in patients with DLB have been linked to reduced CBF in the left ventral occipital gyrus and bilateral parietal areas [25]. In our study, compared to patients who did not experience visual hallucinations, patients with new-onset Lewy body disease who experienced visual hallucinations exhibited significantly lower CBF in the frontal lobe. In addition, the frontal lobe CBF was significantly lower in the medial prefrontal gyri in patients with visual hallucinations than in those without visual hallucinations, for reasons that are yet unclear. Reduced CBF affected the occipital lobe, temporal lobe, parietal lobe, and frontal lobe, in that order. These findings together with the link between Lewy bodies and

visual hallucinations suggest that the presence of a large number of Lewy bodies in the frontal lobes may indirectly reflect the reduced frontal lobe CBF in patients with visual hallucinations. The appearance of visual hallucinations may be affected by reduced nerve function, not only in the occipital lobe but also in a wide area extending to the medial frontal area. The relationship between the reduced CBF in anterior brain regions and the higher brain dysfunction associated with these anterior regions needs to be clarified and the pathology of nerve fiber routes should be explored.

Z-scores used in this study were based on normal database values. The utility of Z-scores for ²³¹I-IMP SPECT imaging in the differentiation between Alzheimer's disease (AD) and DLB and other dementia and degenerative changes has been reported [26]. Furthermore, in cases of Alzheimer's dementia, Z-scores were shown to correlate inversely with the Mini-Mental State Examination and the Clinical Global Impression-Severity Illness scores [27]. Therefore, we believe our data are clinically meaningful.

Visual hallucinations are present in a substantial proportion of patients with PD, reportedly affecting 15.8% to 74% of patients, including some with recent-onset PD [28–30]. Notably, the frequency of visual hallucinations was reported to be 44.4% in DLB [31]. The occurrence of visual hallucinations among patients with DLB is marked and outweighs that among patients with PD (62.5% vs 20.0%) [32]. In a recent meta-analysis, the pooled prevalence of visual hallucinations was shown to be 28.2% and 61.8% among patients with PD and those with DLB, respectively [33]. Thus, the extreme difference in the prevalence of visual hallucinations between our study patients with PD and those with DLB is not unusual. As visual hallucinations can appear early in patients with PD, the occurrence of visual hallucinations is not relied upon for a differential diagnosis of DLB (vs PD). Nuclear imaging, however, appears to be reliable for distinguishing between the two diseases.

Our study was limited in that it was a single-center study that included a small number of patients. In addition, the disease had reached H&Y stage III or IV in some patients by the time of the scintigraphic examination, despite the study only including patients with new-onset Lewy body disease. Some of the patients were older adults, and the ability of these patients to perform activities of daily living was indeed impaired. Despite the mixed study group, our study showed that reduced CBF is observed in cases of DLB and in patients suffering hallucinations, regardless of the H&Y stage. The manifestations of

Lewy body disease vary depending on the version of the disease. There is the presence of heterogeneity and some subgroup variation in early-stage PD [34]. Multicenter prospective studies with larger numbers of patients are needed to confirm our findings.

Conclusions

In conclusion, the results of our study showed that the CBF is reduced in several areas of the cerebral cortex and suggest an association between reduced blood flow in the frontal lobe and the appearance of visual hallucinations in patients with new-onset Lewy body disease.

Conflict of interest

Yukinori Okada received the lecture fee from AstraZeneca and Beyer not applicable the COI value in Japan, and the authors of this work have nothing to disclose for this study.

Acknowledgments

The authors thank Dr. Tsutomu Kamo of the Noborito Neurology Clinic and Prof. Tina Tajima of the St. Marianna University School of Medicine for their valuable advice regarding the study design.

References

- Dias JA, Felgueiras MM, Sanchez JP, et al. The prevalence of Parkinson's disease in Portugal. A population approach. *Eur J Epidemiol.* 1994; 10(6): 763–767, doi: [10.1007/BF01719295](https://doi.org/10.1007/BF01719295), indexed in Pubmed: [7672060](https://pubmed.ncbi.nlm.nih.gov/7672060/).
- Cheng HC, Ulane CM, Burke RE. Clinical progression in Parkinson disease and the neurobiology of axons. *Ann Neurol.* 2010; 67(6): 715–725, doi: [10.1002/ana.21995](https://doi.org/10.1002/ana.21995), indexed in Pubmed: [20517933](https://pubmed.ncbi.nlm.nih.gov/20517933/).
- Obeso JA, Stamelou M, Goetz CG, et al. Past, present, and future of Parkinson's disease: A special essay on the 200th Anniversary of the Shaking Palsy. *Mov Disord.* 2017; 32(9): 1264–1310, doi: [10.1002/mds.27115](https://doi.org/10.1002/mds.27115), indexed in Pubmed: [28887905](https://pubmed.ncbi.nlm.nih.gov/28887905/).
- Barnes J, David AS. Visual hallucinations in Parkinson's disease: a review and phenomenological survey. *J Neurol Neurosurg Psychiatry.* 2001; 70(6): 727–733, doi: [10.1136/jnnp.70.6.727](https://doi.org/10.1136/jnnp.70.6.727), indexed in Pubmed: [11385004](https://pubmed.ncbi.nlm.nih.gov/11385004/).
- Iaccarino L, Sala A, Caminiti SP, et al. The brain metabolic signature of visual hallucinations in dementia with Lewy bodies. *Cortex.* 2018; 108: 13–24, doi: [10.1016/j.cortex.2018.06.014](https://doi.org/10.1016/j.cortex.2018.06.014), indexed in Pubmed: [30098477](https://pubmed.ncbi.nlm.nih.gov/30098477/).
- Imabayashi E, Soma T, Sone D, et al. Validation of the cingulate island sign with optimized ratios for discriminating dementia with Lewy bodies from Alzheimer's disease using brain perfusion SPECT. *Ann Nucl Med.* 2017; 31(7): 536–543, doi: [10.1007/s12149-017-1181-4](https://doi.org/10.1007/s12149-017-1181-4), indexed in Pubmed: [28547521](https://pubmed.ncbi.nlm.nih.gov/28547521/).
- Imon Y, Matsuda H, Ogawa M, et al. SPECT image analysis using statistical parametric mapping in patients with Parkinson's disease. *J Nucl Med.* 1999; 40(10): 1583–1589, indexed in Pubmed: [10520695](https://pubmed.ncbi.nlm.nih.gov/10520695/).
- Imamura T, Ishii K, Sasaki M, et al. Regional cerebral glucose metabolism in dementia with Lewy bodies and Alzheimer's disease: a comparative study using positron emission tomography. *Neurosci Lett.* 1997; 235(1-2): 49–52, doi: [10.1016/s0304-3940\(97\)00713-1](https://doi.org/10.1016/s0304-3940(97)00713-1), indexed in Pubmed: [9389593](https://pubmed.ncbi.nlm.nih.gov/9389593/).
- Imabayashi E, Yokoyama K, Tsukamoto T, et al. The cingulate island sign within early Alzheimer's disease-specific hypoperfusion volumes of interest is useful for differentiating Alzheimer's disease from dementia with Lewy bodies. *EJNMMI Res.* 2016; 6(1): 67, doi: [10.1186/s13550-016-0224-5](https://doi.org/10.1186/s13550-016-0224-5), indexed in Pubmed: [27620458](https://pubmed.ncbi.nlm.nih.gov/27620458/).
- Minoshima S, Frey KA, Koeppe RA, et al. A diagnostic approach in Alzheimer's disease using three-dimensional stereotactic surface projections of fluorine-18-FDG PET. *J Nucl Med.* 1995; 36(7): 1238–1248, indexed in Pubmed: [7790950](https://pubmed.ncbi.nlm.nih.gov/7790950/).
- Yamazaki T, Inui Y, Ichihara T, et al. Clinical utility of the normal database of I-iodoamphetamine brain perfusion single photon emission computed tomography for statistical analysis using computed tomography-based attenuation correction: a multicenter study. *Ann Nucl Med.* 2019; 33(11): 835–841, doi: [10.1007/s12149-019-01395-0](https://doi.org/10.1007/s12149-019-01395-0), indexed in Pubmed: [31414335](https://pubmed.ncbi.nlm.nih.gov/31414335/).
- Vander Borght T, Minoshima S, Giordani B, et al. Cerebral metabolic differences in Parkinson's and Alzheimer's diseases matched for dementia severity. *J Nucl Med.* 1997; 38(5): 797–802, indexed in Pubmed: [9170449](https://pubmed.ncbi.nlm.nih.gov/9170449/).
- Gibb WR, Lees AJ. The relevance of the Lewy body to the pathogenesis of idiopathic Parkinson's disease. *J Neurol Neurosurg Psychiatry.* 1988; 51(6): 745–752, doi: [10.1136/jnnp.51.6.745](https://doi.org/10.1136/jnnp.51.6.745), indexed in Pubmed: [2841426](https://pubmed.ncbi.nlm.nih.gov/2841426/).
- McKeith IG, Dickson DW, Lowe J, et al. Consortium on DLB. Diagnosis and management of dementia with Lewy bodies: third report of the DLB Consortium. *Neurology.* 2005; 65(12): 1863–1872, doi: [10.1212/01.wnl.0000187889.17253.b1](https://doi.org/10.1212/01.wnl.0000187889.17253.b1), indexed in Pubmed: [16237129](https://pubmed.ncbi.nlm.nih.gov/16237129/).
- Fahn S, Elton RL. Members of the UPDRS Development Committee. Unified Parkinson's Disease Rating Scale. In: Fahn S, Marsden CD, Goldstein M, Calne DB, ed. *Recent Developments in Parkinson's Disease, Vol 2.* Macmillan Healthcare Information, Florham Park, NJ 1987: 153–163.
- Fällmar D, Lijja J, Danfors T, et al. Z-score maps from low-dose F-FDG PET of the brain in neurodegenerative dementia. *Am J Nucl Med Mol Imaging.* 2018; 8(4): 239–246, indexed in Pubmed: [30245916](https://pubmed.ncbi.nlm.nih.gov/30245916/).
- Pasquier J, Michel B, Brenot-Rossi I, et al. Value of 99mTc-ECD SPET for the diagnosis of dementia with Lewy bodies. *Eur J Nucl Med Mol Imaging.* 2002; 29(10): 1342–1348, doi: [10.1007/s00259-002-0919-x](https://doi.org/10.1007/s00259-002-0919-x), indexed in Pubmed: [12271417](https://pubmed.ncbi.nlm.nih.gov/12271417/).
- Ishii K, Yamaji S, Kitagaki H, et al. Regional cerebral blood flow difference between dementia with Lewy bodies and AD. *Neurology.* 1999; 53(2): 413–416, doi: [10.1212/wnl.53.2.413](https://doi.org/10.1212/wnl.53.2.413), indexed in Pubmed: [10430439](https://pubmed.ncbi.nlm.nih.gov/10430439/).
- Shimizu S, Hanyu H, Hirao K, et al. Deep gray matter hyperperfusion with occipital hypoperfusion in dementia with Lewy bodies. *Eur J Neurol.* 2007; 14(11): 1299–1301, doi: [10.1111/j.1468-1331.2007.01951.x](https://doi.org/10.1111/j.1468-1331.2007.01951.x), indexed in Pubmed: [17877736](https://pubmed.ncbi.nlm.nih.gov/17877736/).
- Kikuchi A, Takeda A, Kimpara T, et al. Hypoperfusion in the supplementary motor area, dorsolateral prefrontal cortex and insular cortex in Parkinson's disease. *J Neurol Sci.* 2001; 193(1): 29–36, doi: [10.1016/s0022-510x\(01\)00641-4](https://doi.org/10.1016/s0022-510x(01)00641-4), indexed in Pubmed: [11718747](https://pubmed.ncbi.nlm.nih.gov/11718747/).
- Kawasaki Y, Ohtaki J, Toba K, et al. Relationship of Alzheimer disease severity and 99mTc-ECD SPECT brain blood-flow imaging (in Japanese). *J Kyorin Med Soc.* 2007; 38: 21–28.
- Livingston KE, Escobar A. Anatomical bias of the limbic system concept. A proposed reorientation. *Arch Neurol.* 1971; 24(1): 17–21, doi: [10.1001/archneur.1971.00480310045003](https://doi.org/10.1001/archneur.1971.00480310045003), indexed in Pubmed: [5538598](https://pubmed.ncbi.nlm.nih.gov/5538598/).
- Harding AJ, Broe GA, Halliday GM. Visual hallucinations in Lewy body disease relate to Lewy bodies in the temporal lobe. *Brain.* 2002; 125(Pt 2): 391–403, doi: [10.1093/brain/awf033](https://doi.org/10.1093/brain/awf033), indexed in Pubmed: [11844739](https://pubmed.ncbi.nlm.nih.gov/11844739/).
- Gallagher DA, Parkkinen L, O'Sullivan SS, et al. Testing an aetiological model of visual hallucinations in Parkinson's disease. *Brain.* 2011; 134(Pt 11): 3299–3309, doi: [10.1093/brain/awr225](https://doi.org/10.1093/brain/awr225), indexed in Pubmed: [21921019](https://pubmed.ncbi.nlm.nih.gov/21921019/).
- Nagahama Y, Okina T, Suzuki N, et al. Neural correlates of psychotic symptoms in dementia with Lewy bodies. *Brain.* 2010; 133(Pt 2): 557–567, doi: [10.1093/brain/awp295](https://doi.org/10.1093/brain/awp295), indexed in Pubmed: [19920063](https://pubmed.ncbi.nlm.nih.gov/19920063/).
- Ishii K, Ito K, Nakanishi A, et al. Computer-assisted system for diagnosing degenerative dementia using cerebral blood flow SPECT and 3D-SSP: a multicenter study. *Jpn J Radiol.* 2014; 32(7): 383–390, doi: [10.1007/s11604-014-0329-6](https://doi.org/10.1007/s11604-014-0329-6), indexed in Pubmed: [24838777](https://pubmed.ncbi.nlm.nih.gov/24838777/).
- Kirino E. Three-dimensional stereotactic surface projection in the statistical analysis of single photon emission computed tomography data

- for distinguishing between Alzheimer's disease and depression. *World J Psychiatry*. 2017; 7(2): 121–127, doi: [10.5498/wjp.v7.i2.121](https://doi.org/10.5498/wjp.v7.i2.121), indexed in Pubmed: [28713690](https://pubmed.ncbi.nlm.nih.gov/28713690/).
28. Aarsland D, Larsen JP, Cummins JL, et al. Prevalence and clinical correlates of psychotic symptoms in Parkinson disease: a community-based study. *Arch Neurol*. 1999; 56(5): 595–601, doi: [10.1001/archneur.56.5.595](https://doi.org/10.1001/archneur.56.5.595), indexed in Pubmed: [10328255](https://pubmed.ncbi.nlm.nih.gov/10328255/).
 29. Coelho M, Marti MJ, Tolosa E, et al. Late-stage Parkinson's disease: the Barcelona and Lisbon cohort. *J Neurol*. 2010; 257(9): 1524–1532, doi: [10.1007/s00415-010-5566-8](https://doi.org/10.1007/s00415-010-5566-8), indexed in Pubmed: [20411272](https://pubmed.ncbi.nlm.nih.gov/20411272/).
 30. Hely MA, Reid WGJ, Adena MA, et al. The Sydney multicenter study of Parkinson's disease: the inevitability of dementia at 20 years. *Mov Disord*. 2008; 23(6): 837–844, doi: [10.1002/mds.21956](https://doi.org/10.1002/mds.21956), indexed in Pubmed: [18307261](https://pubmed.ncbi.nlm.nih.gov/18307261/).
 31. Matar E, Ehgoetz Martens KA, Halliday GM, et al. Clinical features of Lewy body dementia: insights into diagnosis and pathophysiology. *J Neurol*. 2020; 267(2): 380–389, doi: [10.1007/s00415-019-09583-8](https://doi.org/10.1007/s00415-019-09583-8), indexed in Pubmed: [31650254](https://pubmed.ncbi.nlm.nih.gov/31650254/).
 32. Savica R, Grossardt BR, Bower JH, et al. Incidence of dementia with Lewy bodies and Parkinson disease dementia. *JAMA Neurol*. 2013; 70(11): 1396–1402, doi: [10.1001/jamaneurol.2013.3579](https://doi.org/10.1001/jamaneurol.2013.3579), indexed in Pubmed: [24042491](https://pubmed.ncbi.nlm.nih.gov/24042491/).
 33. Eversfield CL, Orton LD. Auditory and visual hallucination prevalence in Parkinson's disease and dementia with Lewy bodies: a systematic review and meta-analysis. *Psychol Med*. 2019; 49(14): 2342–2353, doi: [10.1017/S0033291718003161](https://doi.org/10.1017/S0033291718003161), indexed in Pubmed: [30474581](https://pubmed.ncbi.nlm.nih.gov/30474581/).
 34. Szeto JY, O'Callaghan C, Shine JM, et al. The relationships between mild cognitive impairment and phenotype in Parkinson's disease. *NPJ Parkinsons Dis*. 2015; 1: 15015, doi: [10.1038/npjparkd.2015.15](https://doi.org/10.1038/npjparkd.2015.15), indexed in Pubmed: [28725684](https://pubmed.ncbi.nlm.nih.gov/28725684/).

Detection of a second primary cancer in a ¹⁸F-fluorocholine PET/CT – multicentre retrospective analysis on a group of 1345 prostate cancer patients

Paulina Cegla¹, Katarzyna Scibisz-Dziedzic², Kamila Witkowska³, Anna Kubiak⁴, Ewa Wierzchoslawska^{5, 6}, Witold Kycler^{7, 8}, Beata Chrapko², Rafal Czepczynski^{3, 9}

¹Department of Nuclear Medicine, Greater Poland Cancer Center, Poznan, Poland

²Chair and Department of Nuclear Medicine, Medical University of Lublin, Lublin, Poland

³Department of Nuclear Medicine, Affidea Poznan, Poland

⁴Greater Poland Cancer Registry, Greater Poland Cancer Centre, Poznan, Poland

⁵Department of Electroradiology, Poznan University of Medical Sciences, Poznan, Poland

⁶Radiology Department, Greater Poland Cancer Centre, Poznan, Poland

⁷Gastrointestinal Surgical Oncology Department, Greater Poland Cancer Centre, Poznan, Poland

⁸Department of Head and Neck Surgery, Poznan University of Medical Sciences, Poznan, Poland

⁹Department of Endocrinology, Metabolism and Internal Medicine, Poznan University of Medical Sciences, Poznan, Poland

[Received 8 VIII 2021; Accepted 31 XII 2021]

Abstract

Background: Aim of this study was to evaluate the rate of incidental detection of second primary cancer (SPC) at ¹⁸F-fluorocholine ([¹⁸F]FCH) positron emission tomography/computed tomography (PET/CT) performed in prostate cancer patients.

Material and methods: A retrospective analysis was performed on a group of 1345 prostate cancer patients, who underwent [¹⁸F]FCH PET/CT study because of suspicion of recurrence (n = 937) or for initial staging (n = 408). Images were acquired after intravenous injection [¹⁸F]FCH with a mean activity of 200 ± 75 MBq (5.4 ± 2 mCi), from the top of the head to the half of the thigh. The confirmation of second primary cancer was obtained from the cancer registry.

Results: Based on the [¹⁸F]FCH PET/CT scans, a second primary cancer was suspected in 89 patients (6.6%). Of these, a malignancy was histologically confirmed in 26 patients (29% of all suspected findings and 1.9% of the complete cohort). Lung cancer (including adenocarcinoma, neuroendocrine cancer) was diagnosed in 13 patients (50%) and hematologic neoplasm (including chronic lymphocytic leukemia, Hodgkin lymphoma, follicular lymphoma, and multiple myeloma) in 5 patients (19%). ¹⁸F-fluorocholine PET/CT also revealed esophageal cancer, mesothelioma, testicular, renal, bladder, and colorectal cancer in individual patients, non-keratinizing squamous cell carcinoma (SCC) of the skin as well as head and neck SCC with unknown primary.

Conclusion: We conclude that incidental detection of a second primary cancer in prostate cancer patients using [¹⁸F]FCH PET/CT is not very common and that lung cancer and hematologic malignancies are most frequently detected.

KEY words: positron emission tomography/computed tomography; prostate cancer; second primary cancer

Nucl Med Rev 2022; 25, 1: 25–30

Correspondence to: Paulina Cegla, Department of Nuclear Medicine, Greater Poland Cancer Center, Garbary 15, 61-866 Poznan, Poland, phone: +48 618850789, fax: +48 618850785, e-mail: paulina.cegla@gmail.com

Introduction

Prostate cancer (PCa) ranks 2nd in incidence and 5th in mortality in men worldwide, accounting for 1.3 million newly diagnosed cases and 359.00 deaths per annum [1]. The term 'second primary cancer' (SPC) is used to describe a malignancy that appears unrelated to treated or untreated primary malignancy and that might occur months or years after primary diagnosis. In general, SPC is seen in ca. 15% of cancer patients, leading to increased morbidity and mortality. When suspicion of an SPC is raised, the metastasis of the first primary malignancy should be excluded at first [2, 3].

Standard positron emission tomography/computed tomography (PET/CT) examination with ¹⁸F-Fluorodeoxyglucose (¹⁸F) FDG has a limited value in the diagnosis of prostate cancer and, for this reason, some other radiopharmaceuticals, including tracers based on the metabolism of choline are used, e.g. ¹¹C-choline or ¹⁸F-fluorocholine [4–6]. Radiolabelled choline accumulation in prostate cancer can be observed because of its integration into membranes of the proliferating tumor cells [7]. PET/CT with the radiolabeled choline plays an important role in the initial staging, evaluation of recurrence, and dissemination of prostate cancer [8–11]. The detection of SPC is clinically relevant since comorbidities, including concomitant malignancies, may pose a clinical problem in men with prostate cancer.

The aim of this study was to evaluate the rate of incidental detection of a second primary cancer at [¹⁸F]FCH PET/CT in patients with prostate cancer.

Material and methods

The retrospective, multicenter analysis was performed in 1345 prostate cancer patients, who underwent standard [¹⁸F]FCH PET/CT examination in three nuclear medicine departments between May 2009 and October 2019 because of the suspicion of recurrence (n = 937) or for the initial staging (n = 408). The images were acquired from skull vertex to mid-thigh 45–60 min after IV injection of 200 ± 75 MBq (5.4 ± 2 mCi) of [¹⁸F]FCH. All patients fasted for 6 h before examination and they gave their written informed consent. The images were acquired with different scanners depending on the study site: Gemini TF 16 (Philips), Discovery ST or Discovery IQ (GE Healthcare), Biograph mCT S(64)-4R (Siemens). All PET/CT images were fused and viewed using a dedicated workstation in sagittal, coronal, and transverse planes.

The inclusion criteria for SPC included unspecific [¹⁸F]FCH uptake, not related to patients' previous clinical history. From the selected group of suspected SPC, [¹⁸F]FCH PET images, as well as reports, were re-reviewed for the independent nuclear medicine specialists, and the confirmation of SPC was obtained from the histopathological examination of the suspected lesions. The final SPC diagnosis was retrieved from the local and national cancer registries and was defined using the Warren and Gates' criteria [12].

Results

Based on the [¹⁸F]FCH PET/CT scans, an SPC was suspected in 89 patients (6.6%) from the whole analyzed group. Of these, a malignancy was confirmed in 26 patients (29.2% of all suspected findings and 1.9% of the complete cohort). Most of the patients were

referred to [¹⁸F]FCH PET/CT examination for suspicion of recurrence (n = 21 patients) and only 5 of them for initial staging. The characteristics of patients with confirmed SPC are shown in Table 1.

The most common SPC was lung cancer (including adenocarcinoma, neuroendocrine cancer), which was diagnosed in 13 patients (50%), and hematologic malignancy (including chronic lymphocytic leukemia, Hodgkin lymphoma, follicular lymphoma, and multiple myeloma diagnosed in 5 patients (19.2%) (Fig. 1). ¹⁸F-fluorocholine PET/CT also revealed a low-differentiated adenocarcinoma of the esophagus, mesothelioma, a testicular seminoma (Fig. 2), renal cancer, a bladder and colorectal cancer in individual patients. Furthermore, a non-keratinizing squamous cell carcinoma (SCC) of the skin was diagnosed in one patient. In another patient, [¹⁸F]FCH PET/CT showed increased uptake in cervical lymph nodes that were histologically verified as SCC metastases and the primary malignancy remained undetected (cancer of unknown primary syndrome). All patients with confirmed SPC underwent treatment first for SPC (because in most cases it was more aggressive) and only in a patient with chronic lymphocytic leukemia, first, the progression of PCa was treated.

Discussion

Second primary cancers are relatively rare, reported in a wide range of 0.4–17% of PET/CT scans [13–20]. The detection of SPC has been more frequently reported for PET/CT scans using [¹⁸F] FDG than using [¹⁸F]FCH. A quite high number of SPC is found in patients with head and neck cancer, lymphoma, and gynecological malignancies [13–20]. The risk of development of any SPC increases with time from initial cancer diagnosis [21]. Detection of SPC in prostate cancer patients using a tracer other than [¹⁸F]FDG is very rare, with a frequency of 1.54–13%, with the specificity of 47–90% and sensitivity of 84–100% [22, 23], however, several authors found an SPC in [¹⁸F]FCH PET/CT study (Tab. 2) with SUV_{max} value for SPC ranged from 2.7–15.

To our knowledge, this is the largest cohort of [¹⁸F]FCH PET/CT scans reviewed retrospectively for the detection of SPC. A confirmed synchronous malignancy was detected in 1.9% of patients, but potentially malignant findings were much more frequent, accounting for as much as 6.6% of all scans, suggesting a relatively low specificity of this imaging modality.

Other authors reported an incidental uptake of [¹⁸F]FCH in the head and neck of patients with prostate cancer. An incidental uptake of [¹⁸F]FCH in the head and neck region was found in 8 patients examined for prostate cancer staging or restaging [27]. However, only in two cases, malignancy was proven histologically, in other cases the increased uptake was associated with a benign finding. In our study, one patient showed enlarged cervical lymph nodes with elevated uptake of [¹⁸F]FCH (SUV_{max} 1.8) and after further work-up, the SCC with unknown primary malignancy was diagnosed. Calabria et al. reported [¹⁸F]FCH-positive findings unrelated to PCa in 48 out of 300 patients (16%), but only a few of them were finally confirmed as malignant diseases (colorectal cancer, multiple myeloma, and bladder cancer) [28].

Pieterman et al. compared ¹¹C-choline and [¹⁸F]FDG in the diagnosis of primary lung cancer and reported no significant differences between these two tracers, however, [¹⁸F]FDG was more accurate in the detection of nodal involvement than ¹¹C-choline [29].

Table 1. Characteristics of patients with a second primary cancer detected in ¹⁸F-fluorocholine

N ^o	Age	Indication to [¹⁸ F]FCH PET/CT	PSA (ng/mL)	Second primary cancer	SUV _{max} of the second primary cancer
1	56	PCa recurrence	0.426	Lung adenocarcinoma	2.3
2	75	PCa recurrence	4.23	Lung adenocarcinoma	8.2
3	61	PCa recurrence	6.37	Lung adenocarcinoma	2.5
4	63	PCa recurrence	0.54	Neuroendocrine lung cancer	2.4
5	80	PCa staging	n/a	Lung adenocarcinoma	4.6
6	65	PCa staging	10.4	Chronic lymphocytic leukemia	3.8
7	56	PCa recurrence	0.01	Hodgkin lymphoma	4.7
8	75	PCa recurrence	2.6	Testicular seminoma	5.3
9	72	PCa recurrence	0.003	Colorectal cancer	5.7
10	63	PCa recurrence	3.76	Solid lung cancer	2.6
11	65	PCa recurrence	47.58	Adenocarcinoma of the esophagus	7.7
12	78	PCa recurrence	30.0	Multiple myeloma	3.4
13	71	PCa recurrence	11.68	Clear cell renal cancer	4.9
14	71	PCa staging	20.0	Follicular lymphoma	4.5
15	75	PCa recurrence	0.06	Lung adenocarcinoma	5.1
16	63	PCa staging	7.29	Lung adenocarcinoma	4.8
17	75	PCa recurrence	n/a	Lung adenocarcinoma	1.2
18	59	PCa staging	3.65	Lung adenocarcinoma	3.2
19	74	PCa recurrence	0.3	Mesothelioma	5.4
20	79	PCa recurrence	5.74	Bladder cancer	11.0
21	67	PCa recurrence	10.78	Lung adenocarcinoma	2.2
22	69	PCa recurrence	0.08	Non-keratinizing cutaneous SCC	4.1
23	65	PCa recurrence	9.47	Chronic lymphocytic leukemia	3.3
24	75	PCa recurrence	0.57	Lung adenocarcinoma	6.0
25	86	PCa recurrence	2.53	Lung adenocarcinoma	1.8
26	73	PCa recurrence	1.06	SCC with unknown primary malignancy	1.8

n/a — not available; PCa — prostate cancer; SCC — squamous cell carcinoma; SUV_{max} — maximum standardized uptake value

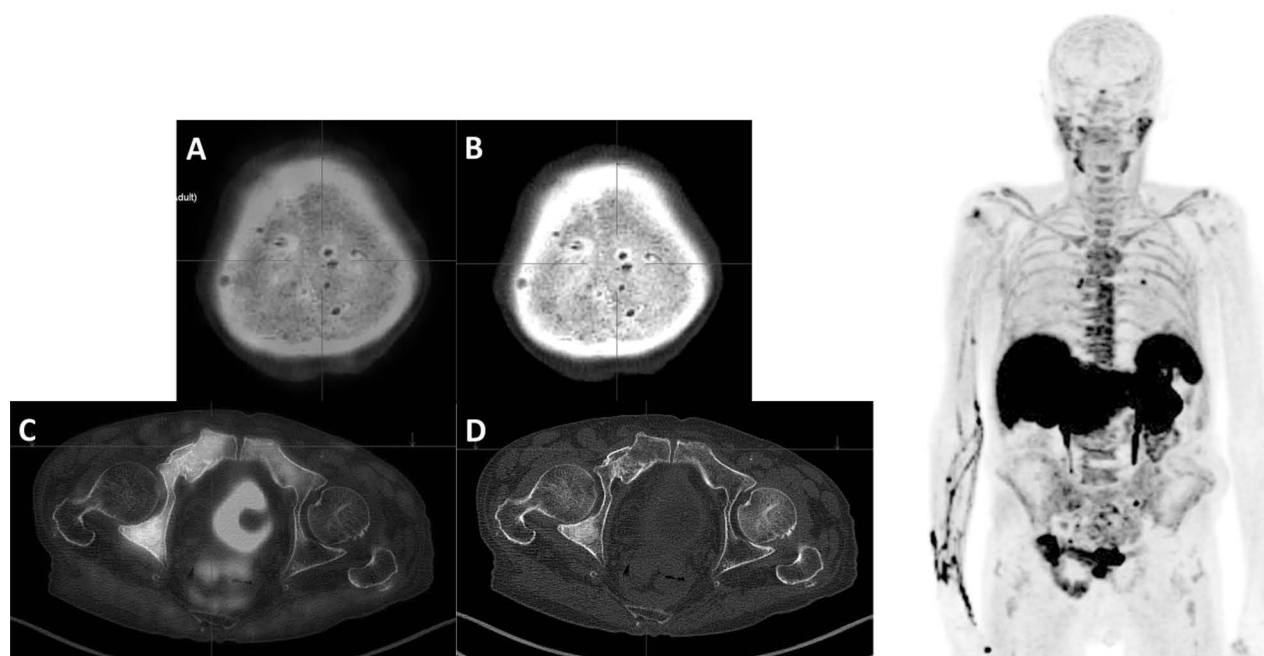


Figure 1. 78-year-old man with PCa, PSA 30.0 [ng/ml] and synchronous multiple myeloma. **A** — PET/CT fusion without increased [¹⁸F]FCH uptake in the skull but with osteolytic lesions in CT. **B** — CT showing osteolytic lesions of the multiple myeloma in the skull. **C** — PET/CT fusion image with extensive prostate metastases in the right iliac bone. **D** — CT with bone remodeling as a result of metastatic changes

Table 2. Second primary cancers detected at ^{18}F -fluorocholine positron emission tomography/computed tomography (PET/CT) in patients with biochemical prostate cancer recurrence — overview of the literature

Author	PCa treatment (s)	Age	PSA (ng/mL)	Second primary cancer histology	Second primary cancer treatment
Sollini M. et al. [24]	RP (2004) + ADT	72	0.11	NSCLC — Adenocarcinoma	CHT + palliative EBRT
	RP (1998) + salvage EBRT (2009)	71	0.08	NSCLC — n/a	CHT
	EBRT (1996)	80	2.62	NSCLC — n/a	patient refused any treatment
	RP (2003)	80	8.77	Melanoma — Melanoma metastases	excision of melanoma metastases
	EBRT (2003) + ADT	71	3.16	NSCLC — n/a	lung lobectomy + salvage EBRT
	RP (2012)	74	1.4	NSCLC — n/a	lung lobectomy + salvage EBRT
	RP (2012) + ADT	80	0.3	Colorectal cancer — n/a	anterior resection of rectum + ADT
Buroni F. et al. [25]	BRT	71	2.86	DLBCL	CHT
Tuscano et al. [26]	n/a	66	5.2	posterior wall of sigmoid colon — mucinous adenocarcinoma	surgical resection

RP — radical prostatectomy; BRT — brachytherapy; ADT — androgen deprivation therapy; EBRT — external beam radiation therapy; DLBCL — Diffuse Large B Cell Lymphoma; CHT — chemotherapy; NSCLC — non-small-cell lung cancer; n/a — not available

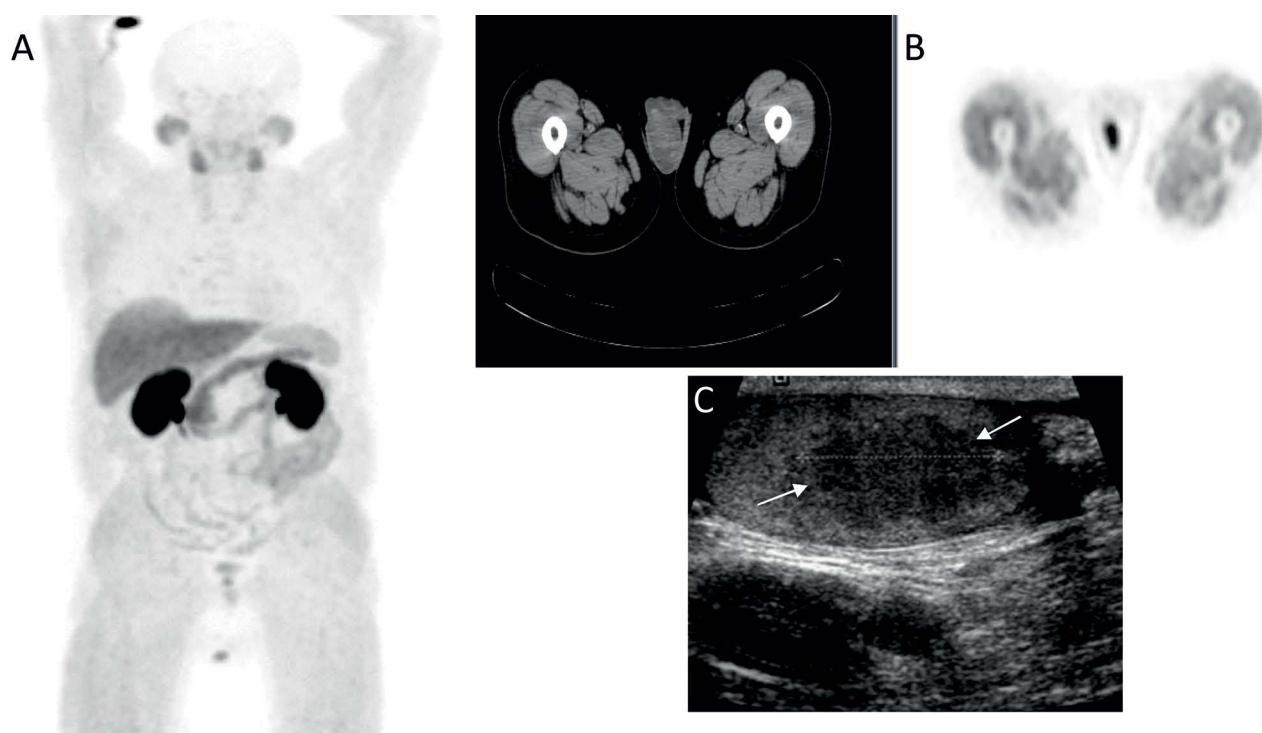


Figure 2. 75-year-old man with PCa, T-PSA 2.6 [ng/mL] and synchronous testicular seminoma. **A** — MIP image without typical metastatic changes of PCa. **B** — increased ^{18}F FCH uptake in the right testicle. **C** — hypoechoic mass with increased vascularity in the ultrasound, typical for seminoma

It is well-known that ^{18}F FCH PET/CT shows optimal diagnostic accuracy when used in patients with relatively high concentrations of prostate-specific antigen (PSA), at least above 1.0 ng/mL [30]. As shown in Table 1, there were several patients who were reported to PET/CT despite PSA levels below that cut-off value. The retrospective analysis of these cases showed that clinical deterioration rather than PSA concentration was a major indication to PET/CT. The clinical symptoms, like loss of weight or dyspnea, had driven the diagnostic process to the exclusion of PCa progression before initiating further symptom-oriented diagnosis. In general, patients with low PSA concentrations would benefit more from ^{68}Ga Ga-PSMA PET/CT — a radiopharmaceutical known for its higher sensitivity in the detection of PCa relapse in the presence of lower

cancer burden [30], however, due to better local availability ^{18}F FCH PET/CT was applied instead. Although, as expected, the scan was negative with respect to the PCa in all cases with PSA < 1.0 ng/mL, the patients benefited from the earlier detection of the second primary malignancies, so that an adequate treatment could be initiated immediately.

Our retrospective study has several drawbacks. The study group was not homogenous from the technical point of view, since images were obtained using four different PET/CT scanners in three centers over a long period of 10 years. Although all the scanners were equipped with 16-slice CT and the imaging parameters were similar, the impact of differences in qualitative parameters on the diagnostic accuracy cannot be excluded. On the

other hand, it would not be possible to collect such a large study cohort on the basis of experience gathered in one center only or a shorter interval. Our analysis was limited to the histopathologically confirmed malignancies, reported to the cancer registers. Positively verified lesions accounted for 29% of all suspected lesions, but we have to keep in mind that this number might be underestimated. It cannot be excluded that some cases were lost to analysis if the findings reported in [¹⁸F]FCH PET/CT were not subjected to further verification due to the patient's refusal or poor clinical condition that led to disqualification from invasive diagnostic procedures. Conversely, we did not analyze benign findings (false-positive results), so that adequate statistical analysis of the diagnostic accuracy of this method could not be performed and this will be considered in our next paper.

Conclusions

The study showed that incidental detection of a second primary cancer in prostate cancer patients using [¹⁸F]FCH PET/CT is not very common and that lung cancer and hematologic malignancies belong to the most frequent cancers detected. Therefore, each unusual radiotracer uptake that is unlikely to be related to prostate cancer should be verified with other methods, including histopathology.

Conflict of interest

The authors declare no conflict of interest.

References

- Bray F, Ferlay J, Soerjomataram I, et al. Global cancer statistics 2018: GLOBOCAN estimates of incidence and mortality worldwide for 36 cancers in 185 countries. *CA Cancer J Clin.* 2018; 68(6): 394–424, doi: [10.3322/caac.21492](https://doi.org/10.3322/caac.21492), indexed in Pubmed: [30207593](https://pubmed.ncbi.nlm.nih.gov/30207593/).
- Feller L, Lemmer J. New 'second primary' cancers. *SADJ.* 2012; 67(4): 175–178, indexed in Pubmed: [23198353](https://pubmed.ncbi.nlm.nih.gov/23198353/).
- Nielsen SF, Nordestgaard BG, Bojesen SE. Associations between first and second primary cancers: a population-based study. *CMAJ.* 2012; 184(1): E57–E69, doi: [10.1503/cmaj.110167](https://doi.org/10.1503/cmaj.110167), indexed in Pubmed: [22125331](https://pubmed.ncbi.nlm.nih.gov/22125331/).
- Vali R, Loidl W, Pirich C, et al. Imaging of prostate cancer with PET/CT using (18)F-Fluorocholine. *Am J Nucl Med Mol Imaging.* 2015; 5(2): 96–108, indexed in Pubmed: [25973332](https://pubmed.ncbi.nlm.nih.gov/25973332/).
- Kwee SA, DeGrado TR, Talbot JN, et al. Cancer imaging with fluorine-18-labeled choline derivatives. *Semin Nucl Med.* 2007; 37(6): 420–428, doi: [10.1053/j.semnuclmed.2007.07.003](https://doi.org/10.1053/j.semnuclmed.2007.07.003), indexed in Pubmed: [17920349](https://pubmed.ncbi.nlm.nih.gov/17920349/).
- Beheshti M, Haroon A, Bomanji JB, et al. Fluorocholine PET/computed tomography: physiologic uptake, benign findings, and pitfalls. *PET Clin.* 2014; 9(3): 299–306, doi: [10.1016/j.cpet.2014.03.001](https://doi.org/10.1016/j.cpet.2014.03.001), indexed in Pubmed: [25030393](https://pubmed.ncbi.nlm.nih.gov/25030393/).
- Yoshimoto M, Waki A, Yonekura Y, et al. Characterization of acetate metabolism in tumor cells in relation to cell proliferation: acetate metabolism in tumor cells. *Nucl Med Biol.* 2001; 28(2): 117–122, doi: [10.1016/s0969-8051\(00\)00195-5](https://doi.org/10.1016/s0969-8051(00)00195-5), indexed in Pubmed: [11295421](https://pubmed.ncbi.nlm.nih.gov/11295421/).
- Evangelista L, Cimitan M, Zattoni F, et al. Comparison between conventional imaging (abdominal-pelvic computed tomography and bone scan) and [(18)F]choline positron emission tomography/computed tomography imaging for the initial staging of patients with intermediate- to high-risk prostate cancer: A retrospective analysis. *Scand J Urol.* 2015; 49(5): 345–353, doi: [10.3109/21681805.2015.1005665](https://doi.org/10.3109/21681805.2015.1005665), indexed in Pubmed: [25649494](https://pubmed.ncbi.nlm.nih.gov/25649494/).
- Fanti S, Minozzi S, Castellucci P, et al. PET/CT with (11)C-choline for evaluation of prostate cancer patients with biochemical recurrence: meta-analysis and critical review of available data. *Eur J Nucl Med Mol Imaging.* 2016; 43(1): 55–69, doi: [10.1007/s00259-015-3202-7](https://doi.org/10.1007/s00259-015-3202-7), indexed in Pubmed: [26450693](https://pubmed.ncbi.nlm.nih.gov/26450693/).
- Picchio M, Messa C, Landoni C, et al. Value of [11C]choline-positron emission tomography for re-staging prostate cancer: a comparison with [18F]fluorodeoxyglucose-positron emission tomography. *J Urol.* 2003; 169(4): 1337–1340, doi: [10.1097/01.ju.0000056901.95996.43](https://doi.org/10.1097/01.ju.0000056901.95996.43), indexed in Pubmed: [12629355](https://pubmed.ncbi.nlm.nih.gov/12629355/).
- Gauvin S, Rompré-Brodeur A, Chaussé G, et al. F-fluorocholine positron emission tomography-computed tomography (F-FCH PET/CT) for staging of high-risk prostate cancer patients. *Can Urol Assoc J.* 2019; 13(4): 84–91, doi: [10.5489/cuaj.5142](https://doi.org/10.5489/cuaj.5142), indexed in Pubmed: [30273114](https://pubmed.ncbi.nlm.nih.gov/30273114/).
- Warren S, Gates O. Multiple primary malignant tumors: A survey of the literature and statistical study. *Am J Cancer.* 1932; 16: 1358–1414.
- Chun-Sing W, Nan-Jie G, Yiu-Ching C. Prevalence of synchronous second primary malignancy: identification using whole body PET/CT imaging. *Clin Imaging.* 2014; 38(2): 179–186, doi: [10.1016/j.clinimag.2013.09.001](https://doi.org/10.1016/j.clinimag.2013.09.001), indexed in Pubmed: [24210360](https://pubmed.ncbi.nlm.nih.gov/24210360/).
- Garcheva M, Zlatareva D, Gocheva L. Positron emission tomography combined with computed tomography for diagnosis of synchronous tumors. *Klin Onkol.* 2014; 27(4): 283–286, doi: [10.14735/amko2014283](https://doi.org/10.14735/amko2014283), indexed in Pubmed: [25115718](https://pubmed.ncbi.nlm.nih.gov/25115718/).
- Moletta L, Bissoli S, Fantin A, et al. PET/CT incidental detection of second tumor in patients investigated for pancreatic neoplasms. *BMC Cancer.* 2018; 18(1): 531, doi: [10.1186/s12885-018-4469-4](https://doi.org/10.1186/s12885-018-4469-4), indexed in Pubmed: [29728085](https://pubmed.ncbi.nlm.nih.gov/29728085/).
- Pang L, Liu G, Shi H, et al. Nineteen cases with synchronous multiple primary cancers studied by 18 F-FDG PET/CT. *Hell J Nucl Med.* 2017; 20(1): 36–40, doi: [10.1967/s002449910504](https://doi.org/10.1967/s002449910504), indexed in Pubmed: [28315906](https://pubmed.ncbi.nlm.nih.gov/28315906/).
- Gunes BY, Akbayir O, Demirci E, et al. Clinical, pathological and (18)F-FDG PET/CT findings in synchronous primary vaginal and endometrial cancers. *Hell J Nucl Med.* 2016; 19(2): 170–172, doi: [10.1967/s002449910374](https://doi.org/10.1967/s002449910374), indexed in Pubmed: [27331214](https://pubmed.ncbi.nlm.nih.gov/27331214/).
- Plachta M, Cholewiński W, Burchardt E, et al. Strategy and early results of treatment of advanced cervical cancer patients with synchronous cancers observed in PET-CT imaging. *Ginekol Pol.* 2017; 88(9): 475–480, doi: [10.5603/GPa.2017.0087](https://doi.org/10.5603/GPa.2017.0087), indexed in Pubmed: [29057432](https://pubmed.ncbi.nlm.nih.gov/29057432/).
- Strobel K, Haerle SK, Stoeckli SJ, et al. Head and neck squamous cell carcinoma (HNSCC)--detection of synchronous primaries with (18) F-FDG-PET/CT. *Eur J Nucl Med Mol Imaging.* 2009; 36(6): 919–927, doi: [10.1007/s00259-009-1064-6](https://doi.org/10.1007/s00259-009-1064-6), indexed in Pubmed: [19205699](https://pubmed.ncbi.nlm.nih.gov/19205699/).
- Miyazaki T, Sohda M, Higuchi T, et al. Effectiveness of FDG-PET in screening of synchronous cancer of other organs in patients with esophageal cancer. *Anticancer Res.* 2014; 34(1): 283–287, indexed in Pubmed: [24403475](https://pubmed.ncbi.nlm.nih.gov/24403475/).
- Amer MH. Multiple neoplasms, single primaries, and patient survival. *Cancer Manag Res.* 2014; 6: 119–134, doi: [10.2147/CMAR.S57378](https://doi.org/10.2147/CMAR.S57378), indexed in Pubmed: [24623992](https://pubmed.ncbi.nlm.nih.gov/24623992/).
- How Kit N, Dugué AE, Sevin E, et al. Pairwise comparison of 18F-FDG and 18F-FCH PET/CT in prostate cancer patients with rising PSA and known or suspected second malignancy. *Nucl Med Commun.* 2016; 37(4): 348–355, doi: [10.1097/MNM.0000000000000457](https://doi.org/10.1097/MNM.0000000000000457), indexed in Pubmed: [26642435](https://pubmed.ncbi.nlm.nih.gov/26642435/).
- García JR, Ponce A, Canales M, et al. [Detection of second tumors in 11C-choline PET/CT studies performed due to biochemical recurrence of prostate cancer]. *Rev Esp Med Nucl Imagen Mol.* 2014; 33(1): 28–31, doi: [10.1016/j.rem.2013.01.007](https://doi.org/10.1016/j.rem.2013.01.007), indexed in Pubmed: [23499124](https://pubmed.ncbi.nlm.nih.gov/23499124/).
- Sollini M, Pasqualetti F, Perri M, et al. Detection of a second malignancy in prostate cancer patients by using [(18)F]Choline PET/CT: a case series. *Cancer Imaging.* 2016; 16(1): 27, doi: [10.1186/s40644-016-0085-1](https://doi.org/10.1186/s40644-016-0085-1), indexed in Pubmed: [27581366](https://pubmed.ncbi.nlm.nih.gov/27581366/).

25. Buroni FE, Persico MG, Lodola L, et al. Malignant Lymphoma Imaged by 18F-Fluoro-Choline PET-CT in a Patient with Prostate Cancer: a Case Report and Review of Literature. *STJ Cancer*. 2017; 1(1002).
26. Tuscano C, Russi EG, Al Sayyad S, et al. An Incidental Finding of Mucinous Colon Cancer by (18)F-Choline PET/CT Determining a Change in Clinical Management of a Patient with Recurrent Prostate Adenocarcinoma. *Case Rep Oncol Med*. 2014; 2014: 297031, doi: [10.1155/2014/297031](https://doi.org/10.1155/2014/297031), indexed in Pubmed: [25197590](https://pubmed.ncbi.nlm.nih.gov/25197590/).
27. Hodolic M, Huchet V, Balogova S, et al. Incidental uptake of (18)F-fluoro-choline (FCH) in the head or in the neck of patients with prostate cancer. *Radiol Oncol*. 2014; 48(3): 228–234, doi: [10.2478/raon-2013-0075](https://doi.org/10.2478/raon-2013-0075), indexed in Pubmed: [25177236](https://pubmed.ncbi.nlm.nih.gov/25177236/).
28. Calabria F, Chiaravalloti A, Ciccio C, et al. PET/CT with 18 F-choline: Physiological whole bio-distribution in male and female subjects and diagnostic pitfalls on 1000 prostate cancer patients: 18 F-choline PET/CT bio-distribution and pitfalls. A southern Italian experience. *Nucl Med Biol*. 2017; 51: 40–54, doi: [10.1016/j.nucmedbio.2017.04.004](https://doi.org/10.1016/j.nucmedbio.2017.04.004), indexed in Pubmed: [28575697](https://pubmed.ncbi.nlm.nih.gov/28575697/).
29. Pieterman RM, Que TH, Elsinga PH, et al. Comparison of (11)C-choline and (18)F-FDG PET in primary diagnosis and staging of patients with thoracic cancer. *J Nucl Med*. 2002; 43(2): 167–172, indexed in Pubmed: [11850480](https://pubmed.ncbi.nlm.nih.gov/11850480/).
30. Giovacchini G, Giovannini E, Leoncini R, et al. PET and PET/CT with radiolabeled choline in prostate cancer: a critical reappraisal of 20 years of clinical studies. *Eur J Nucl Med Mol Imaging*. 2017; 44(10): 1751–1776, doi: [10.1007/s00259-017-3700-x](https://doi.org/10.1007/s00259-017-3700-x), indexed in Pubmed: [28409220](https://pubmed.ncbi.nlm.nih.gov/28409220/).

The efficacy of melatonin against radiotoxicity of iodine-131 and its response to treatment in hyperthyroid patients: a randomized controlled trial

Soudabe Alidadi^{1,4}, Ali Shabestani Monfared², Mehrangiz Amiri³, Ebrahim Zabih⁴, Ehsan Assadollahi⁴, Amir Gholami³, Zoleika Moazezi⁵, Zeinab Abedian⁴

¹Student Research Committee, Babol University of Medical Sciences, Babol, I.R. Iran

²Cancer Research Center, Health Research Institute, Babol University of Medical Sciences, Babol, I.R. Iran

³Department of Radiology and Radiotherapy, School of Medicine, Babol University of Medical Sciences, Babol, I.R. Iran

⁴Cellular and Molecular Biology Research Center, Health Research Institute, Babol University of Medical Sciences, Babol, I.R. Iran

⁵Department of Endocrinology, Rohani Hospital, Babol University of Medical Sciences, Babol, Iran

[Received 13 VIII 2021; Accepted 30 XI 2021]

Abstract

Background: Since melatonin is a non-toxic compound with proven radioprotective effects, we aimed to investigate its efficacy in an in-vivo setting in hyperthyroid patients who are treated with iodine-131. This double-blind placebo-controlled study was conducted on hyperthyroid patients referred to nuclear medicine centers in Babol, Iran. We excluded patients suffering from hypertension treated with warfarin, autoimmune diseases, genetic diseases, cancers, smokers, chemical wounded, radiology and radiotherapy workers, and those who were treated with chemotherapy agents. Patients were randomly assigned to receive a capsule containing 300 mg of melatonin powder or a placebo. Just before receiving iodine-131, blood samples were taken from individuals. All 52 female patients received 10 to 20 mCi iodine-131 for treating hyperthyroidism. A second blood sample was taken one hour after the administration of iodine-131.

Material and methods: To determine the chromosomal damages before and after receiving radioiodine, we performed the cytokinesis-block micronucleus assay. Also, at phase 2, 6 months follow-up was performed, in which patients' positive responses to treatment were compared.

Results: The findings of this study indicate that the difference in micronucleus formation between the placebo and melatonin groups is not significant. However, a significant difference in the 6 months follow-up revealed that 61.5% and 85.7% of patients had a positive response to treatment in the placebo and melatonin groups, respectively.

Conclusions: As one of the first studies dealing with the human in-vivo assessment on the radioprotective effects of melatonin, it was concluded that melatonin has a non-significant positive impact on reducing the rate of chromosomal damages in hyperthyroid patients treated with iodine-131. Nevertheless, the outcome of treatment was significantly higher by melatonin compared to the placebo group.

KEY words: hyperthyroidism; melatonin; radiation

Nucl Med Rev 2022; 25, 1: 31–36

Correspondence to: Ali Shabestani Monfared, Cancer Research Center, Babol University of Medical Sciences, Ganjafrooz St., Babol, Iran
 e-mail: monfared1345@gmail.com

Introduction

Iodine-131 therapy is widely used to treat hyperthyroidism, which has turned into the treatment of choice for reversible hyperthyroidism [1]. However, a recent increase has been reported in the overall incidence of cancer among patients with hyperthyroidism that had been treated with radioactive iodine [2]. Chromosomal damages in peripheral lymphocytes have also been reported in patients with Graves' disease treated with iodine-131 [3]. Ionizing radiations interact with biological systems and cause the formation of free radicals or production of reactive oxygen species (ROS), which attack different cellular components, including DNA, membrane proteins, and lipids, leading to severe cell damages [4]. The antioxidant defense system could control the influx of ROS, which involves enzymatic and non-enzymatic components. The antioxidant system consists of antioxidant molecules with low molecular weight, such as glutathione, melatonin, vitamin E, folic acid, and different antioxidant enzymes [5].

Since the cell damage caused by radiation has been primarily attributed to the harmful effects of free radicals, molecules with free radicals scavenging properties will be especially useful as a radiation protector [6, 7]. Various radio-protectors have been made to increase the therapeutic index of ionizing radiation that selectively reduces the cytotoxic effects of normal tissues [8] However, most of them cause serious side effects, and some are toxic at doses required for radiation protector [9].

It has been shown that melatonin can be an immune-stimulant [10, 11] and an antioxidant [7, 12, 13]. Melatonin acts in a synergistic mechanism as a direct scavenger of free radicals (14) and an indirect antioxidant through stimulating activities on the performance of antioxidant enzymes and by inhibitory activity on the function of pro-oxidant enzymes [6]. Also, due to its compact size and high lipophilic feature, melatonin easily passes through the membrane and reaches all cellular biological components [15]. The results of numerous studies suggest that acute and chronic toxicity due to melatonin is minimal [6, 7].

Chromosomal abnormalities can be assessed merely by examining the number of micronuclei [by Micronuclei (MN) method] in dividing cells that have been stopped in the cytokinesis phase, which is a numeric or structural index for chromosomal changes [16, 17]. Peripheral blood lymphocytes are circulating throughout the body, including the thyroid, which will experience in vivo chromosomal damages [18, 19]. Therefore, examining the micronuclei in the peripheral blood lymphocytes can be used as a real "biological dosimeter" for exposure to radiation of patients who receive radiation therapy [20].

Although many in-vitro studies have shown that human blood lymphocytes treatment with melatonin can reduce the number of micronuclei induced by gamma radiation [6, 7], the effectiveness of this treatment as in-vivo is still being investigated.

Given the increasing use of radioactive iodine to treat hyperthyroidism, investigation to find a suitable radiation protector to reduce radiation-induced chromosomal damages in the body would be useful. Since melatonin is a non-toxic substance and has been proven to have radioprotective effects, this study aimed to assess the radioprotective effect of melatonin against chromosomal damage caused by iodine therapy in peripheral blood lymphocytes using MN assay also a 6 months follow up was performed which patients' response were compared.

Material and methods

Design

This double-blind placebo-controlled parallel study was conducted on 60 women with equal randomization. We have used simple random allocation to distribute patients in groups to minimize selection bias, and the sequence generation or allocation concealment steps and the implementation step were done by different persons. Consent has been obtained from each patient after a full explanation of the purpose and nature of all procedures used. The mean age of participants was 46.01 ± 14.66 and diagnosed with hyperthyroidism who have been referred to 2 nuclear medicine centers (Beheshti and Alborz) in Babol, Iran, to be treated with iodine-131. The MN assay of samples was done in The Cellular and Molecular Biology Research Center, Babol University of Medical Sciences, Babol, Iran. The MN data of 8 participants were missed because their sample was destroyed and did not yield analysis. Finally, we had 52 patients, 24 in the placebo and 28 patients in the study groups for MN analysis. However, in 6 months follow up, the data of 54 patients have obtained which 26 of them were in placebo and 28 in the melatonin group. Individuals with hypertension and those treated with warfarin, those who have autoimmune diseases, genetic diseases and cancer, smokers, chemical wounded, radiology and radiotherapy workers, and those treated chemotherapy agents were excluded from the study. Before starting the study, informed consent was obtained from all participants, which was set according to the guidelines by the National Committee for Ethics in biomedical research. This study has been registered in the Iranian Registry of Clinical Trials (IRCT); registry No: IRCT2014090419045N1, and we did not any important changes to methods after trial commencement. The investigation was approved by the Babol University of Medical Sciences ethical committee.

All patients using methimazole to control hyperthyroidism discontinued their medication seven days before radioiodine therapy. The initiation time for intervention in all patients was considered from 8 to 9 am.

Melatonin powder was prepared from Pure Bulk Company (USA) and was placed in a capsule under sterile conditions. A total of 30 capsules containing 300 mg of melatonin and 30 placebo capsules containing starch were prepared, and the capsules were blindly coded by an expert pharmacologist. One hour before the administration of iodine-131, a capsule containing 300 mg of melatonin or placebo was administered orally to patients on a random basis. One hour later, immediately before administration of iodine-131, an initial blood sample as the T (1) was taken from patients, and the second blood sample as T (2) was taken one hour after receiving iodine-131. In this period, all patients were clinically monitored, and side effects known for melatonin such as a headache, dizziness, nausea, and lethargy were recorded, if occurred.

Outcomes

From each sample, 500 microliters of whole blood were added to 4.5 mL of the culture medium RPMI 1640 (Gibco, USA), which contained 10% fetal bovine serum, 0.1 mL/5 mL phytohemagglutinin (Gibco, USA), antibiotics (penicillin 100 IU/mL, streptomycin 100 μ g/mL) and 2 mM glutamine (Sigma, USA). The cultures were placed in the incubator under 37 ± 1 °C and 5% CO₂ conditions. Cytochalasin B (Sigma, USA) at a concentration of 6 μ g/mL

was added to the medium after 44 hours. After 72 hours of incubation, the cells were isolated by centrifuging and re-suspended in the cold potassium chloride at a concentration of 0.075 M for 8 minutes at 1500 g. Then, they were washed three times with the fixator solution (containing methanol and acetic acid at a ratio of 1:5). The fixed cells were then spread on perfectly clean slides, dried for 24 hours at room temperature, and then stained by Giemsa (10%). The slides were examined with a magnification of 1 000 times to count the number of micronuclei in binucleated cells fixed in cytokinesis that their cytoplasm had been preserved entirely. To be considered as a micronucleus, those with cell diameters of 1/16 to 1/3 of the main cell nucleus, not connected to the main nucleus or had no overlapping, were counted. For each patient, 1000 binucleated cells were counted in each of the samples T (1) and T (2), and the number of micronuclei was recorded.

Blood samples from 8 patients who participated in the study were destroyed in the process of cell culture or staining. Finally, the counting was done on blood samples from 52 patients.

Data analysis was performed by paired sample t-test comparing mean MN before and after iodine therapy within groups. Independent samples t-test was done for comparing the quantity of MN between two study and placebo groups, respectively. The p values lower than 5% were considered as significant for this study, and the results were presented at a 95% confidence interval.

The sample sizes of 23 in each group achieve 91.25% power to reject the null hypothesis of equal means when the population means the difference is $\mu_1 - \mu_2 = 9.0 - 10.0 = -1.0$ with a standard deviation for both groups of 1.0 and with an alpha of 0.05 using a two-sided two-sample equal-variance t-test. After the dropout rate of 20%, the inflated sample size was determined as 29 patients.

As the second outcome, the patients were followed up by an endocrinologist 6 months after treatment, and the response to treatment was assessed among them. Patients with euthyroidism or hypothyroidism state were considered as a positive response to treatment, and those with hyperthyroidism were considered as treatment failure.

Results

From 60 included patients, the MN data of 8 participants were missed because their sample was destroyed and did not yield analysis. Finally, we had 24 in the placebo and 28 patients in melatonin groups for MN analysis, but our 6 months follow-up, the data of 26 patients of the placebo, and 28 patients in the melatonin group were analyzed. Patients who received placebo capsules before radioiodine therapy called the "Placebo" group and patients who received melatonin called the "Melatonin" group. The average age in the groups was 46.82 ± 12.40 and 44.62 ± 15.7 , respectively. The average iodine-131 dosage received by the placebo group patients was 12.70 ± 3.59 mCi, while the dosage for the melatonin group accounted for 13.17 ± 3.31 mCi. There was no significant difference between the 2 groups at the significance level of 95% ($p = 0.807$). The average numbers of micronucleus before treatment with iodine-131 for placebo and melatonin groups were as 5.87 ± 3.59 and 5.50 ± 2.86 , respectively ($p = 0.677$). The average numbers of micronuclei after treatment for placebo and melatonin groups were also as 10.13 ± 4.85 and 9.96 ± 5.34 ,

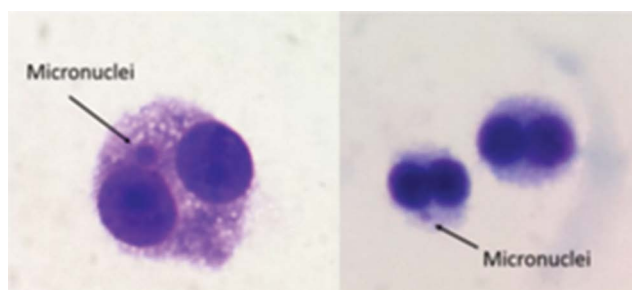


Figure 1. Typical binucleated lymphocytes with micronuclei in patients who received iodine-131 in the placebo group

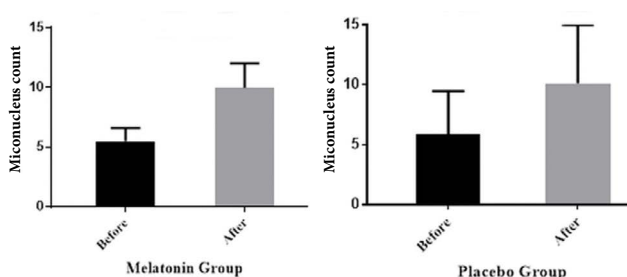


Figure 2. Average number of cells with micronuclei per 1000 cells counted for patients with melatonin (right) and placebo (left) groups before and after treatment with iodine-131

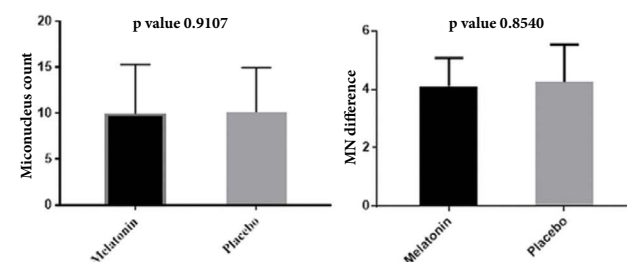


Figure 3. The mean (right) and MN (differences between the number of micronuclei before and after treatment with iodine-131) (left) per 1000 cells counted for patients of melatonin and placebo groups

respectively ($p = 0.910$). Typical micronucleated binucleate cells are shown in Figure 1.

The data on the micronuclei count before treating with iodine-131 and after the treatment is shown in Figure 2 for both groups. According to this chart, treatment with iodine-131 in both groups has increased the number of micronuclei. In both groups, the difference between the number of micronuclei before and after treatment with iodine-131 is significant (Placebo group: $p < 0.0001$; Melatonin group: $p < 0.0001$).

Figure 3 shows the comparison of MN in 2 groups after iodine therapy also MN, which represent the difference in the number of micronuclei before and after treatment with iodine-131 in the 2 placebo and melatonin groups. As shown in Figure 3, MN is 4.25 ± 3.05 for the placebo group, and 4.10 ± 2.51 for the

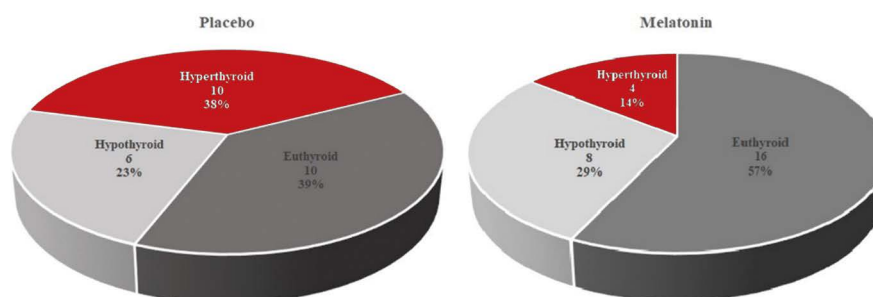


Figure 4. The treatment outcome in placebo and melatonin groups in a 6 month follow-up

melatonin group. However, there was no statistically significant ($p = 0.854$).

The patients participating in the trial were monitored clinically in the intervening period until the end of the treatment process for 2 hours. Eight subjects in the placebo group (33.33%) and nine patients in the melatonin group (29.0%) experienced the above complications. It should be noted that none of the patients experienced an acute symptom requiring remedial action.

Figure 4 shows the treatment outcome in the placebo and melatonin groups in separation. The information showed that 62% and 86% of patients had an excellent response to treatment in the placebo and melatonin groups, respectively. The results of the chi-square test showed that the difference in treatment outcome in the 2 groups was statistically significant ($p = 0.043$).

Discussion

Previous studies, which had been performed on in-vitro human and animal models, have shown that melatonin can be useful in reducing radiation-induced genotoxic damages [9, 21–30]. The current trial was carried out for the first time in the in-vivo environment and human subjects.

Data from this study indicate that treatment with iodine-131 at doses of 10 to 20 mCi significantly induces genetic damages in patients' blood lymphocytes. The doubled number of micronuclei in samples after administration of iodine was an appropriate marker for this hypothesis. Gil et al. [31] studied the DNA damages by the Micronuclei method in peripheral lymphocytes of patients with thyroid cancer after treatment with iodine-131. The number of micronuclei in cells from patients significantly increased one month after the treatment. Ballardín et al. [32] reported the 4-fold increase in the number of micronuclei in the seventh day after treatment in patients who had received therapeutic doses of iodine-131. However, the number of micronuclei then slowly fell and reached the baseline at day 180 after the treatment. In the three-month follow-up of hyperthyroid patients treated with iodine-131, Gutiérrez et al. [33] showed that the number of micronuclei in blood lymphocytes of patients would increase after treatment with iodine-131 increases, which is dose-dependent. Dardano et al. [34] also found in their study that administering iodine-131 to treat hyperthyroidism in patients would cause a significant increase in the number of micronuclei in peripheral blood lymphocytes, which gradually decreased after 21 days and reached to the baseline at day 90 after the treatment. The increasing trend in

the number of micronuclei as our study has been seen in all the mentioned previous studies. The differences in the increase in various studies may be explained due to different doses of iodine. According to these results, one can say that the micronuclei test can be used as a valuable endpoint and sensitive method for the biological study of iodine-131 radiation to assess the genetic damages in patients.

Iodine-131 is a useful radionuclide for the treatment of hyperthyroidism, but it has been reported that iodine therapy may increase the risk of secondary cancers due to genotoxic effects. Metso et al. observed a significant increase in the incidence of secondary cancers in the 10-year follow-up of patients who had received iodine-131 to treat hyperthyroidism [2]. The research carried out by Iyer et al. [35] suggests that the incidence of leukemia significantly increased in patients after treatment with iodine-131. This finding was also seen similarly in Sawka et al. study [36].

Two-third of chromosomal damages caused by ionizing radiations are created by generated free radicals. Due to the ability to collect the free radicals, antioxidants are capable of reducing adverse effects of ionizing radiation on living systems, including chromosomal damages [37]. Melatonin efficiency, as a naturally occurring compound in the human body, has been reviewed and approved regarding radiation protection in numerous studies. In this study, the number of micronuclei in the group receiving melatonin decreased compared to the group receiving a placebo. A significant reduction of chromosomal damages caused by gamma rays in the presence of melatonin had been seen in human and animal studies. Vijayalaxmi et al. [27] treated the human peripheral blood cells in the in-vitro environment with melatonin. The cells were then irradiated with gamma rays. Lymphocytes being in the melatonin-rich environment before exposure showed a significant and dose-dependent reduction in the frequency of radiation-induced chromosome damage compared to control cells. In another study by Reiter et al. [28], some volunteers received a single oral dose of 300 mg melatonin, and their blood samples were collected before receiving melatonin as well as 1 and 2 hours after receiving melatonin. Samples collected in the in-vitro environment were irradiated by cesium-137 gamma-ray at a dose of 150 cGy and were then studied regarding chromosomal abnormalities and micronucleus. During observations, the highest concentration of melatonin was seen in human serum and leukocytes in samples collected one hour after oral administration of melatonin. Consequently, a further reduction was seen in the incidence of genetic abnormalities and

micronucleus in this group (one hour after oral administration) of the blood samples.

Badr et al. [29] observed the radioprotective effect of melatonin when melatonin had been already added to the culture medium of blood lymphocytes and showed that melatonin should be present in the cell at the time of radiation so that it can play its radioprotective role. Kopjar et al. [38] found that peripheral blood lymphocytes treatment with melatonin can be involved in reducing the number of micronuclei after radiation. An in-vitro study conducted by Rostami et al. [37] showed the radioprotective effect of melatonin when the lymphocytes had been treated with melatonin. It should be noted that the highest radioprotective effect on blood lymphocytes was observed in their study one hour after adding melatonin. Similarly, in this study, the effect of melatonin was investigated one hour after oral administration.

These findings may suggest that melatonin might be able to act effectively as a radioprotector. Two hypotheses can be involved in the radioprotective effect of melatonin;

Melatonin may "directly" prevent chromosome damage by collecting free radicals caused by ionizing radiations before they damage the genetic material. Thus, the expansion of the initial damages in the cellular DNA may be significantly reduced.

Melatonin can "indirectly" change the rate of final chromosome damage by activating oxidative repair enzymes. As a result, the damaged DNA in irradiated cells of patients who have already received melatonin would be restored. Also, melatonin may indirectly stimulate the intracellular signals for genes involved in the synthesis of proteins participating in DNA restoration [9].

The literature published about the effects of melatonin suggests that both proposed hypotheses may be correct [39]. The small size and high lipophilicity of melatonin make it possible for this molecule to pass all biological membranes and enter any cell and even into the cellular compartments [12]. Melatonin is widely distributed within cells with the highest concentration at the nucleus [40]. Melatonin tendency for dispersion and accumulation in the nucleus as well as its ability to collect free radicals can be a direct and effective medium for in situ conservation in cells against damages induced by ionizing radiations [26].

Another feature, which probably increases the efficiency of melatonin in reducing oxidative stress is related to its second and third produced metabolites appearing to be efficient scavengers [41]. Some studies have shown an anti-tumor effect for melatonin as it slows down the cell cycle [42].

Conclusions

This study showed that the percentage of those people in the placebo group who had been treated with iodine-131 with no favorable response to treatment (having hyperthyroidism after 6 months of treatment with iodine-131) was higher than the melatonin group. In other words, treatment success in the group receiving the melatonin was higher than control. However, any conclusion about this observation requires further investigation with a larger population and a more precise measurement of the melatonin levels in serum at each stage of sampling.

As a general conclusion, this was the first study examining human in-vivo assessment on the radioprotective effects of

melatonin, and melatonin has a positive but not significant effect on reducing the rate of MN. Nevertheless, after 6 month follow-up, the treatment success was higher in the group which received Melatonin. However, future studies with a more extensive study population, longer follow-up (6 months), use of different melatonin doses, and utilizing further biochemical, cytogenetic methods will be recommended.

Financial support

This work is financially supported by the Deputy of research and technology, Babol University of Medical Sciences.

Compliance with ethical standards

The Authors declare compliance of the study with all ethical standards. Iranian Registry of Clinical Trials (IRCT); registry No.: IRCT2014090419045N1.

Conflict of interest

There is no conflict of interest.

References

- Streetman DD, Khanderia U. Diagnosis and treatment of Graves disease. *Ann Pharmacother.* 2003; 37(7-8): 1100–1109, doi: [10.1345/aph.1C299](https://doi.org/10.1345/aph.1C299), indexed in Pubmed: [12841824](https://pubmed.ncbi.nlm.nih.gov/12841824/).
- Metso S, Auvinen A, Huhtala H, et al. Increased cancer incidence after radioiodine treatment for hyperthyroidism. *Cancer.* 2007; 109(10): 1972–1979, doi: [10.1002/cncr.22635](https://doi.org/10.1002/cncr.22635), indexed in Pubmed: [17393376](https://pubmed.ncbi.nlm.nih.gov/17393376/).
- Ballardin M, Barsacchi R, Bodei L, et al. Oxidative and genotoxic damage after radio-iodine therapy of Graves' hyperthyroidism. *Int J Radiat Biol.* 2004; 80(3): 209–216, doi: [10.1080/0955300042000205555](https://doi.org/10.1080/0955300042000205555), indexed in Pubmed: [15244374](https://pubmed.ncbi.nlm.nih.gov/15244374/).
- Mansour HH, Hafez HF, Fahmy NM, et al. Protective effect of N-acetylcysteine against radiation induced DNA damage and hepatic toxicity in rats. *Biochem Pharmacol.* 2008; 75(3): 773–780, doi: [10.1016/j.bcp.2007.09.018](https://doi.org/10.1016/j.bcp.2007.09.018), indexed in Pubmed: [18028880](https://pubmed.ncbi.nlm.nih.gov/18028880/).
- Sharma S, Haldar C. Melatonin prevents X-ray irradiation induced oxidative damage in peripheral blood and spleen of the seasonally breeding rodent, *Funambulus pennanti* during reproductively active phase. *Int J Radiat Biol.* 2006; 82(6): 411–419, doi: [10.1080/09553000600774105](https://doi.org/10.1080/09553000600774105), indexed in Pubmed: [16846976](https://pubmed.ncbi.nlm.nih.gov/16846976/).
- Karbownik M, Reiter RJ. Antioxidative effects of melatonin in protection against cellular damage caused by ionizing radiation. *Proc Soc Exp Biol Med.* 2000; 225(1): 9–22, doi: [10.1046/j.1525-1373.2000.22502.x](https://doi.org/10.1046/j.1525-1373.2000.22502.x), indexed in Pubmed: [10998194](https://pubmed.ncbi.nlm.nih.gov/10998194/).
- Reiter RJ, Tan DX, Herman TS, et al. Melatonin as a radioprotective agent: a review. *Int J Radiat Oncol Biol Phys.* 2004; 59(3): 639–653, doi: [10.1016/j.ijrobp.2004.02.006](https://doi.org/10.1016/j.ijrobp.2004.02.006), indexed in Pubmed: [15183467](https://pubmed.ncbi.nlm.nih.gov/15183467/).
- Brenner B, Wasserman L, Beery E, et al. Variable cytotoxicity of amifostine in malignant and non-malignant cell lines. *Oncol Rep.* 2003; 10(5): 1609–1613, indexed in Pubmed: [12883748](https://pubmed.ncbi.nlm.nih.gov/12883748/).
- Reiter RJ, Meltz ML, Herman TS. Melatonin: possible mechanisms involved in its 'radioprotective' effect. *Mutat Res.* 1998; 404(1-2): 187–189, doi: [10.1016/s0027-5107\(98\)00112-2](https://doi.org/10.1016/s0027-5107(98)00112-2), indexed in Pubmed: [9729375](https://pubmed.ncbi.nlm.nih.gov/9729375/).
- Guerrero JM, Reiter RJ. A brief survey of pineal gland-immune system interrelationships. *Endocr Res.* 1992; 18(2): 91–113, doi: [10.1080/07435809209035401](https://doi.org/10.1080/07435809209035401), indexed in Pubmed: [1516565](https://pubmed.ncbi.nlm.nih.gov/1516565/).

11. Carrillo-Vico A, Lardone PJ, Alvarez-Sánchez N, et al. Melatonin: buffering the immune system. *Int J Mol Sci.* 2013; 14(4): 8638–8683, doi: [10.3390/ijms14048638](https://doi.org/10.3390/ijms14048638), indexed in Pubmed: [23609496](https://pubmed.ncbi.nlm.nih.gov/23609496/).
12. Reiter RJ, Tan DX, Osuna C, et al. Actions of melatonin in the reduction of oxidative stress. A review. *J Biomed Sci.* 2000; 7(6): 444–458, doi: [10.1007/BF02253360](https://doi.org/10.1007/BF02253360), indexed in Pubmed: [11060493](https://pubmed.ncbi.nlm.nih.gov/11060493/).
13. Rodriguez C, Mayo JC, Sainz RM, et al. Regulation of antioxidant enzymes: a significant role for melatonin. *J Pineal Res.* 2004; 36(1): 1–9, doi: [10.1046/j.1600-079x.2003.00092.x](https://doi.org/10.1046/j.1600-079x.2003.00092.x), indexed in Pubmed: [14675124](https://pubmed.ncbi.nlm.nih.gov/14675124/).
14. Galano A, Tan DX, Reiter RJ. On the free radical scavenging activities of melatonin's metabolites, AFMK and AMK. *J Pineal Res.* 2013; 54(3): 245–257, doi: [10.1111/jpi.12010](https://doi.org/10.1111/jpi.12010), indexed in Pubmed: [22998574](https://pubmed.ncbi.nlm.nih.gov/22998574/).
15. Reiter RJ, Tan DX, Cabrera J, et al. The oxidant/antioxidant network: role of melatonin. *Biol Signals Recept.* 1999; 8(1-2): 56–63, doi: [10.1159/000014569](https://doi.org/10.1159/000014569), indexed in Pubmed: [10085463](https://pubmed.ncbi.nlm.nih.gov/10085463/).
16. Fenech M, Morley AA. Cytokinesis-block micronucleus method in human lymphocytes: effect of in vivo ageing and low dose X-irradiation. *Mutat Res.* 1986; 161(2): 193–198, doi: [10.1016/0027-5107\(86\)90010-2](https://doi.org/10.1016/0027-5107(86)90010-2), indexed in Pubmed: [3724773](https://pubmed.ncbi.nlm.nih.gov/3724773/).
17. Gutiérrez S, Carbonell E, Galofré P, et al. Micronuclei induction by 131I exposure: study in hyperthyroidism patients. *Mutat Res.* 1997; 373(1): 39–45, doi: [10.1016/s0027-5107\(96\)00185-6](https://doi.org/10.1016/s0027-5107(96)00185-6), indexed in Pubmed: [9015151](https://pubmed.ncbi.nlm.nih.gov/9015151/).
18. Baugnet-Mahieu L, Lemaire M, Léonard ED, et al. Chromosome aberrations after treatment with radioactive iodine for thyroid cancer. *Radiat Res.* 1994; 140(3): 429–431, indexed in Pubmed: [7972697](https://pubmed.ncbi.nlm.nih.gov/7972697/).
19. Kacher R, Legal J, Schlumberger M, et al. Biological dosimetry in patients treated with iodine-131 for differentiated thyroid carcinoma. *J Nucl Med.* 1996; 37(11): 1860–1864, indexed in Pubmed: [8917193](https://pubmed.ncbi.nlm.nih.gov/8917193/).
20. Watanabe N, Yokoyama K, Kinuya S, et al. Radiotoxicity after iodine-131 therapy for thyroid cancer using the micronucleus assay. *J Nucl Med.* 1998; 39(3): 436–440, indexed in Pubmed: [9529288](https://pubmed.ncbi.nlm.nih.gov/9529288/).
21. Assayed ME, Abd El-Aty AM. Protection of rat chromosomes by melatonin against gamma radiation-induced damage. *Mutat Res.* 2009; 677(1-2): 14–20, doi: [10.1016/j.mrgentox.2009.04.016](https://doi.org/10.1016/j.mrgentox.2009.04.016), indexed in Pubmed: [19465147](https://pubmed.ncbi.nlm.nih.gov/19465147/).
22. Tahamtan R, Haddadi G, Tavassoli A. The evaluation of melatonin effect against the early effect of ionizing radiation induced lung injury. *Journal of Fasa University of Medical Sciences.* 2014; 4(1): 120–126.
23. Yilmaz S, Yilmaz E. Effects of melatonin and vitamin E on oxidative-antioxidative status in rats exposed to irradiation. *Toxicology.* 2006; 222(1-2): 1–7, doi: [10.1016/j.tox.2006.02.008](https://doi.org/10.1016/j.tox.2006.02.008), indexed in Pubmed: [16564611](https://pubmed.ncbi.nlm.nih.gov/16564611/).
24. Shirazi A, Fardid R, Mihandoost E. Protective effect of low dose melatonin on radiation-induced damage to rat liver. *J Biomed Phys Eng.* 2012; 2(2): 66–71.
25. El-Missiry MA, Fayed TA, El-Sawy MR, et al. Ameliorative effect of melatonin against gamma-irradiation-induced oxidative stress and tissue injury. *Ecotoxicol Environ Saf.* 2007; 66(2): 278–286, doi: [10.1016/j.ecoenv.2006.03.008](https://doi.org/10.1016/j.ecoenv.2006.03.008), indexed in Pubmed: [16793135](https://pubmed.ncbi.nlm.nih.gov/16793135/).
26. Reiter RJ, Meltz ML. Melatonin protects human blood lymphocytes from radiation-induced chromosome damage. *Mutat Res.* 1995; 346(1): 23–31, doi: [10.1016/0165-7992\(95\)90065-9](https://doi.org/10.1016/0165-7992(95)90065-9), indexed in Pubmed: [7530326](https://pubmed.ncbi.nlm.nih.gov/7530326/).
27. Vijayalaxmi, Reiter RJ, Sewerynek E, et al. Marked reduction of radiation-induced micronuclei in human blood lymphocytes pretreated with melatonin. *Radiat Res.* 1995; 143(1): 102–106, indexed in Pubmed: [7597136](https://pubmed.ncbi.nlm.nih.gov/7597136/).
28. Vijayalaxmi, Reiter RJ, Herman TS, et al. Melatonin and radioprotection from genetic damage: in vivo/in vitro studies with human volunteers. *Mutat Res.* 1996; 371(3-4): 221–228, doi: [10.1016/s0165-1218\(96\)90110-x](https://doi.org/10.1016/s0165-1218(96)90110-x), indexed in Pubmed: [9008723](https://pubmed.ncbi.nlm.nih.gov/9008723/).
29. Badr FM, El Habit OH, Harraz MM. Radioprotective effect of melatonin assessed by measuring chromosomal damage in mitotic and meiotic cells. *Mutat Res.* 1999; 444(2): 367–372, doi: [10.1016/s1383-5718\(99\)00103-5](https://doi.org/10.1016/s1383-5718(99)00103-5), indexed in Pubmed: [10521676](https://pubmed.ncbi.nlm.nih.gov/10521676/).
30. Bhatia AL, Manda K. Study on pre-treatment of melatonin against radiation-induced oxidative stress in mice. *Environ Toxicol Pharmacol.* 2004; 18(1): 13–20, doi: [10.1016/j.etap.2004.05.005](https://doi.org/10.1016/j.etap.2004.05.005), indexed in Pubmed: [21782731](https://pubmed.ncbi.nlm.nih.gov/21782731/).
31. Monteiro Gil O, Oliveira NG, Rodrigues AS, et al. Cytogenetic alterations and oxidative stress in thyroid cancer patients after iodine-131 therapy. *Mutagenesis.* 2000; 15(1): 69–75, doi: [10.1093/mutage/15.1.69](https://doi.org/10.1093/mutage/15.1.69), indexed in Pubmed: [10640533](https://pubmed.ncbi.nlm.nih.gov/10640533/).
32. Ballardín M, Gemignani F, Bodei L, et al. Formation of micronuclei and of clastogenic factor(s) in patients receiving therapeutic doses of iodine-131. *Mutat Res.* 2002; 514(1-2): 77–85, doi: [10.1016/s1383-5718\(01\)00323-0](https://doi.org/10.1016/s1383-5718(01)00323-0), indexed in Pubmed: [11815246](https://pubmed.ncbi.nlm.nih.gov/11815246/).
33. Gutiérrez S, Carbonell E, Galofré P, et al. Cytogenetic damage after 131I-iodine treatment for hyperthyroidism and thyroid cancer. A study using the micronucleus test. *Eur J Nucl Med.* 1999; 26(12): 1589–1596, doi: [10.1007/s002590050499](https://doi.org/10.1007/s002590050499), indexed in Pubmed: [10638411](https://pubmed.ncbi.nlm.nih.gov/10638411/).
34. Dardano A, Ballardín M, Ferdeghini M, et al. Anticlastogenic effect of Ginkgo biloba extract in Graves' disease patients receiving radioiodine therapy. *J Clin Endocrinol Metab.* 2007; 92(11): 4286–4289, doi: [10.1210/jc.2007-0597](https://doi.org/10.1210/jc.2007-0597), indexed in Pubmed: [17711926](https://pubmed.ncbi.nlm.nih.gov/17711926/).
35. Iyer NG, Morris LGT, Tuttle RM, et al. Rising incidence of second cancers in patients with low-risk (T1N0) thyroid cancer who receive radioactive iodine therapy. *Cancer.* 2011; 117(19): 4439–4446, doi: [10.1002/cncr.26070](https://doi.org/10.1002/cncr.26070), indexed in Pubmed: [21432843](https://pubmed.ncbi.nlm.nih.gov/21432843/).
36. Sawka AM, Thabane L, Parlea L, et al. Second primary malignancy risk after radioactive iodine treatment for thyroid cancer: a systematic review and meta-analysis. *Thyroid.* 2009; 19(5): 451–457, doi: [10.1089/thy.2008.0392](https://doi.org/10.1089/thy.2008.0392), indexed in Pubmed: [19281429](https://pubmed.ncbi.nlm.nih.gov/19281429/).
37. Rostami A, Moosavi SA, Dianat Moghadam H, et al. Micronuclei assessment of the radioprotective effects of melatonin and vitamin C in human lymphocytes. *Cell J.* 2016; 18(1): 46–51, doi: [10.22074/cellj.2016.3986](https://doi.org/10.22074/cellj.2016.3986), indexed in Pubmed: [27054118](https://pubmed.ncbi.nlm.nih.gov/27054118/).
38. Kopjar N, Miocić S, Ramić S, et al. Assessment of the radioprotective effects of amifostine and melatonin on human lymphocytes irradiated with gamma-rays in vitro. *Arh Hig Rada Toksikol.* 2006; 57(2): 155–163, indexed in Pubmed: [16832970](https://pubmed.ncbi.nlm.nih.gov/16832970/).
39. Sewerynek E, Lewiński A. Melatonin inhibits mitotic activity of adrenocortical cells in vivo and in organ culture. *J Pineal Res.* 1989; 7(1): 1–12, doi: [10.1111/j.1600-079x.1989.tb00436.x](https://doi.org/10.1111/j.1600-079x.1989.tb00436.x), indexed in Pubmed: [2724051](https://pubmed.ncbi.nlm.nih.gov/2724051/).
40. Reiter RJ. Oxidative damage to nuclear DNA: amelioration by melatonin. *NEL Review. Neuro Endocrinol Lett.* 1999; 20(3-4): 145–150, indexed in Pubmed: [11462105](https://pubmed.ncbi.nlm.nih.gov/11462105/).
41. Reiter RJ, Tan DX, Gitto E, et al. Pharmacological utility of melatonin in reducing oxidative cellular and molecular damage. *Pol J Pharmacol.* 2004; 56(2): 159–170, indexed in Pubmed: [15156066](https://pubmed.ncbi.nlm.nih.gov/15156066/).
42. De Salvia R, Fiore M, Aglitti T, et al. Inhibitory action of melatonin on H2O2- and cyclophosphamide-induced DNA damage. *Mutagenesis.* 1999; 14(1): 107–112, doi: [10.1093/mutage/14.1.107](https://doi.org/10.1093/mutage/14.1.107), indexed in Pubmed: [10474831](https://pubmed.ncbi.nlm.nih.gov/10474831/).

Optimized method for normal range estimation of standardized uptake values (SUVmax, SUVmean) in liver SPECT/CT images with somatostatin analog [^{99m}Tc]-HYNIC-TOC (Tektrotyd)

Hanna Piwowarska-Bilska^{ORCID}, Sara Kurkowska^{ORCID}, Bożena Birkenfeld^{ORCID}
 Department of Nuclear Medicine, Pomeranian Medical University, Szczecin, Poland

[Received 12 XI 2021; Accepted 29 XII 2021]

Abstract

Background: ^{99m}Tc-hydrazinonicotinyl-Tyr3-octreotide ([^{99m}Tc]-HYNIC-TOC [Tektrotyd]) is a radiopharmaceutical used for the diagnosis of lesions with overexpression of somatostatin receptors. The purpose of this study was to optimize the method and estimate normal ranges for standardized uptake values of Tektrotyd in healthy livers.

Material and methods: An analysis of standardized uptake value (SUVs) normal ranges was performed for images acquired in a selected “healthy group” of 42 patients evaluated for neuroendocrin tumors. The “pathological group” comprised 20 patients with liver lesions detected by scintigraphic imaging. Normal ranges for radiopharmaceutical uptake values were estimated based on the quantitative analysis of images acquired with a GE Healthcare NM/CT 850 gamma camera.

Results: The method for healthy liver segmentation in single photon emission computed tomography/computed tomography (SPECT/CT) was optimized. The normal range of SUVs for the liver was: standardized uptake value body weight (SUVbw) max [5.2–14.0] g/mL and standardized uptake value lean body mass (SUVlbm) [3.5–9.5] g/mL. The relative standard error (relative SE) of activity concentration estimated in the phantom study for the largest hot spheres was: $\phi = 37$ mm — 5.9%, $\phi = 28$ mm — 7.1%, $\phi = 22$ mm — 11.4%, and $\phi = 17$ mm — 22%.

Conclusions: Segmentation in the mid-coronal computed tomography (CT) image, at one-fourth of the height of the liver measured from the top, with a medium-sized volume of interest (VOI) outlined on a given transverse SPECT slice was regarded as the optimal method for estimating normal ranges for standardized uptake values. It is necessary to standardize quantification methods in the SPECT/CT studies. Our work is a step forward in obtaining standardization of SPECT/CT SUV calculation methods. Calculations for radiopharmaceutical uptake in tumors with volumes smaller than 5 mL are biased with a significant measurement error.

KEY words: quantitative SPECT/CT; SUV; standardized uptake value; [^{99m}Tc]-HYNIC-TOC; Tektrotyd

Nucl Med Rev 2022; 25, 1: 37–46

Correspondence to: Hanna Piwowarska-Bilska,
 Department of Nuclear Medicine, Pomeranian Medical University,
 Unii Lubelskiej 1, 71-344 Szczecin, Poland
 e-mail: hanna.piwowarska@pum.edu.pl

Introduction

SPECT/CT and positron emission tomography/computed tomography (PET/CT) imaging with radiolabeled analogues of somatostatin plays an important role in the diagnosis and monitoring of patients with neuroendocrine tumors (NET). These techniques offer additional metabolic information and higher specificity than conventional magnetic resonance imaging (MRI) or CT [1, 2]. Radioisotope studies of somatostatin receptors are used for diagnostic purposes and in the process of qualifying patients for peptide receptor radionuclide therapy (PRRT). The somatostatin analog [^{99m}Tc]-HYNIC-TOC (Tektrotyd), manufactured in Poland, has been used for over a decade in many European countries for imaging NET with SPECT/CT. This radiopharmaceutical is characterized by a high affinity for somatostatin receptors type 2 (SSTR2), a lower affinity for SSTR3 and SSTR5, optimal physical parameters, and biodistribution. In 2003 Gabriel et al. [3] reported a higher sensitivity of [^{99m}Tc]-HYNIC-TOC as compared to [^{111}In]-diethylenetriaminepentaacetic acid-d-phenylalanine-octreotide ([^{111}In]-DTPA-octreotide [Octreoscan]) for the detection of neuroendocrine tumors. Tektrotyd has many advantages with respect to Octreoscan, including better physical characteristics of [^{99m}Tc] compared to [^{111}In], which makes it more suitable for SPECT/CT imaging; shorter half-life; lower radiation burden; lower physiological liver and bowel uptake [4]. Therefore, Tektrotyd is a good alternative to [^{68}Ga]-DOTA-Peptide in medical centers where PET/CT or [^{68}Ge]/[^{68}Ga] generators are not available [5, 6, 7].

In PET/CT imaging, the quantitative assessment of uptake by NET measured by SUV is a standard procedure [8, 9]. Modern SPECT/CT systems offer quantitative imaging. Physicians referring their patients for imaging with [^{99m}Tc]-HYNIC-TOC expect quantitative data on radionuclide uptake by tumors. However, standardized uptake values (SUVs) when presented without an estimated normal range for SUV do not provide any important or conclusive diagnostic information.

In clinical practice, the qualification of patients for PRRT with somatostatin analogs is based, among others, on the assessment of the intensity of uptake in tumors with a semiquantitative visual scoring system, known as Krenning score, which consists of a scale from 0 to 4 and uses the liver and spleen as reference organs [10]. Moreover, it has been found that the maximum standardized uptake value (SUVmax) is strongly correlated with Krenning score [11]. Quantitative nuclear medicine is diagnostically and therapeutically more effective than qualitative because visual analysis of SPECT/CT images can be subjective and not repeatable [12].

The primary purpose of this study was to optimize the method for the segmentation of healthy liver in order to estimate normal ranges for SUV. The detailed aims of the study were to estimate normal ranges for standardized uptake values (SUVmax, mean standardized uptake value [SUVmean]) in SPECT/CT images of healthy liver acquired using Tektrotyd and a GE Healthcare NM/CT 850 gamma camera, and to estimate the accuracy of SUV measurements performed in a body phantom.

In addition to the absolute normal standardized uptake values of Tektrotyd, we also calculated the relative ranges for the following ratios: SUV spleen/SUV liver and SUV liver/SUV gluteus medius which

may help to overcome the problem of the individual presence of somatostatin receptors in healthy patients.

Material and methods

Patient images

An analysis of normal ranges for SUV was performed for images acquired in a selected "healthy group" of 42 patients (29 men, 13 women, mean age 60 years) evaluated for NET. They had a physiological liver distribution of Tektrotyd, as well as normal results of selected biochemical liver tests (aspartate aminotransferase test [AST] and alanine aminotransferase test [ALT]) and normal results of CT or MRI scan of the abdomen. The "pathological group" comprised 20 patients (13 men and 7 women, mean age 61 years) with hot liver lesions detected by scintigraphy. In this group, 58 hot lesions in the livers were described. All of these patients were diagnosed before SPECT/CT examinations, based on the biopsy results of the primary lesion. Histopathological examination revealed NET of the gastrointestinal tract in 18 of these patients and the carcinoid of the lung in 2 other patients. SPECT/CT was performed to assess the severity of the disease.

Patient SPECT/CT scans were acquired 2–5 hours following the injection of 483–765 Megabecquerel (MBq) of the radiopharmaceutical. Syringe activity for each patient was measured before and after the injection of Tektrotyd. SUVs in SPECT/CT images were calculated with the Q.Metrix option of Xeleris 4.0 software.

Normal ranges for radiopharmaceutical uptake values were estimated based on the quantitative analysis of images acquired with a GE Healthcare NM/CT 850 gamma camera. The following SPECT/CT acquisition parameters were used: low energy high resolution (LEHR) collimator, 120 projections, projection time 20 s, matrix 128 x 128, dual-energy windows: emission 126.5–154.6 keV, scatter 114.0–126.0 keV, and low dose CT after SPECT mode. The reconstruction parameters were: 5 iterations and 15 subsets, without a reconstruction filter. Segmentation of regions of interest (ROIs) in patient images and phantom images was performed at a 50% cut-off threshold for the background. The volumes of interest (VOIs) were drawn in the reconstructed SPECT images by manually adjusting the threshold of an isocontour such that the ROI boundaries coincided with the boundaries of the fused CT image.

Optimization of the method for estimating normal range for SUV in the liver

The quantification of the images began with the clinical optimization of the liver segmentation method in the images of healthy subjects.

1) Segmentation of the entire area of the liver without the regions of extrahepatic bile ducts

During the quantitative analysis, SPECT and CT images of the same liver slices were displayed. Correct liver segmentation in SPECT slices was anatomically monitored on the corresponding CT slices. The segmentation technique involved the outlining of the entire liver area, without the extrahepatic bile ducts, on individual transverse slices (Fig. 1). ROIs were outlined on every fourth SPECT transverse slice. As a result, VOIs were created on 3D images covering a considerable portion of the liver, with a mean volume of 1296 ± 299 mL.

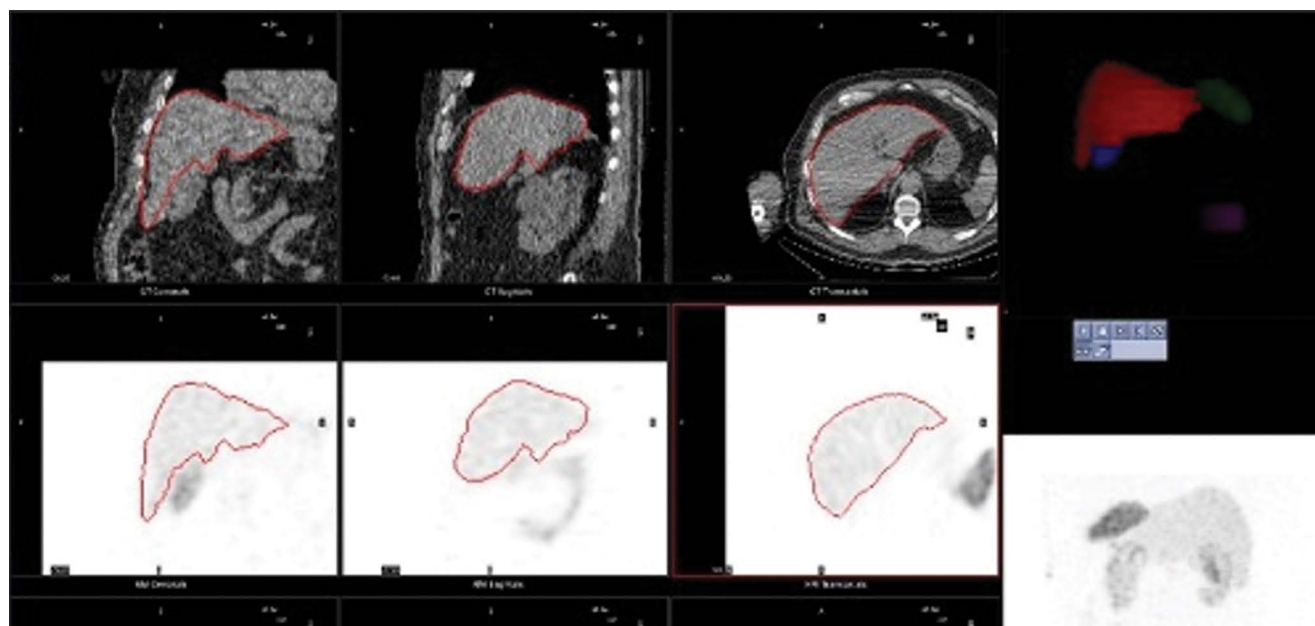


Figure 1. Liver segmentation method 1 with Q.Metrix option of Xeleris 4.0 software

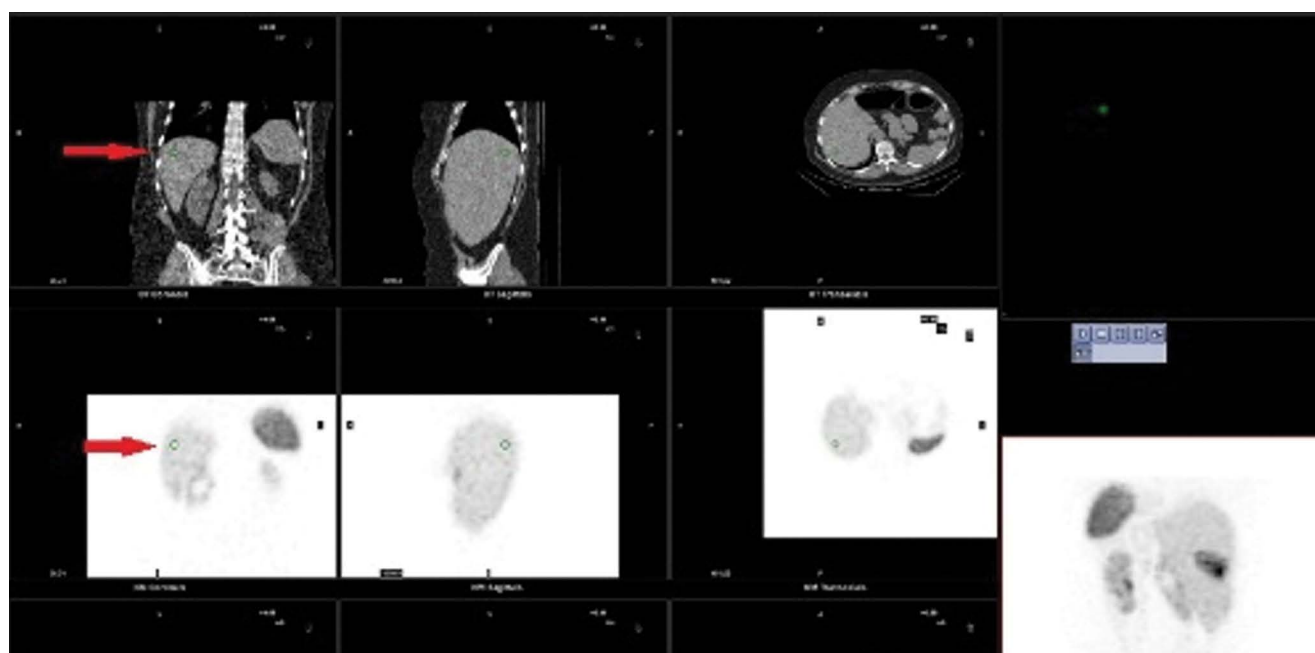


Figure 2. Small liver volume of interest (VOI) — segmentation method 2

2) Method for the segmentation of a small liver VOI on the established slice

A CT slice corresponding to the SPECT slice showing the Th11 and Th12 vertebra was displayed. A liver fragment of the mean volume 2.5 ± 0.7 mL was segmented at the level of the intervertebral disc between Th11 and Th12 (Fig. 2), within peripheral localization of liver segments V and VI.

3) Segmentation method for the medium-sized liver VOI at 1/4 of the height of the liver (measured from the top)

Segmentation was performed as follows: in the mid-coronal CT image of the patient's liver, one-fourth of the height of the liver from the top was determined. Then, on the given transverse SPECT slice, the ROI outlining the liver was selected (Fig. 3). The mean size of the VOI created with this method was 31.1 ± 7.7 mL within liver segments VII and VIII.

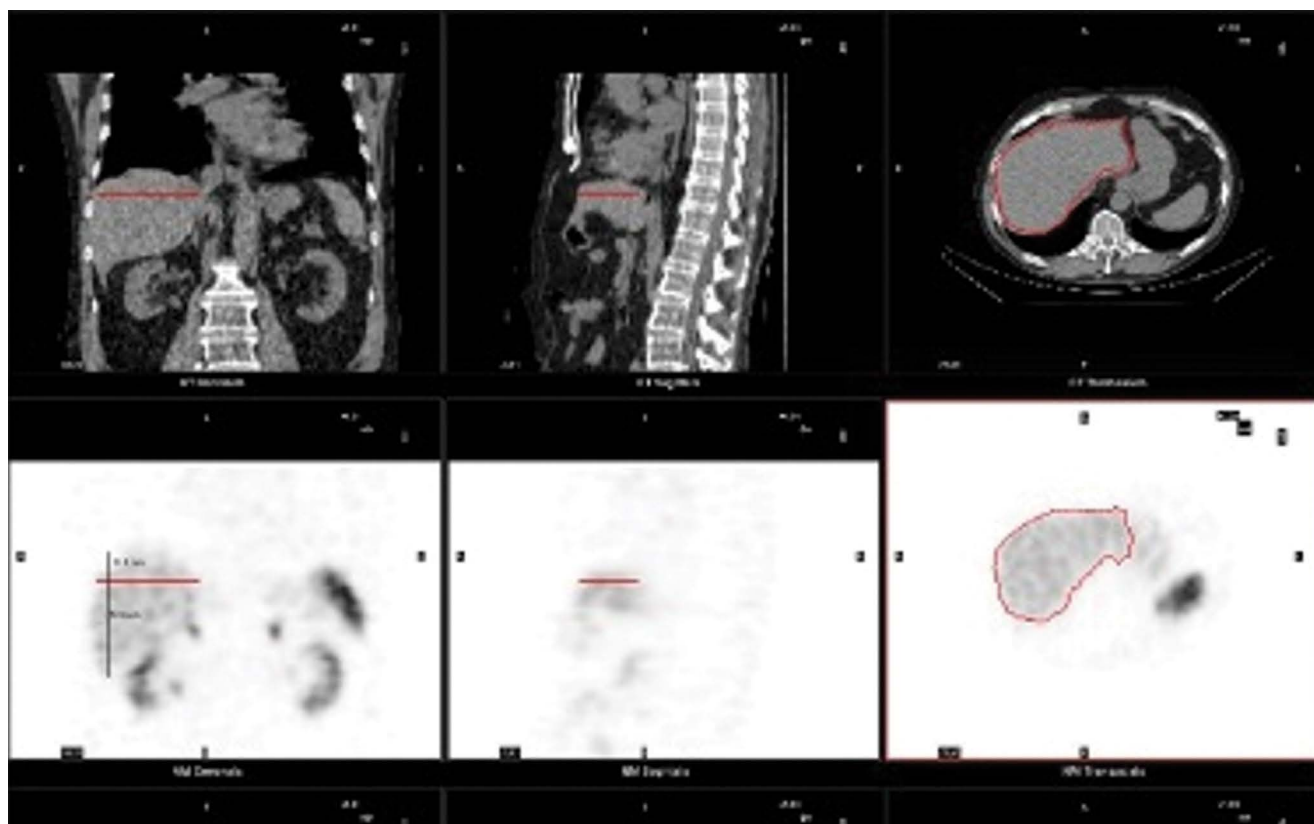


Figure 3. Medium liver volume of interest (VOI) — segmentation method 3

After completing the segmentation with each of the described methods, we calculated SUVbw max, SUVbm mean, SUVlbm max, and SUVlbm mean for each outlined VOI.

SUVbw and SUVlbm were calculated using the following formulas [13–15]:

$$SUV_{bw} = \frac{\text{SPECT image Pixels uptake (Bq/ml)} \times \text{weight (g)}}{\text{Actual activity}} \quad (1)$$

$$SUV_{lbm} = \frac{\text{SPECT image Pixels uptake (Bq/ml)} \times \text{LBM (kg)}}{\text{Actual activity} \times 1000} \quad (2)$$

where:

Actual activity: activity during scanning,

$$\text{pixels uptake (Bq/ml)} = 37 \times 10^3 \times \frac{60}{\text{SPECTSensitivity (counts/min/}\mu\text{Ci)} \times T (s) \times \text{ml}} \quad (3)$$

where T-scan duration in seconds.

for males:

$$\text{LBM in kg} = 1.10 \times (\text{weight in kg}) - 120 \times \frac{(\text{weight in kg})}{(\text{height in cm})^2} \quad (4)$$

for females:

$$\text{LBM in kg} = 1.07 \times (\text{weight in kg}) - 148 \times \frac{(\text{weight in kg})}{(\text{height in cm})^2} \quad (5)$$

Data were processed using Statistica 13.1 software. The normality of data distribution for SUV was verified with the Shapiro-Wilk test at the significance level $\alpha = 0.05$. The normal range for SUVs for healthy livers was determined using the formula: normal range = (mean -2SD ; mean $+2\text{SD}$).

Method for the determination of SUVs in the group with liver lesions

For images with numerous liver lesions, up to five abnormal hot spheres were segmented each time: with the lowest, moderate, and highest SUV. This method enabled the inclusion of the whole range of lesions, assuring also that the ones with relatively low uptake of the radiopharmaceutical were considered in the quantitative analysis.

Method for the determination of SUVs in other tissues

The spleen and the gluteus medius muscle have a relatively uniform distribution of radiopharmaceuticals in the tissues. The accumulation of radiopharmaceuticals by the gluteus medius is usually very low and may correspond with the background activity of the peripheral blood circulation. The accumulation of radiopharmaceuticals in the spleen is usually very high, and its value may correspond with that for hot lesions. Due to the individual differences of radiopharmaceutical accumulation in particular tissues, quantitative data on the physiological uptake of $^{99\text{m}}\text{Tc}$ -Tektrotyd by the spleen and the gluteus medius may be useful in the diagnostic interpretation of SUV measured in the liver.

We calculated the SUV spleen/SUV liver ratios in 42 patients and the SUV liver/SUV gluteus medius ratios in 38 patients (in 4 patients gluteus medius muscles were not visible in the SPECT/CT images). VOI in the spleen region was segmented based on SPECT

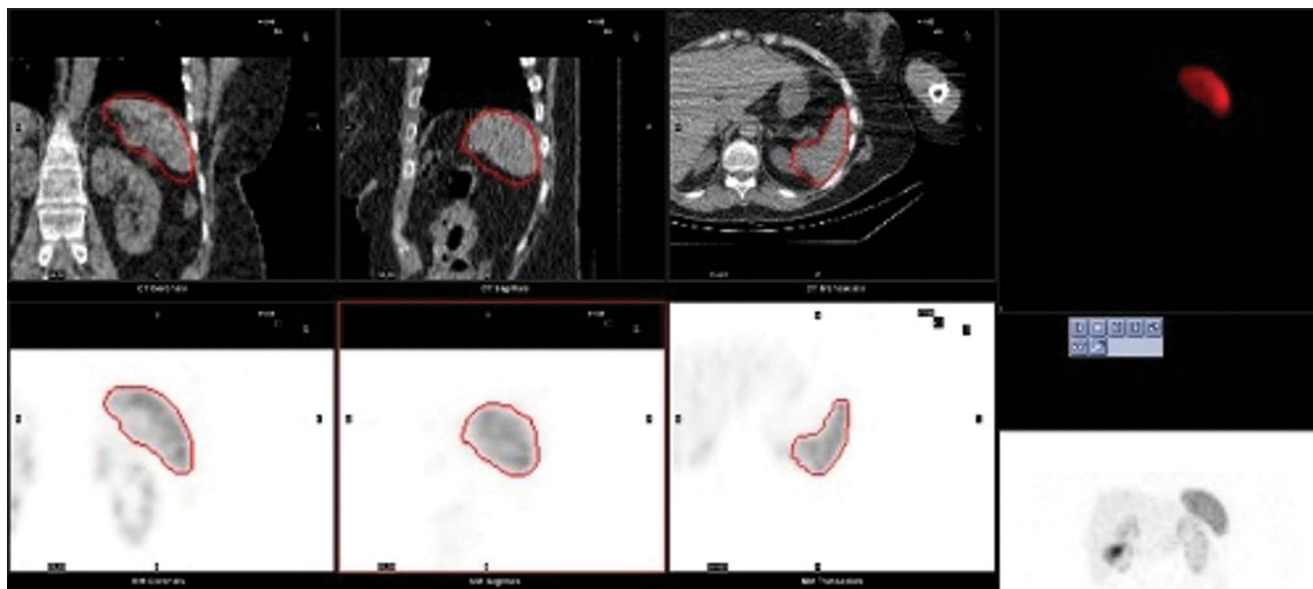


Figure 4. Segmentation of the spleen in single photon emission computed tomography (SPECT) slices

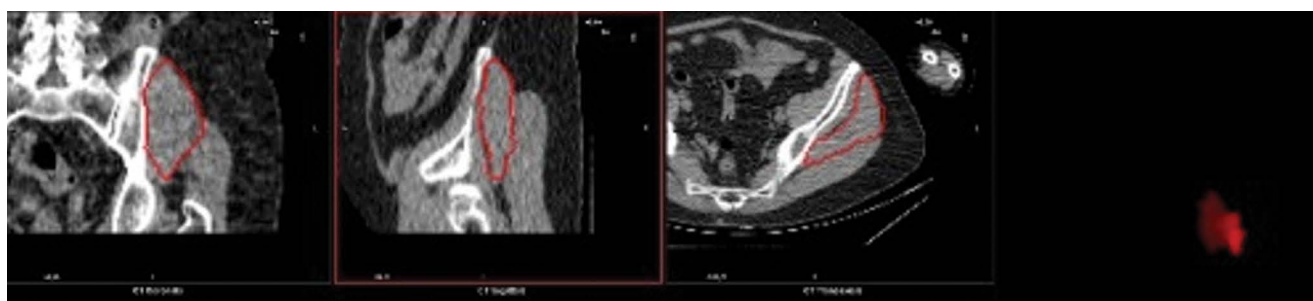


Figure 5. Segmentation of the gluteus medius muscle in computed tomography (CT) slices

and CT slices. VOI in the gluteus medius muscle was segmented based on CT slices. Figures 4 and 5 present the method for outlining VOI within the spleen and the gluteus medius muscle.

Estimation of the accuracy of SUV measurements

SPECT/CT acquisitions were performed using the National Electrical Manufacturers Association, International Electrotechnical Commission (NEMA IEC) Body Phantom with 6 hot spheres of different diameters: 10 mm, 13 mm, 17 mm, 22 mm, 28 mm, and 37 mm. The acquisition protocol and reconstruction parameters were identical to those used during imaging studies involving patients. SUVs are directly proportional to the activity concentration in the measured VOIs, and therefore the accuracy of the SUV measurement is closely related to the accuracy of the activity concentration measurement. Based on activity measurements performed with a calibrated activity meter and the results of image quantification, the relative standard error of mean activity concentration for VOIs in 6 spheres was determined. Figure 6 presents the segmentation of hot spheres in the NEMA IEC Body Phantom.

Results

Patients with healthy liver

1) Results of liver measurement

Results obtained for the quantification of SPECT/CT slices of healthy livers are presented in Table 1.

2) Results of measurements for the spleen and gluteus medius muscle

Table 2 presents SUV_{bw} and SUV_{lbm} for the spleen and gluteus medius muscle.

3) Standardized uptake value ratios: spleen/liver and liver/gluteus medius muscle

Table 3 presents normal ranges for SUV spleen/SUV liver ratios.

Table 4 presents normal ranges for SUV liver/SUV gluteus medius muscle ratios.

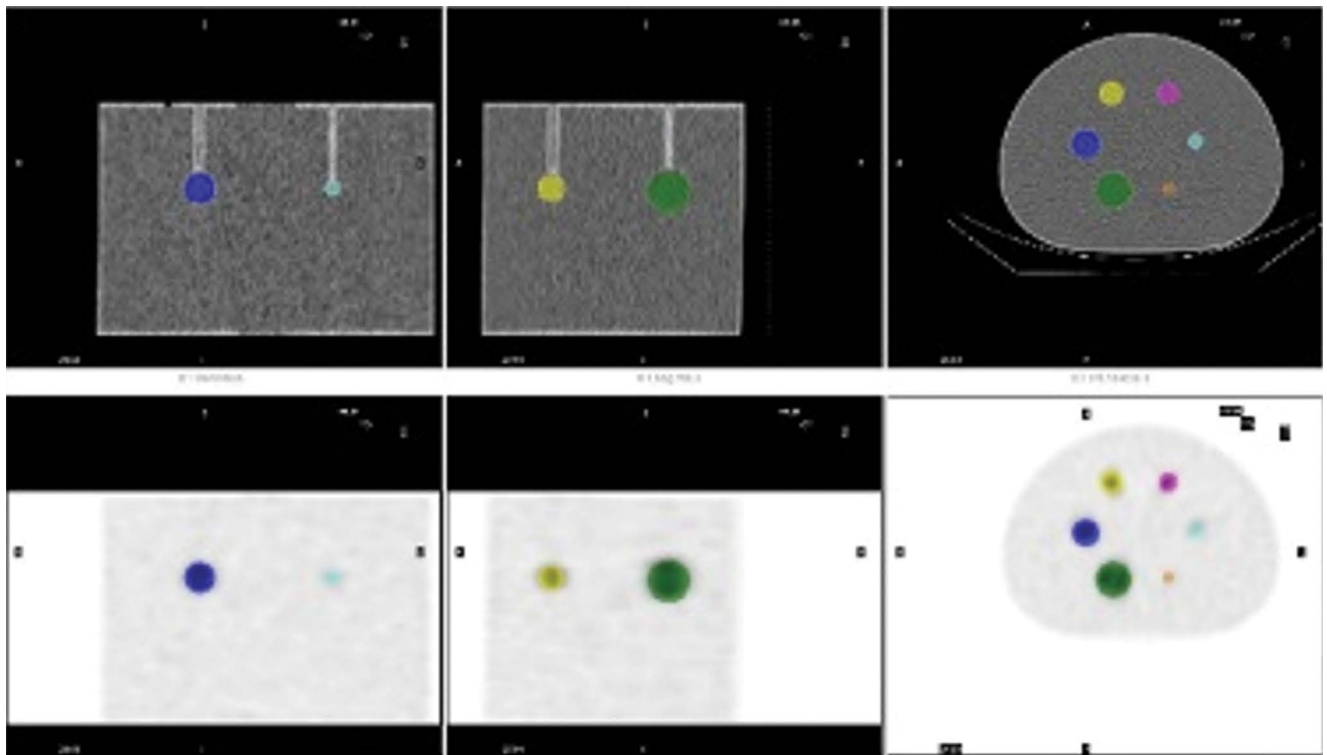


Figure 6. Segmentation of 6 hot spheres in the NEMA IEC Body Phantom; The RC — recovery coefficients curve was also plotted for hot spheres

Table 1. Standardized uptake value based on body weight (SUVbw) and standardized uptake value lean body mass (SUVlbm) measured in single photon emission computed tomography/ computed tomography (SPECT/CT) slices of healthy livers using three methods. The table presents normal ranges for SUVs for each segmentation method

	SUVbw max [g/mL]	SUVbw mean [g/mL]	SUVlbm max [g/mL]	SUVlbm mean [g/mL]
Method 1				
mean liver VOI: 1292.2 ± 299.1 mL				
Shapiro-Wilk test results	W = 0.96 p = 0.20	W = 0.95 p = 0.08	W = 0.98 p = 0.47	W = 0.98 p = 0.64
mean ± SD	12.6 ± 2.7	4.8 ± 1.3	8.4 ± 1.8	3.2 ± 0.8
minimum value–maximum value	7.7–19.0	2.5–9.1	4.4–11.5	1.5–4.8
normal range:	7.2–18.0	2.2–7.4	4.8–12.0	1.6–4.8
Method 2				
mean liver VOI: 2.5 ± 0.7 mL				
Shapiro-Wilk test results	W = 0.99 p = 0.86	W = 0.98 p = 0.58	W = 0.97 p = 0.23	W = 0.97 p = 0.28
mean ± SD	8.4 ± 2.3	5.8 ± 1.7	5.7 ± 1.4	4.0 ± 1.1
minimum value–maximum value	3.5–13.7	2.6–9.7	2.9–7.9	2.0–5.8
normal range:	3.8–13.0	2.4–9.2	2.9–8.5	1.8–6.2
Method 3				
mean liver VOI: 30.8 ± 7.7 mL				
Shapiro-Wilk test results	W = 0.99 p = 0.89	W = 0.94 p = 0.06	W = 0.97 p = 0.22	W = 0.98 p = 0.76
mean ± SD	9.6 ± 2.2	4.9 ± 1.3	6.5 ± 1.5	3.3 ± 0.9
minimum value–maximum value	4.9–15.2	2.6–9.4	2.3–9.1	1.5–5.0
normal range:	5.2–14.0	2.3–7.5	3.5–9.5	1.5–5.1

SD — standard deviation; SUVbw — standardized uptake value normalized to body weight; SUVlbm — standardized uptake value normalized to lean body mass; VOI — volume of interest

Table 2. Standardized uptake value based on body weight (SUVbw) and standardized uptake value lean body mass (SUVlbm) measured in single photon emission computed tomography/ computed tomography SPECT/CT slices of the spleen and gluteus medius muscle

	SUVbw max	SUVbw mean	SUVlbm max	SUVlbm mean
Spleen				
mean ± SD	39.3 ± 13.9	19.5 ± 4.4	26.22 ± 8.1	13.08 ± 3.0
mean volume: 236 ± 101 mL				
Gluteus medius				
mean ± SD	2.4 ± 0.7	0.5 ± 0.2	1.6 ± 0.5	0.4 ± 0.6
mean volume: 108 ± 34 mL				

SUVbw — standardized uptake value normalized to body weight; SUVlbm — standardized uptake value normalized to lean body mass

Table 3. Normal ranges for the standardized uptake value (SUV) spleen / standardized uptake value (SUV) liver ratios determined for each of the three segmentation methods and four standardized uptake values

	SUVbw max ratio	SUVbw mean ratio	SUVlbm max ratio	SUVlbm mean Ratio
Method 1				
mean ± SD	3.2 ± 0.9	4.2 ± 1.1	3.2 ± 0.9	4.2 ± 1.1
normal range:	1.4–5.0	2.0–6.4	1.4–5.0	2.0–6.4
Method 2				
mean ± SD	4.9 ± 1.5	3.6 ± 1.2	4.8 ± 1.4	3.4 ± 1.0
normal range:	1.9–7.9	1.2–6.0	2.0–7.6	1.4–5.4
Method 3				
mean ± SD	4.2 ± 1.2	4.1 ± 1.1	4.2 ± 1.2	4.1 ± 1.1
normal range:	1.8–6.6	1.9–6.3	1.8–6.6	1.9–6.3

SUVbw — standardized uptake value normalized to body weight; SUVlbm — standardized uptake value normalized to lean body mass

Table 4. Normal ranges for the SUV liver/SUV gluteus medius muscle ratios determined for each of the three segmentation methods and four SUVs

	SUVbw max ratio	SUVbw mean ratio	SUVlbm max ratio	SUVlbm mean ratio
Method 1				
mean ± SD	4.9 ± 1.5	3.6 ± 1.2	4.8 ± 1.4	3.5 ± 1.0
normal range:	1.9–7.9	1.2–6.0	2.0–7.6	1.5–5.5
Method 2				
mean ± SD	3.6 ± 1.1	13.1 ± 5.3	3.6 ± 1.1	12.9 ± 5.8
normal range:	1.4–5.8	2.5–23.7	1.4–5.8	1.3–24.5
Method 3				
mean ± SD	4.3 ± 1.3	11.2 ± 4.3	4.2 ± 1.3	10.8 ± 4.7
normal range:	1.7–6.9	2.6–19.8	1.6–6.8	1.4–20.2

SUVbw — standardized uptake value normalized to body weight; SUVlbm — standardized uptake value normalized to lean body mass

Patients with hot liver lesions

Quantitative analysis was performed for 58 lesions. The mean VOI for lesions was 22.7 ± 46.2 mL (range: 1.1–277.9 mL). 65% of the hot lesions had a volume greater than 5 mL.

Results obtained for the quantification of SPECT/CT slices of livers with hot lesions are presented in Table 5.

Estimation of the accuracy of SUV measurements

Relative errors of spheres' volume and activity concentration measurements obtained for SPECT/CT images of the NEMA IEC Body Phantom are presented in Table 6.

Figure 7 presents the RCmax (recovery coefficient curve) for the accuracy of spheres' activity concentration measurements in SPECT/CT images.

Discussion

Standardization of quantitative SPECT/CT is currently a crucial clinical problem. The feasibility of absolute quantification in SPECT/CT imaging was confirmed by different studies more than 10 years ago [16–19], but no standard quantification procedures, clinical analyses, or principles for the validation of equipment have been established to this day.

Table 5. Results of quantitative analysis of SPECT/CT slices of livers with hot lesions.

	SUVbw max	SUVbw mean	SUVlbm max	SUVlbm mean
Mean value [g/mL]	37.6 ± 27.1	21.0 ± 13.8	27.7 ± 20.3	15.5 ± 10.3
range [g/mL]	13.3–129.9	7.1–70.3	6.3–95.8	3.4–52.2

SUVbw — standardized uptake value normalized to body weight; SUVlbm — standardized uptake value normalized to lean body mass

Table 6. Relative errors of spheres' volume and activity concentration measurements. Ac_{measured} — activity concentration measured with a dose calibrator was 255 kBq/mL.

	Vt	Vi	SE _{Vi}	Ac _{in image} mean	SE _{Ac in image}
Sphere diameter [mm]	True sphere volume [mL]	Sphere volume in image [mL]	Relative standard error of volume [%]	Activity concentration mean in image [kBq/mL]	Relative standard error of activity concentration [%]
10	0.5	0.4	20.0	90	64.7
13	1.2	1.3	-8.3	130	49.0
17	2.6	2.3	11.6	199	22.0
22	5.6	5.0	10.7	226	11.4
28	11.5	10.7	6.9	237	7.1
37	26.5	25.7	3.0	240	5.9

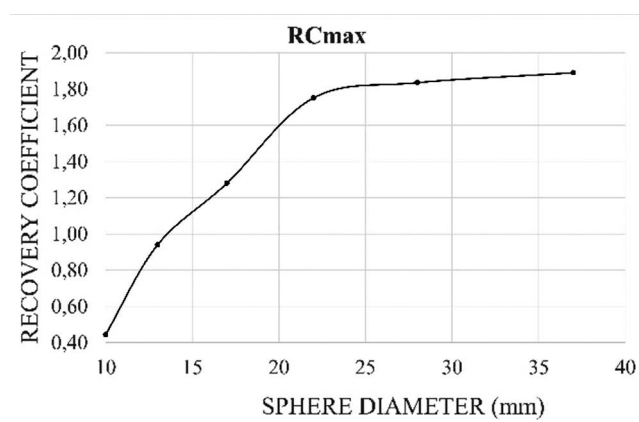


Figure 7. Recovery coefficient (RCmax) curve. Recovery coefficients were determined as the ratio of the maximum activity concentration measured in the image ($Ac_{\text{in image}}^{\text{max}}$) to the activity concentration measured with a dose calibrator (Ac_{measured})

Determination of the normal range of SUVs in studies is difficult because of very significant differences in the uptake of different radiopharmaceuticals associated with several biological and physical factors [20]. Firstly, the pharmacokinetics of the injected radiopharmaceutical depends on the metabolism of the examined patient. Secondly, the images are acquired at different time points following the injection of the radiopharmaceutical because of the limited availability of the gamma camera. The calculation of SUV involves measurements obtained using two instruments — a gamma camera and an activity meter. Therefore, inaccurate calibration of either instrument may influence the level of accuracy in the SUV measurement. There are also other factors affecting the variability of SUV, including the quality of image reconstruction, the efficiency of corrections for the scatter and attenuation of radiation in the patient's tissues, and the limited resolution of gamma camera

detectors, which create difficulties with the segmentation of selected regions of interest. Determination of absolute SUV is a complex task, but it is achievable [21].

A significant problem investigated in our study was to determine the optimal method for measuring SUV in healthy liver tissue. Method 1, which involved the segmentation of the entire liver region (except the extrahepatic bile ducts), although very laborious, seemed to be the most appropriate in the initial phase of analysis. The disadvantage of this method was the possibility of covering many intrahepatic bile ducts in a segmented large VOI (mean volume 1292 mL). Method 2 involved the segmentation of a small regular fragment of the liver (mean VOI: 2.5 mL) and was used because physicians prefer a technique that does not require a precise outlining of tissue contours for the estimation of SUVmax in ROI. The disadvantage of this method was the lack of reproducibility with respect to the anatomical location of the selected liver fragment in the examined patients. The position of the intervertebral disc between Th11 and Th12 may correspond to very different liver segments in different patients. Method 3, used in the presented study, was regarded by the authors as the optimal technique for VOI segmentation and the assessment of normal ranges for SUV. It allowed for reproducible localization of the medium VOI (with a mean volume of 31 mL) within liver segments VII and VIII (in transverse SPECT slices from different patients), based on the dimensional analysis of its coronal and sagittal CT slices.

All mean values of SUVbw max, SUVbw mean, SUVlbm max, and SUVlbm mean calculated for hot liver lesions in the "pathological group" were several times higher than the upper limits of normal ranges for SUVs obtained with all methods.

The effect of biological and physical factors on the variability of SUV (different biokinetics of the radiopharmaceutical in patients, different time intervals between the injection and start of SPECT/CT acquisition) can be limited by using relative SUV ratios: SUV spleen/SUV liver and SUV liver/SUV gluteus medius muscle. Normal ranges for SUV spleen/SUV liver ratios calculated in our

study have lower variance (an average of 19%) compared to normal ranges for SUV liver. The variance of the mean normal range for the SUV liver/SUV gluteus medius ratio has the same feature, except for SUVmean estimated.

Phantom validation revealed good accuracy (maximum relative SE ~ 11%) of the volume and concentration measurement in hot spheres with diameters: 22, 28, and 37 mm (VOI 5.6, 11.5, and 26.5 mL, respectively). The clinical results for the accuracy of concentration measurements obtained in our study for the three largest spheres were consistent with the results reported by the GE Healthcare laboratory [13]. The accuracy of the activity concentration measurement for a sphere with a 17 mm diameter (volume 2.6 mL) in our study was 8% lower than the accuracy obtained by the GE Healthcare laboratory. SUVs calculated for hot liver lesions with volumes smaller than 5 mL are biased with a significant measurement error.

The shape of RCmax corresponds with recovery coefficients reported by other researchers [21–23].

Conclusions

Segmentation in the mid-coronal CT image, at one-fourth of the height of the liver measured from the top, with a medium-sized VOI outlined on a given transverse SPECT slice was regarded as the optimal method for estimating normal ranges for standardized uptake values.

It is necessary to standardize quantification methods in the SPECT/CT studies. Our work is a step forward in obtaining standardization of SPECT/CT SUV calculation methods.

Calculations for radiopharmaceutical uptake in tumors with volumes smaller than 5 mL are biased with a significant measurement error.

Availability of data and material

The datasets generated during and/or analyzed during the current study are available from the corresponding author on reasonable request.

Authors' contributions

All authors contributed to the study's conception and design. Material preparation, data collection and analysis were performed by Sara Kurkowska, Hanna Piwowska-Bilska and Bozena Birkenfeld. The first draft of the manuscript was written by Hanna Piwowska-Bilska and all authors commented on previous versions of the manuscript. All authors read and approved the final manuscript.

Ethics approval and consent to participate

Ethical approval was waived by the local Ethics Committee of Pomeranian Medical University in view of the retrospective nature of the study and all the procedures being performed were part of the routine care.

Conflict of interest






The authors declare that they have no competing interests.

References

- Schillaci O, Spanu A, Palumbo B, et al. SPECT/CT in neuroendocrine tumours. *Clin Transl Imaging*. 2014; 2(6): 477–489, doi: [10.1007/s40336-014-0091-x](https://doi.org/10.1007/s40336-014-0091-x).
- Sharma P, Singh H, Bal C, et al. PET/CT imaging of neuroendocrine tumors with (68)Gallium-labeled somatostatin analogues: An overview and single institutional experience from India. *Indian J Nucl Med*. 2014; 29(1): 2–12, doi: [10.4103/0972-3919.125760](https://doi.org/10.4103/0972-3919.125760), indexed in Pubmed: [24591775](https://pubmed.ncbi.nlm.nih.gov/24591775/).
- Gabriel M, Decristoforo C, Donnemiller E, et al. An inpatient comparison of 99m Tc-EDDA/HYNIC-TOC with 111 In-DTPA-octreotide for diagnosis of somatostatin receptor-expressing tumors. *J Nucl Med*. 2003; 44(5): 708–16, indexed in Pubmed: [12732671](https://pubmed.ncbi.nlm.nih.gov/12732671/).
- Briganti V, Cuccurullo V, Berti V, et al. Tc-EDDA/HYNIC-TOC is a New Opportunity in Neuroendocrine Tumors of the Lung (and in other Malignant and Benign Pulmonary Diseases). *Curr Radiopharm*. 2020; 13(3): 166–176, doi: [10.2174/1874471013666191230143610](https://doi.org/10.2174/1874471013666191230143610), indexed in Pubmed: [31886756](https://pubmed.ncbi.nlm.nih.gov/31886756/).
- Artiko V, Sobic-Saranovic D, Pavlovic S, et al. The clinical value of scintigraphy of neuroendocrine tumors using (99m)Tc-HYNIC-TOC. *J BUON*. 2012; 17(3): 537–542, indexed in Pubmed: [23033296](https://pubmed.ncbi.nlm.nih.gov/23033296/).
- Trogrlic M, Težak S. Incremental value of Tc-HYNIC-TOC SPECT/CT over whole-body planar scintigraphy and SPECT in patients with neuroendocrine tumours. *Nuklearmedizin*. 2017; 56(3): 97–107, doi: [10.3413/Nukmed-0851-16-10](https://doi.org/10.3413/Nukmed-0851-16-10), indexed in Pubmed: [28164207](https://pubmed.ncbi.nlm.nih.gov/28164207/).
- Yamaga LY, Neto GC, da Cunha ML, et al. 99mTc-HYNIC-TOC increased uptake can mimic malignancy in the pancreas uncinatate process at somatostatin receptor SPECT/CT. *Radiol Med*. 2016; 121(3): 225–228, doi: [10.1007/s11547-015-0593-2](https://doi.org/10.1007/s11547-015-0593-2), indexed in Pubmed: [26558391](https://pubmed.ncbi.nlm.nih.gov/26558391/).
- Boellaard R, O'Doherty MJ, Weber WA, et al. FDG PET and PET/CT: EANM procedure guidelines for tumour PET imaging: version 1.0. *Eur J Nucl Med Mol Imaging*. 2010; 37(1): 181–200, doi: [10.1007/s00259-009-1297-4](https://doi.org/10.1007/s00259-009-1297-4), indexed in Pubmed: [19915839](https://pubmed.ncbi.nlm.nih.gov/19915839/).
- European Medicines Agency. Assessment report. SomaKit TOC International non-proprietary name: edotreotide Procedure No. EMEA/H/C/004140/0000. EMA/734748/2016 Committee for Medicinal Products for Human Use (CHMP). 2016.
- Krenning EP, Bakker WH, Breeman WA, et al. Localisation of endocrine-related tumours with radioiodinated analogue of somatostatin. *Lancet*. 1989; 1(8632): 242–244, doi: [10.1016/s0140-6736\(89\)91258-0](https://doi.org/10.1016/s0140-6736(89)91258-0), indexed in Pubmed: [2563413](https://pubmed.ncbi.nlm.nih.gov/2563413/).
- Hope TA, Calais J, Zhang Li, et al. 111 In-Pentetreotide Scintigraphy Versus Ga-DOTATATE PET: Impact on Krenning Scores and Effect of Tumor Burden. *J Nucl Med*. 2019; 60(9): 1266–1269, doi: [10.2967/jnumed.118.223016](https://doi.org/10.2967/jnumed.118.223016), indexed in Pubmed: [30850506](https://pubmed.ncbi.nlm.nih.gov/30850506/).
- Beck M, Sanders JC, Ritt P, et al. Longitudinal analysis of bone metabolism using SPECT/CT and (99m)Tc-diphosphono-propanedicarboxylic acid: comparison of visual and quantitative analysis. *EJNMMI Res*. 2016; 6(1): 60, doi: [10.1186/s13550-016-0217-4](https://doi.org/10.1186/s13550-016-0217-4), indexed in Pubmed: [27464623](https://pubmed.ncbi.nlm.nih.gov/27464623/).
- NM Quantification. Q.Metrix for SPECT/CT Package. White Paper, DOC1951185, GE Healthcare 2017.
- Kim CK, Gupta NC, Chandramouli B, et al. Standardized uptake values of FDG: body surface area correction is preferable to body weight correction. *J Nucl Med*. 1994; 35(1): 164–167, indexed in Pubmed: [8271040](https://pubmed.ncbi.nlm.nih.gov/8271040/).
- Sugawara Y, Zasadny KR, Neuhoff AW, et al. Reevaluation of the standardized uptake value for FDG: variations with body weight and methods for correction. *Radiology*. 1999; 213(2): 521–525, doi: [10.1148/radiology.213.2.r99nv37521](https://doi.org/10.1148/radiology.213.2.r99nv37521), indexed in Pubmed: [10551235](https://pubmed.ncbi.nlm.nih.gov/10551235/).
- Zeintl J, Vija AH, Yahil A, et al. Quantitative accuracy of clinical 99mTc SPECT/CT using ordered-subset expectation maximization with 3-dimensional resolution recovery, attenuation, and scatter correction. *J Nucl Med*. 2010; 51(6): 921–928, doi: [10.2967/jnumed.109.071571](https://doi.org/10.2967/jnumed.109.071571), indexed in Pubmed: [20484423](https://pubmed.ncbi.nlm.nih.gov/20484423/).

17. Vandervoort E, Celler A, Harrop R. Implementation of an iterative scatter correction, the influence of attenuation map quality and their effect on absolute quantitation in SPECT. *Phys Med Biol.* 2007; 52(5): 1527–1545, doi: [10.1088/0031-9155/52/5/020](https://doi.org/10.1088/0031-9155/52/5/020), indexed in Pubmed: [17301469](https://pubmed.ncbi.nlm.nih.gov/17301469/).
18. Willowson K, Bailey DL, Baldock C. Quantitative SPECT reconstruction using CT-derived corrections. *Phys Med Biol.* 2008; 53(12): 3099–3112, doi: [10.1088/0031-9155/53/12/002](https://doi.org/10.1088/0031-9155/53/12/002), indexed in Pubmed: [18495976](https://pubmed.ncbi.nlm.nih.gov/18495976/).
19. Shcherbinin S, Celler A, Belhocine T, et al. Accuracy of quantitative reconstructions in SPECT/CT imaging. *Phys Med Biol.* 2008; 53(17): 4595–4604, doi: [10.1088/0031-9155/53/17/009](https://doi.org/10.1088/0031-9155/53/17/009), indexed in Pubmed: [18678930](https://pubmed.ncbi.nlm.nih.gov/18678930/).
20. Huang SC. Anatomy of SUV. Standardized uptake value. *Nucl Med Biol.* 2000; 27(7): 643–646, doi: [10.1016/s0969-8051\(00\)00155-4](https://doi.org/10.1016/s0969-8051(00)00155-4), indexed in Pubmed: [11091106](https://pubmed.ncbi.nlm.nih.gov/11091106/).
21. Peters SMB, van der Werf NR, Segbers M, et al. Towards standardization of absolute SPECT/CT quantification: a multi-center and multi-vendor phantom study. *EJNMMI Phys.* 2019; 6(1): 29, doi: [10.1186/s40658-019-0268-5](https://doi.org/10.1186/s40658-019-0268-5), indexed in Pubmed: [31879813](https://pubmed.ncbi.nlm.nih.gov/31879813/).
22. Gnesin S, Leite Ferreira P, Malterre J, et al. Phantom Validation of Tc-99m Absolute Quantification in a SPECT/CT Commercial Device. *Comput Math Methods Med.* 2016; 2016: 4360371, doi: [10.1155/2016/4360371](https://doi.org/10.1155/2016/4360371), indexed in Pubmed: [28096891](https://pubmed.ncbi.nlm.nih.gov/28096891/).
23. Collarino A, Pereira Arias-Bouda LM, Valdés Olmos RA, et al. Experimental validation of absolute SPECT/CT quantification for response monitoring in breast cancer. *Med Phys.* 2018; 45(5): 2143–2153, doi: [10.1002/mp.12880](https://doi.org/10.1002/mp.12880), indexed in Pubmed: [29572848](https://pubmed.ncbi.nlm.nih.gov/29572848/).

Optimal activity of [¹⁸F]FDG for Hodgkin lymphoma imaging performed on PET/CT camera with BGO crystals

Mirosław Dziuk^{1,2}, Ewa Witkowska-Patena^{1,2}, Agnieszka Gizewska^{1,2}, Andrzej Mazurek^{1,2}, Anna Pieczonka³, Magdalena Koza¹, Marina Gerszewska¹, Zbigniew Podgajny³, Marta Chojnowska²

¹Affidea PET/CT Warsaw, Poland

²Department of Nuclear Medicine, Military Institute of Medicine, Warsaw, Poland

³Dolnoslaskie Affidea PET/CT Centre, Wrocław, Poland

[Received 17 XI 2021; Accepted 29 XII 2021]

Abstract

Background: We aimed to find the minimum feasible activity of fluorodeoxyglucose ([¹⁸F]FDG) in positron emission tomography/computed tomography (PET/CT) of Hodgkin lymphoma patients performed on a camera with bismuth germanate (BGO) crystals.

Material and methods: Ninety-one [¹⁸F]FDG PET/CT scans (each in seven Bayesian Penalized Likelihood [BPL] reconstructions with varying acquisition time per bed position — 2 min, 1.5 min, 1 min, 50 s, 40 s, 30 s, and 20 s) were independently assessed by three physicians to evaluate image quality. Mean administered activity was 3.0 ± 0.1 MBq/kg and mean uptake time was 54.0 ± 8.7 min. The series quality was subjectively marked on a 1–10 scale and then ranked 1–7 based on the mean mark. Interobserver rank correlation and intraclass correlation within each series for the three observers were calculated. Phantom studies were also performed to determine if reduced acquisition time can be directly translated into a reduced activity.

Results: Time series were marked and ranked unanimously — the longer the time of acquisition the higher the mark and rank. The interobserver agreement in the ranking was excellent (100%) with a kappa coefficient of 1.00 (95% CI [0.83–1.0]). The general intraclass correlation coefficient (agreement between the marks observers gave each time series) was very high (0.945, 95% CI [0.936–0.952]) and was higher the shorter the time per bed. According to all three observers only the series with 2 min and 1.5 min acquisition time were appropriate for assessment (mean mark ≥ 7). In phantom studies there was a linear correlation between time per bed, administered activity, and number of total prompts detected by a scanner. Hence, a reduction of acquisition time of 25% (from 2 min to 1.5 min) could be directly translated into a 25% activity reduction (from 3.0 to 2.25 MBq/kg).

Conclusions: In patients with HL, [¹⁸F]FDG activity can be reduced by up to 25% when using a BGO crystal camera, without substantial impact on image quality.

KEY words: activity reduction; [¹⁸F]FDG; PET/CT; Hodgkin lymphoma; BGO

Nucl Med Rev 2022; 25, 1: 47–53

Introduction

The dual-modality positron emission tomography/computed tomography (PET/CT) is nowadays a primary imaging method for

a wide range of oncologic, cardiologic, and neurologic diseases. It is used at various stages of the treatment process—from diagnosis and primary staging to treatment response assessment [1–4].

Despite its many advantages, PET/CT is a diagnostic method associated with notable radiation exposure and that may raise concern. During a PET/CT scan patients receive radiation both from the radiotracer and from the CT. The effective dose of the 18F-2-fluoro-2-deoxy-D-glucose ([¹⁸F]FDG) PET/CT may reach 25–30 mSv, depending on the CT protocol (high-dose diagnostic

Correspondence to: Ewa Witkowska-Patena, Department of Nuclear Medicine, Military Institute of Medicine, Szaserow 128, 04-141 Warsaw, Poland, e-mail: ewitkowska-patena@wim.mil.pl

CT vs low-dose CT for anatomic localization); the radiotracer activity (the effective dose of 18F-FDG is 0.019 mSv/MBq); the anatomical region; and the number of body parts imaged [5–7].

According to the guidelines (based on phantom experiments, theoretical estimations, and retrospective studies on heterogeneous populations), the administered activity of [¹⁸F]FDG should be 3.5–7 MBq/kg [8–13]. Currently, however, activities smaller than 4.0 MBq/kg are usually injected. In order to comply with the ALARA principle, which states that the activity administered should be As Low As Reasonably Achievable, PET/CT protocols are constantly optimized in order to further reduce the effective dose without compromising the image quality. In order to reduce the CT dose, we may: decrease the tube voltage, tube current or the exposure time, and minimize the Z-axis coverage. In the PET protocol, we may: use 3D acquisition mode or time-of-flight reconstruction, apply novel reconstruction algorithms such as Bayesian penalized likelihood (BPL), increase acquisition time per bed, and, finally, reduce the injected activity [8, 10, 14, 15].

The aim of the study was to determine the minimum feasible [¹⁸F]FDG activity that would not compromise the quality of images in patients with Hodgkin lymphoma obtained from a PET/CT scanner with bismuth germanium oxide (BGO) detectors.

Material and methods

Patients

We retrospectively evaluated 18F-FDG PET/CT scans of patients with Hodgkin lymphoma (HL) referred to the Dolnoslaskie Afidea PET/CT Centre for disease staging or response assessment between January 2017 and October 2018. Patient and PET/CT scan characteristics are summarized in Table 1.

Table 1. Characteristics of patients and performed positron emission/computed tomography (PET/CT) scans

CHARACTERISTIC	VALUE
Number of PET/CT scans	91
Number of patients	50
Gender	33 (66%) women, 17 (34%) men
Age	
mean ± SD	38.7 ± 16.5 years
median (range)	34.0 (12.0 – 85.0) years
Weight	
mean ± SD	71.0 ± 13.5 kg
median (range)	69.0 (37.0 – 101.0) kg
BMI	
mean ± SD	24.8 ± 4.2
median (range)	24.3 (14.8 – 35.4)
Administered activity	
mean ± SD	211.3 ± 40.3 MBq
median (range)	208.3 (110.7 – 318.1) MBq
Administered activity per kg	
mean ± SD	3.0 ± 0.1 MBq/kg
median (range)	3.0 (2.7 – 3.3) MBq/kg
Uptake time	
mean ± SD	54.0 ± 8.7 min
median (range)	52.0 (45.0 – 77.0) min

BMI — body mass index; MBq — megabecquerels; SD — standard deviation

Imaging protocol

PET/CT imaging was performed using a 5-ring PET/CT system Discovery IQ with BGO crystals (GE Healthcare, Chicago, Illinois, US). A scout view and a non-contrast-enhanced low-dose helical 16-slice CT scan were performed for attenuation correction of the PET emission data and for anatomic localization.

The CT scan was acquired with a tube voltage of 100–140 kV, current modulation, and pitch of 1.375:1. The X-ray tube rotation time was 0.6 s. The CT reconstructions were performed with a standard kernel with a slice thickness of 1.25 mm. Computed tomography dose index (CTDIvol) ranged from 1.19 to 7.02 mGy (depending on patient body mass).

Immediately after CT scanning, a whole-body three-dimensional PET was acquired. The scan range was from the top of the head to the mid-thighs. For each bed position (24% overlap) a 2 min list mode acquisition was used. The images were then reconstructed with a reduced time per bed of 1.5 min, 1 min, 50 s, 40 s, 30 s, and 20 s. The emission data were corrected for geometrical response and detector efficiency (normalization) as well as for system dead time, random coincidences, scatter, and attenuation. Attenuation corrected images were reconstructed with Bayesian Penalized Likelihood (Q.Clear) algorithm [16–21]. The matrix size was 256 x 256 and the voxel size 2.73 x 2.73 x 2.78 mm³. The resolution recovery algorithm (GE SharpIR) was used. Q.Clear images were reconstructed with beta values of 350, no post-filtering.

Image analysis

PET/CT images were analyzed with GE Healthcare Advantage Workstation (Chicago, Illinois, United States) independently by three experienced nuclear medicine physicians. Each reviewer assessed PET/CT scans in seven-time series (blinded and presented in random order): one standard series with a 2 min acquisition time (1) and six series with reduced acquisition time (2) 1.5 min, (3) 1 min, (4) 50 s, (5) 40 s, (6) 30 s and (7) 20 s. The image quality of each series was graded subjectively on a ten-point scale where “1” was given to images with the poorest quality and “10” to images with the highest quality. Image smoothness, tumor-to-background ratio, and background uptake (measured in the mediastinal blood pool) were taken into consideration. Grades 7–10 were given to images with good or very good quality (appropriate for analysis). Grades 5–6 were given to images with mediocre quality and < 5 to images of poor quality (inappropriate for assessment). The assessing physicians also measured maximum standardized uptake values (SUVmax) of the liver, mediastinal blood pool (MBP), and three random target lesions.

Phantom studies

In order to define whether reduced time per bed can be directly translated into reduced radiotracer activity, phantom studies were performed. A National Electrical Manufacturers Association (NEMA) phantom, a water phantom (GE Healthcare, Chicago, Illinois, US), and a syringe source were used. The NEMA and water phantoms were filled with background activity of 32.3 MBq and 56.1 MBq and then scanned (using the same Discovery IQ PET/CT system) for 2 min, 1.5 min, and 1 min to measure the number of total prompts (depending on the time per bed). Three syringe sources were filled with initial activities of 97.3 MBq, 56.2

MBq, and 57.9 MBq and then scanned after 44 min and 109 min which imitated a 25% and a 50% activity reduction, respectively. The number of total prompts measured was then compared with an estimated number to verify the correlation between the activity and the total number of prompts.

Statistical analysis

SPSS Statistics 25 software (Armonk, New York, US) was used for the statistical analysis. Descriptive analysis was performed by calculating mean, median, standard deviation, and range. Cohen's kappa was used for inter-observer agreement in ranking. The intraclass correlation coefficient (ICC [3;1]) was used to calculate the inter-observer agreement for each series. A *p*-value < 0.05 was considered significant.

Results

The mean and median grade values for image quality were highest for series with the longest acquisition time and decreased with decreasing time per bed (Fig. 1, Tab. 2). Series 1 (2 min per

bed) received the highest points from all three observers, followed by series 2, then series 3, etc. which resulted in the final ranking as shown in Table 1. The interobserver agreement in the ranking was excellent (100%) with a kappa coefficient of 1.00 (95% CI [0.83–1.0]). According to all three observers, only the series with 2 min and 1.5 min acquisition time (series 1 and 2, respectively) were appropriate for assessment (mean mark ≥ 7).

The general intraclass correlation coefficient was very high (0.945, 95% CI [0.936–0.952]) and was higher the shorter the time per bed (Tab. 3, Fig. 2).

In the phantom study, we observed that decreasing time per bed was directly proportional to the decrease in total prompts — a 25% decrease in acquisition time (from 2 min to 1.5 min) resulted in a likewise decrease in total prompts number (Tab. 4).

Phantom studies with the use of the three syringe sources showed the number of total prompts decreased directly proportionally to the administered activity — a 25% activity reduction resulted in a 25% reduction in the total prompts number. The difference in the number of estimated and measured total prompts was ± 5% (Tab. 5).

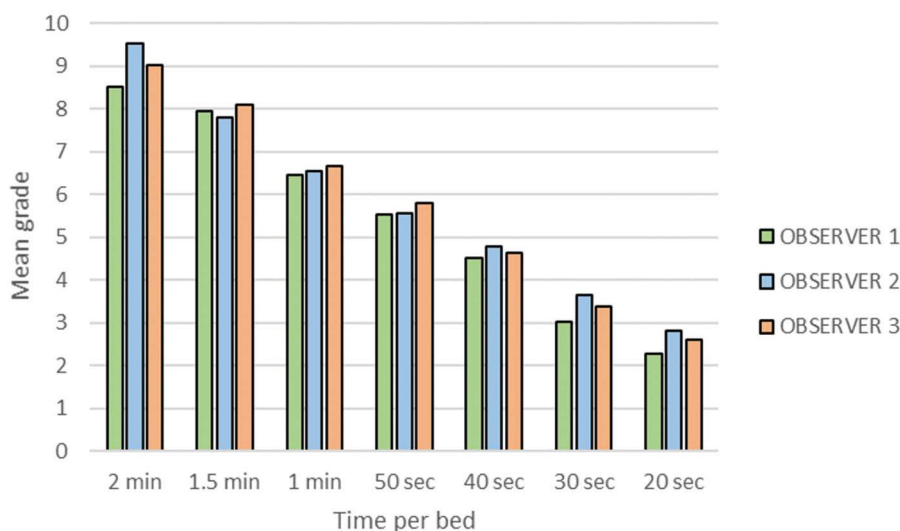


Figure 1. Mean observers' grades for each time per bed series

Table 2. The descriptive statistics of each assessed series (1–7) with their ranks given by the three observers. Series with mean rank ≥ 7 (appropriate for assessment) were highlighted

SERIES	OBSERVER 1						OBSERVER 2						OBSERVER 3						SUM OF PTS	3OBS RANK	MEAN RANK	BEST RANK	WORST RANK
	MN	SD	MDN	NO. OF GRADES	PTS	RANK	MN	SD	MDN	NO. OF GRADES	PTS	RANK	MN	SD	MDN	NO. OF GRADES	PTS	RANK					
2 [min]	8.52	1.2	9	82	7	1.	9.52	0.8	10	85	7	1.	9.03	0.9	9	86	7	1.	21	1.	1.7	1.	1.
1.5 [min]	7.95	1.5	8	86	6	2.	7.79	1	8	85	6	2.	8.1	1.1	8	89	6	2.	18	2.	3.0	2.	2.
1 [min]	6.46	2	6	83	5	3.	6.56	1.1	7	88	5	3.	6.66	1.2	7	87	5	3.	15	3.	4.0	3.	3.
50 [s]	5.53	2.1	5.5	86	4	4.	5.57	1.3	6	88	4	4.	5.8	1.3	6	89	4	4.	13	4.	5.0	4.	4.
40 [s]	4.5	2	4	84	3	5.	4.77	1.2	5	84	3	5.	4.64	1.4	4	88	3	5.	9	5.	6.0	5.	5.
30 [s]	3.01	1.5	3	84	2	6.	3.65	1.1	4	86	2	6.	3.39	1.3	3	87	2	6.	6	6.	7.0	6.	6.
20 [s]	2.28	1.7	2	82	1	7.	2.81	1.1	3	81	1	7.	2.59	1.4	2	86	1	7.	3	7.	8.0	7.	7.

MDN — median; MN — mean; PTS — points; SD — standard deviation; 3OBS RANK — final rank from all observers

Table 3. The inter-observer agreement for each positron emission tomography (PET) series

Series	ICC	95%CI LL	95%CI UL
2 [min]	0.500	0.279	0.662
1.5 [min]	0.628	0.463	0.749
1 [min]	0.727	0.606	0.816
50 [s]	0.713	0.586	0.805
40 [s]	0.777	0.677	0.850
30 [s]	0.834	0.761	0.887
20 [s]	0.859	0.795	0.905
Total	0.945	0.936	0.952

CI – confidence interval; ICC – intra-class correlation coefficient; LL – lower limit; UL – upper limit

Table 4. Total prompts measured in the NEMA and water phantoms for three different acquisition times — 2 min, 1.5 min and 1 min

Time per bed	Total prompts (NEMA phantom)	Total prompts (water phantom)
2 [min]	4.66×10^7	1.49×10^8
1.5 [min]	3.5×10^7	1.12×10^8
(25% decrease)	(24.9% decrease)	(24.8% decrease)
1 [min]	2.34×10^7	7.40×10^7
(50% decrease)	(49.8% decrease)	(50.3% decrease)

NEMA — National Electrical Manufacturers Association

We observed that SUVmax values measured in the liver, MBP, and target lesions were decreasing the longer the time per bed. The target-to-liver and target-to-MBP ratios increased when time per bed was increased (Fig.3, Tab. 6).

Discussion

In our study, we aimed to determine the maximum [¹⁸F] FGD activity reduction on a BGO PET/CT camera that would not compromise the image quality. The minimum feasible activity was defined by proxy — we checked if reduction of acquisition time can be directly translated into activity reduction. We showed that there is a linear correlation between time per bed, administered activity, and the number of total prompts detected by the scanner. Hence, we demonstrated that time per bed reduction is directly proportional to activity reduction. In the visual analysis, we reported that a 25% reduction of time per bed (from 2 min to 1.5 min) did not compromise image quality significantly. This in turn could be translated into a 25% tracer activity reduction — from 3.0 to 2.25

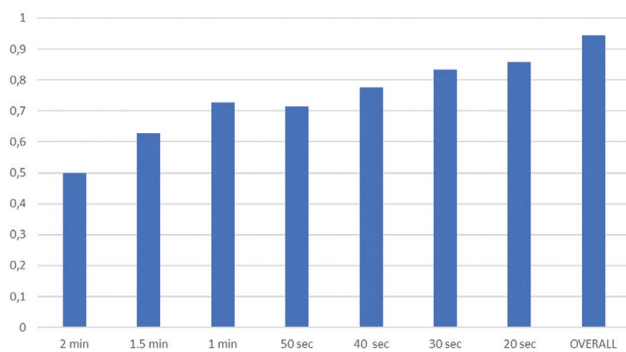


Figure 2. The intra-class correlation coefficient for each PET series; PET — positron emission tomography

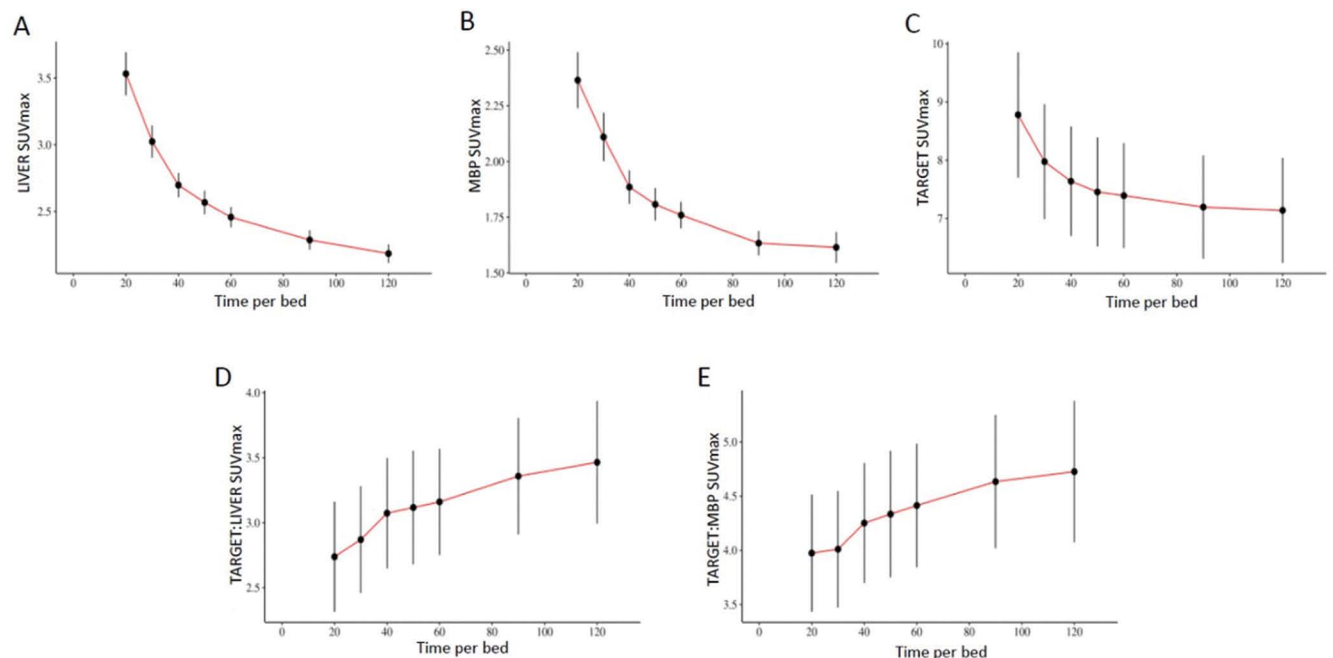
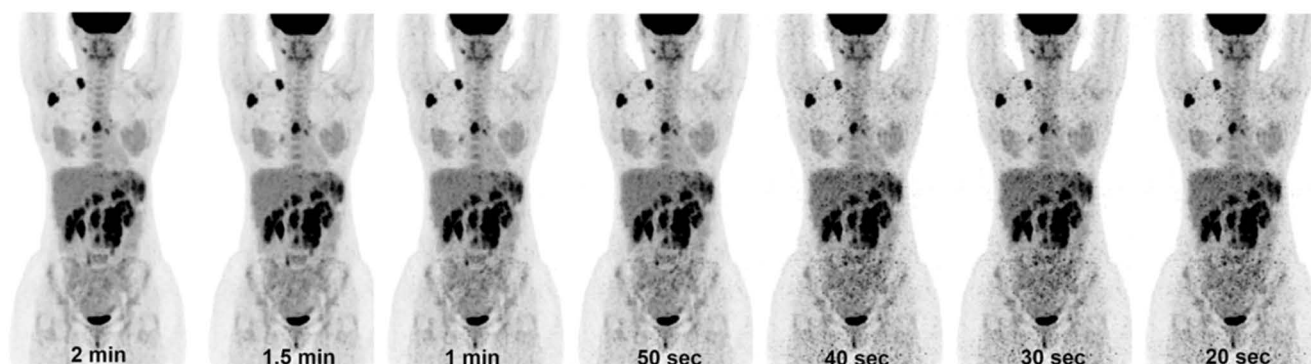


Figure 3. Mean SUVmax values with 95% confidence intervals

Table 5. Decrease in [¹⁸F]FDG activity and number of total prompts in time

No. of syringe	¹⁸ F]FDG activity after time (% decrease)			No. of total prompts measured after time (% decrease)		
	0 [min]	44 [min]	109 [min]	0 [min]	44 [min]	109 [min]
1	97.3 MBq	72.0 MBq (26%)	47.6 MBq (51.1%)	9.88 × 10 ⁸	7.3×10 ⁸ (26.1%)	4.54 × 10 ⁸ (54%)
2	56.2 MBq	44.1 MBq (21.5%)	25.9 MBq (53.9%)	5.29 × 10 ⁸	3.9×10 ⁸ (26.3%)	2.59 × 10 ⁸ (51%)
3	57.9 MBq	43.9 MBq (24.2%)	28.9 MBq (50.1)%	5.26 × 10 ⁸	3.85×10 ⁸ (26.8%)	2.40 × 10 ⁸ (54.4%)

**Figure 4.** Maximum intensity projection images of the same patient with decreasing time per bed

MBq/kg. We reported that administration of reduced activity with 2 min time per bed acquisition is a feasible protocol that does not compromise the image quality.

The radiation dose reduction from PET/CT scans can be achieved by optimizing either PET or CT scanning protocols. It has been robustly shown that various alterations in CT protocols may cut the used radiation by as much as 1/3 (from 8.1 mSv to 5.5 mSv) [22].

According to the European Association of Nuclear Medicine (EANM) recommendations, the minimum administered activity for a gamma camera as we used in the study (with ≤ 30% bed overlap) and a 2 min time per bed should be 7 MBq/kg. The guidelines also state that the dose can be lowered for PET/CT systems with higher sensitivity or improved performance [8]. In our institution — according to national regulations, instructions from the producer of our PET/CT system, available literature, and our personal experience — we routinely administer activities of about 3.7 MBq/kg with an acquisition time of 1.5 min [16, 17].

Experimentally, for the purpose of the study, we have reduced the administered activity to 3.0 MBq/kg. We show that further reduction to 2.25 MBq/kg with 2 min acquisition time might be feasible (Fig. 4). It is in accordance with a study performed on the same type of scanner (GE Discovery IQ) that showed similarly high sensitivity and performance of the camera after the injection of 2.5 MBq/kg of [¹⁸F]FDG. The high sensitivity of the scanner was achieved by adopting several technological solutions such as the 3-dimensional mode, extension of the axial field of view (FOV), and increasing the number of detector rings from 2 to 5 along the FOV [23, 24]. The system also uses a new reconstruction algorithm (Bayesian

penalized likelihood algorithm named Q.Clear) that improves signal-to-noise ratio and standardized uptake value (SUV) quantification. In Q.Clear the noise suppression is controlled by a penalty term beta (the only user-adjusted term in the algorithm). The algorithm also incorporates point-spread-function modeling [25–27].

Prieto et al. showed that an average [¹⁸F]FDG activity reduction of 23.4% (down to 3.57 MBq/kg) is feasible without significant impairment of image quality [28]. On the other hand, Murray et al. reported that emission scans as short as 15 s per bed position sufficiently identified tumor lesions for quantification. The scans were performed on a Gemini TF PET/CT system after injection of 269–411 MBq of [¹⁸F]FDG (3.8–5.9 MBq for a 70 kg patient) [29]. As shown, contemporary PET/CT technology allows for a notable reduction of radiotracer activities compared to the current guidelines.

The findings of this study have to be seen in the light of some limitations. First, the research focused on a single clinical condition — Hodgkin lymphoma. It is highly probable that a 25% activity reduction would also be feasible in other aggressive, FDG-avid lymphomas and malignancies yet it may not be so in the case of indolent tumors. Hence, further research on more heterogeneous groups of patients is needed to explore this subject. Our research is a retrospective study and might show some of the method's inherent limitations such as selection bias or confounding.

Conclusions

In a BGO PET/CT scanner [¹⁸F]FDG activities as low as 2.25 MBq/kg are feasible when Hodgkin lymphoma patients are concerned. The reduced activity is especially important in this setting

Table 6. Maximum standardised uptake values measure in the liver mediastinal blood pool and target lesions

		M	Me	SD	IQR	Min	Max
LIVER SUVmax	20 [s]	3.53	3.40	0.77	0.90	2.10	5.50
	30 [s]	3.02	3.00	0.58	0.80	1.90	5.00
	40 [s]	2.70	2.70	0.44	0.50	1.80	4.00
	50 [s]	2.57	2.60	0.42	0.50	1.70	4.10
	60 [s]	2.46	2.50	0.36	0.40	1.70	3.70
	90 [s]	2.29	2.25	0.35	0.40	1.60	3.20
MBP SUVmax	120 [s]	2.18	2.20	0.33	0.30	1.60	3.20
	20 [s]	2.37	2.30	0.60	0.70	1.20	4.30
	30 [s]	2.11	2.00	0.52	0.50	1.30	3.80
	40 [s]	1.89	1.90	0.36	0.50	1.30	3.10
	50 [s]	1.81	1.80	0.35	0.30	1.10	2.90
	60 [s]	1.76	1.70	0.28	0.30	1.30	2.60
TARGET SUVmax	90 [s]	1.64	1.60	0.26	0.38	1.10	2.40
	120 [s]	1.62	1.60	0.33	0.40	1.00	3.20
	20 [s]	8.78	7.90	4.17	6.12	2.00	23.10
	30 [s]	7.98	7.50	3.82	5.62	2.00	17.70
	40 [s]	7.64	7.23	3.64	5.58	1.90	16.60
	50 [s]	7.45	7.17	3.62	5.57	1.80	16.73
TARGET: LIVER SUVmax	60 [s]	7.38	6.90	3.47	5.17	1.80	16.07
	90 [s]	7.18	7.10	3.41	5.20	1.50	15.67
	120 [s]	7.12	7.00	3.46	5.30	1.40	15.47
	20 [s]	2.74	2.45	1.64	1.59	0.36	11.00
	30 [s]	2.87	2.63	1.59	1.54	0.57	8.70
	40 [s]	3.07	2.83	1.65	2.18	0.66	7.64
TARGET: MBP SUVmax	50 [s]	3.12	2.98	1.69	2.15	0.67	7.53
	60 [s]	3.16	2.97	1.58	2.07	0.72	7.74
	90 [s]	3.36	3.07	1.73	2.48	0.71	7.82
	120 [s]	3.46	3.18	1.83	2.51	0.64	7.73
	20 [s]	3.97	3.38	2.09	2.12	0.69	12.16
	30 [s]	4.01	3.76	2.08	2.94	0.83	9.88
TARGET: MBP SUVmax	40 [s]	4.25	3.72	2.14	3.22	1.12	8.94
	50 [s]	4.33	3.94	2.26	3.02	1.00	9.84
	60 [s]	4.41	4.18	2.21	2.96	1.06	9.45
	90 [s]	4.63	4.41	2.39	3.30	1.07	9.79
	120 [s]	4.73	4.35	2.52	3.68	1.00	10.42

M — mean; Me — median; SD — standard deviation; IQR — interquartile range; Min — minimum; Max — maximum; MBP — mediastinal blood pool; SUVmax — maximum standardised uptake value

because HL patients undergo multiple PET/CT examinations throughout the clinical process.

Ethics approval and consent to participate

The research has been performed in accordance with the Declaration of Helsinki and its further amendments. The study

has been granted ethics committee approval (Military Medical Chamber Ethics Committee, reference no. 150/17, April 28, 2017). Informed consent was obtained from all study participants.

Consent for publication

Consent for publication was obtained from all study participants.

Availability of data and materials

All data generated or analyzed during this study are included in this published article and its supplementary information files.

Conflict of interest

The authors declare that they have no competing interests.

Funding

The authors received no specific funding for this work.

Authors' contributions

MD designed the study, analyzed the data, and contributed to writing the manuscript. EWP designed the study, collected and analyzed the data, and was the main contributor in writing the manuscript. AG and AM collected and analyzed the data. AP, MK, and MG were the main contributors to the phantom experiments. ZP designed the study and collected the data. MC collected the data. All authors read and approved the final manuscript.

References

- Murgu SD. Diagnosing and staging lung cancer involving the mediastinum. *Chest*. 2015; 147(5): 1401–1412, doi: [10.1378/chest.14-1355](https://doi.org/10.1378/chest.14-1355), indexed in Pubmed: [25940251](https://pubmed.ncbi.nlm.nih.gov/25940251/).
- Saraste A, Barbato E, Capodanno D, et al. Imaging in ESC clinical guidelines: chronic coronary syndromes. *Eur Heart J Cardiovasc Imaging*. 2019; 20(11): 1187–1197, doi: [10.1093/ehjci/jez219](https://doi.org/10.1093/ehjci/jez219), indexed in Pubmed: [31642920](https://pubmed.ncbi.nlm.nih.gov/31642920/).
- Cheson BD, Fisher RI, Barrington SF, et al. Recommendations for initial evaluation, staging, and response assessment of Hodgkin and non-Hodgkin lymphoma: the Lugano classification. *J Clin Oncol*. 2014; 32(27): 3059–3068, doi: [10.1200/JCO.2013.54.8800](https://doi.org/10.1200/JCO.2013.54.8800), indexed in Pubmed: [25113753](https://pubmed.ncbi.nlm.nih.gov/25113753/).
- van Waarde A, Marcolini S, de Deyn PP, et al. PET Agents in Dementia: An Overview. *Semin Nucl Med*. 2021; 51(3): 196–229, doi: [10.1053/j.semnuclmed.2020.12.008](https://doi.org/10.1053/j.semnuclmed.2020.12.008), indexed in Pubmed: [33500121](https://pubmed.ncbi.nlm.nih.gov/33500121/).
- Delbeke D, Coleman RE, Guiberteau MJ, et al. Procedure guideline for tumor imaging with 18F-FDG PET/CT 1.0. *J Nucl Med*. 2006; 47(5): 885–895, indexed in Pubmed: [16644760](https://pubmed.ncbi.nlm.nih.gov/16644760/).
- Brix G, Lechel U, Glatting G, et al. Radiation exposure of patients undergoing whole-body dual-modality 18F-FDG PET/CT examinations. *J Nucl Med*. 2005; 46(4): 608–613, indexed in Pubmed: [15809483](https://pubmed.ncbi.nlm.nih.gov/15809483/).
- Quinn B, Dauer Z, Pandit-Taskar N, et al. Radiation dosimetry of 18F-FDG PET/CT: incorporating exam-specific parameters in dose estimates. *BMC Med Imaging*. 2016; 16(1): 41, doi: [10.1186/s12880-016-0143-y](https://doi.org/10.1186/s12880-016-0143-y), indexed in Pubmed: [27317478](https://pubmed.ncbi.nlm.nih.gov/27317478/).
- Boellaard R, Delgado-Bolton R, Oyen WJG, et al. FDG PET/CT: EANM procedure guidelines for tumour imaging: version 2.0. *Eur J Nucl Med Mol Imaging*. 2015; 42(2): 328–354, doi: [10.1007/s00259-014-2961-x](https://doi.org/10.1007/s00259-014-2961-x), indexed in Pubmed: [25452219](https://pubmed.ncbi.nlm.nih.gov/25452219/).

9. Daube-Witherspoon ME, Karp JS, Casey ME, et al. PET Performance Measurements Using the NEMA NU 2-2001 Standard. *J Nucl Med. Society of Nuclear Medicine.* 2002; 43(10): 1398–409, indexed in Pubmed: [12368380](#).
10. Watson CC, Casey ME, Bendriem B, et al. Optimizing injected dose in clinical PET by accurately modeling the counting-rate response functions specific to individual patient scans. *J Nucl Med.* 2005; 46(11): 1825–1834, indexed in Pubmed: [16269596](#).
11. de Groot EH, Post N, Boellaard R, et al. Optimized dose regimen for whole-body FDG-PET imaging. *EJNMMI Res.* 2013; 3(1): 63, doi: [10.1186/2191-219X-3-63](#), indexed in Pubmed: [23938036](#).
12. Chang T, Chang G, Kohlmyer S, et al. Effects of injected dose, BMI and scanner type on NECR and image noise in PET imaging. *Phys Med Biol.* 2011; 56(16): 5275–5285, doi: [10.1088/0031-9155/56/16/013](#), indexed in Pubmed: [21791730](#).
13. Makris NE, Huisman MC, Kinahan PE, et al. Evaluation of strategies towards harmonization of FDG PET/CT studies in multicentre trials: comparison of scanner validation phantoms and data analysis procedures. *Eur J Nucl Med Mol Imaging.* 2013; 40(10): 1507–1515, doi: [10.1007/s00259-013-2465-0](#), indexed in Pubmed: [23754762](#).
14. Karp JS, Surti S, Daube-Witherspoon ME, et al. Benefit of time-of-flight in PET: experimental and clinical results. *J Nucl Med.* 2008; 49(3): 462–470, doi: [10.2967/jnumed.107.044834](#), indexed in Pubmed: [18287269](#).
15. Vallot D, Caselles O, Chaltiel L, et al. A clinical evaluation of the impact of the Bayesian penalized likelihood reconstruction algorithm on PET FDG metrics. *Nucl Med Commun.* 2017; 38(11): 979–984, doi: [10.1097/MNM.0000000000000729](#), indexed in Pubmed: [29045338](#).
16. Reynés-Llompart G, Gámez-Cenzano C, Romero-Zayas I, et al. Performance Characteristics of the Whole-Body Discovery IQ PET/CT System. *J Nucl Med.* 2017; 58(7): 1155–1161, doi: [10.2967/jnumed.116.185561](#), indexed in Pubmed: [28302761](#).
17. Morzenti S, Ponti ED, Guerra L, et al. Performance evaluation of the Discovery IQ - GE PET/CT scanner according to NEMA NU2-2012 standard. *J Nucl Med. Society of Nuclear Medicine.* 2015; 56: 1846.
18. Howard BA, Morgan R, Thorpe MP, et al. Comparison of Bayesian penalized likelihood reconstruction versus OS-EM for characterization of small pulmonary nodules in oncologic PET/CT. *Ann Nucl Med.* 2017; 31(8): 623–628, doi: [10.1007/s12149-017-1192-1](#), indexed in Pubmed: [28689358](#).
19. Teoh EJ, McGowan DR, Bradley KM, et al. Novel penalised likelihood reconstruction of PET in the assessment of histologically verified small pulmonary nodules. *Eur Radiol.* 2016; 26(2): 576–584, doi: [10.1007/s00330-015-3832-y](#), indexed in Pubmed: [25991490](#).
20. Teoh EJ, McGowan DR, Schuster DM, et al. Bayesian penalised likelihood reconstruction (Q.Clear) of F-fluciclovine PET for imaging of recurrent prostate cancer: semi-quantitative and clinical evaluation. *Br J Radiol.* 2018; 91(1085): 20170727, doi: [10.1259/bjr.20170727](#), indexed in Pubmed: [29303359](#).
21. Sampaio Vieira T, Borges Faria D, Azevedo Silva F, et al. The Impact of a Bayesian Penalized Likelihood Reconstruction Algorithm on the Evaluation of Indeterminate Pulmonary Nodules by Dual-Time Point 18F-FDG PET/CT. *Clin Nucl Med.* 2017; 42(7): e352–e354, doi: [10.1097/RLU.0000000000001713](#), indexed in Pubmed: [28525459](#).
22. Tonkopi E, Ross AA, MacDonald A. JOURNAL CLUB: CT dose optimization for whole-body PET/CT examinations. *AJR Am J Roentgenol.* 2013; 201(2): 257–263, doi: [10.2214/AJR.12.10495](#), indexed in Pubmed: [23883207](#).
23. Sломka PJ, Pan T, Germano G. Recent Advances and Future Progress in PET Instrumentation. *Semin Nucl Med.* 2016; 46(1): 5–19, doi: [10.1053/j.semnuclmed.2015.09.006](#), indexed in Pubmed: [26687853](#).
24. Jakoby B, Bercier Y, Watson C, et al. Performance Characteristics of a New LSO PET/CT Scanner With Extended Axial Field-of-View and PSF Reconstruction. *IEEE Transactions on Nuclear Science.* 2009; 56(3): 633–639, doi: [10.1109/tns.2009.2015764](#).
25. Teoh EJ, McGowan DR, Macpherson RE, et al. Phantom and Clinical Evaluation of the Bayesian Penalized Likelihood Reconstruction Algorithm Q.Clear on an LYSO PET/CT System. *J Nucl Med.* 2015; 56(9): 1447–1452, doi: [10.2967/jnumed.115.159301](#), indexed in Pubmed: [26159585](#).
26. Ahn S, Ross SG, Asma E, et al. Quantitative comparison of OSEM and penalized likelihood image reconstruction using relative difference penalties for clinical PET. *Phys Med Biol.* 2015; 60(15): 5733–5751, doi: [10.1088/0031-9155/60/15/5733](#), indexed in Pubmed: [26158503](#).
27. Witkowska-Patena E, Budzyńska A, Giżewska A, et al. Ordered subset expectation maximisation vs Bayesian penalised likelihood reconstruction algorithm in 18F-PSMA-1007 PET/CT. *Ann Nucl Med.* 2020; 34(3): 192–199, doi: [10.1007/s12149-019-01433-x](#), indexed in Pubmed: [31902120](#).
28. Prieto E, Garcia-Velloso MJ, Rodríguez-Fraile M, et al. Significant dose reduction is feasible in FDG PET/CT protocols without compromising diagnostic quality. *Phys Med.* 2018; 46: 134–139, doi: [10.1016/j.ejmp.2018.01.021](#), indexed in Pubmed: [29519399](#).
29. Murray I, Kalemis A, Glennon J, et al. Time-of-flight PET/CT using low-activity protocols: potential implications for cancer therapy monitoring. *Eur J Nucl Med Mol Imaging.* 2010; 37(9): 1643–1653, doi: [10.1007/s00259-010-1466-5](#), indexed in Pubmed: [20428866](#).

Hepatic complications of peptide receptor radionuclide therapy with Lutetium-177 and Yttrium-90 in patients with neuroendocrine neoplasm

Barbara Bober¹, Marek Saracyn¹, Arkadiusz Lubas², Maciej Kolodziej¹, Dorota Brodowska-Kania¹,
Waldemar Kapusta¹, Grzegorz Kaminski¹

¹Department of Endocrinology and Isotope Therapy, Military Institute of Medicine, Warsaw, Poland

²Department of Internal Diseases, Nephrology and Dialysis, Military Institute of Medicine, Warsaw, Poland

[Received 19 01 2022; Accepted 24 01 2022]

Abstract

Neuroendocrine neoplasms (NENs) are a heterogeneous group of tumors originating from neuroendocrine cells spread throughout the body, forming the so-called diffuse endocrine system. The gold standard in treating unresectable or disseminated, progressive, and well-differentiated NENs is therapy with radiolabeled somatostatin analogs (peptide receptor radionuclide therapy — PRRT). PRRT is a method based on peptides combined with beta-emitting radionuclides. The study aimed to assess the early and long-term liver complications after administration of Lutetium-177 or Lutetium-177 combined with Yttrium-90. We enrolled 27 patients treated with [¹⁷⁷Lu]Lu-DOTATATE with an activity of 7.4 GBq (200 mCi) and 9 patients received the tandem treatment [⁹⁰Y]Y-DOTATATE + [¹⁷⁷Lu]Lu-DOTATATE with an activity of 3.7 GBq (50 mCi + 50 mCi). In the assessment of early as well as long-term complications, no significant effect of the applied treatment on the parameters of liver injury was found. Regarding liver function PRRT was a safe treatment for patients with highly or moderately differentiated, unresectable, or diffuse NENs.

KEY words: neuroendocrine neoplasms; treatment of neuroendocrine neoplasms; radioisotope treatment; PRRT; complications of radioisotope treatment

Nucl Med Rev 2022; 25, 1: 54–61

Introduction

Neuroendocrine neoplasms (NENs), formerly called neuroendocrine tumors (NETs), constitute a heterogeneous group of neoplasms. They come from neuroendocrine cells spread throughout the body, forming the so-called diffuse endocrine system (DES). They are considered rare neoplasms, but modern imaging techniques have rapidly increased their detection over the last decades [1–4]. Since 1973, in the United States alone, the number of diagnosed cases of NENs has increased over five times. Currently, the overall incidence rate of NENs is 35 cases per

100,000 persons. The most common location of NENs in the human body is the small intestine, in particular the ileum [5], and 70% of NENs are gastroenteropancreatic (GEP NEN), i.e. about 2% of the general population of gastrointestinal neoplasms [6, 7].

Although the endoscopic or surgical removal of the tumor is the only method of treating the patient ultimately [8–10], the most significant progress in the treatment of highly differentiated NENs of the gastrointestinal tract was achieved by introducing somatostatin analogs (SSA) in 1988 [11]. The analogs bind to the somatostatin receptor causing the inhibition of the cell cycle and inducing a proapoptotic effect. They also have an immunomodulating effect, inhibit angiogenesis, and inhibit the secretion of hormones [12]. Treatment with radioisotope-labeled somatostatin analogs (peptide receptor radionuclide therapy — PRRT) has been used for over 20 years. This method uses peptides combined with radionuclides emitting beta or alpha radiation [13, 14]. In Poland, [⁹⁰Y]Y-DOTATATE was used for the first time in April 2004, and

Correspondence to: Barbara Bober, Department of Endocrinology and Isotope Therapy, Military Institute of Medicine, Szaserów 128, 04–141 Warsaw, Poland; phone: +48 261 816 110, e-mail: barbara.bober@tlen.pl

in February 2006 tandem treatment [^{90}Y]/[^{177}Lu]Lu-DOTATATE was initiated [15].

The current regimen of PRRT treatment consists of 4 administrations of a selected isotope with a specific activity at eight- to twelve-week intervals. The most common side effects are kidney injury and myelosuppression, found relatively rarely in patients treated with PRRT [13]. Acute hematological complications (World Health Organization [WHO] grade 3 or 4) occur in less than 13% of patients receiving Yttrium-90 and 3% of patients receiving Lutetium-177. On the other hand, acute renal complications depend mainly on the radiopharmaceuticals' activity and comorbidities [16–20]. There are limited data on hepatic complications. The Endocrinology and Isotope Therapy Department of the Military Institute of Medicine in Warsaw covers the largest group of patients with NENs undergoing PRRT in Poland and Central and Eastern Europe. Due to the small number of studies and inconclusive results, we decided to assess such complications in this group of patients.

The study aimed to assess the early and long-term hepatic complications after radioisotope treatment using Lutetium-177 or Lutetium-177 in combination with Yttrium-90 in patients with neuroendocrine neoplasm.

Material and methods

Study population

The presented paper is a preliminary study evaluating early and long-term complications of radioisotope treatment in patients with NENs. The study group consisted of 36 patients treated with PRRT due to NENs from November 2017 to June 2019 in the Department of Endocrinology and Isotope Therapy of the Military Institute of Medicine in Warsaw. All patients qualified to PRRT at that time gave their written consent to participate in the study.

The local Bioethics Committee approved the study at the Military Institute of Medicine. All procedures carried out in the study followed the Helsinki Declaration of 1964 and its subsequent changes. Patients to be enrolled had to meet the following inclusion criteria: a) a highly differentiated, progressive neuroendocrine neoplasm defined as Ki-67 < 20% (progression within the last 12 months); b) good expression of somatostatin receptors in a qualifying receptor scintigraphy study (single photon emission computed tomography [SPECT]) or positron emission tomography/computed tomography (PET/CT); c) no more options for surgical treatment possible and d) chronic treatment with long-acting somatostatin analogs. The exclusion criteria were: a) the patient's lack of consent to treatment; b) pregnancy or lactation; c) assessment of the patient's performance status based on the World Health Organization/Eastern Cooperative Oncology Group (WHO/ECOG) status 3 or 4 or the basis of the Karnofsky classification (< 60); d) no uptake of the radiotracer in the somatostatin receptors imaging (SRI); e) bone marrow failure: hemoglobin less than 8 g/dL, platelets less than $80 \times 10^3/\mu\text{L}$, leukocytes below $2 \times 10^3/\mu\text{L}$, lymphocytes below $0.5 \times 10^3/\mu\text{L}$, neutrophils less than $1 \times 10^3/\mu\text{L}$; f) creatinine clearance < 30 mL/min, blood urea nitrogen over 45 mg/dL or serum creatinine concentration over 1.8 mg/dL; g) liver injury (3-fold increase in bilirubin); h) systemic infections; i) glomerulonephritis;

j) interstitial nephritis; k) obstructive nephropathy or l) urinary tract infection.

Treatment strategies

Patients were given an intravenous infusion of [^{177}Lu]Lu-DOTATATE with an activity of 7.4 GBq (200 mCi) or tandem treatment [^{90}Y]-DOTATATE + [^{177}Lu]Lu-DOTATATE with an activity of 3.7 GBq (50 mCi + 50 mCi) (ItraPol and LutaPol, manufacturer: National Center for Nuclear Research, POLATOM Radioisotope Center, Otwock, Poland). In addition, selected biochemical parameters were assessed before and after the radioisotope administration. For two days, patients also received infusions of 10% amino acid solution (Nephroprotect, Fresenius Kabi) (1000 mL on the first day, 500 mL on the second day) and Ringer's solution (2 x 500 mL). Treatment with long-acting somatostatin analogs (octreotide - Sandostatin LAR; Novartis and lanreotide autogel — Somatuline; Ipsen) was discontinued for at least four weeks prior to PRRT administration. The time since completion of prior chemotherapy was more than three months.

In total, the therapy (4 courses) lasted on average nine months (7–11 months). After the fourth course, patients were scheduled for follow-up visits, which were performed approximately 18 months from the start of the therapy (10 months from the end of radioisotope treatment). The following parameters were checked at each stage of the study: serum albumin, alanine aminotransferase (ALT), aspartate aminotransferase (AST), and bilirubin. Detailed procedures are as follows: day 1 — history taking and physical examination, serum albumin, ALT, AST, bilirubin; day 2 — intravenous administration of 1000 mL of positively charged amino acids with a simultaneous infusion of 500 mL Ringer's solution - a continuous infusion of 8 hours, intravenous infusion of radioisotopes [^{177}Lu]Lu-DOTATATE or [^{90}Y]-DOTATATE + [^{177}Lu]Lu-DOTATATE (a radiopharmaceutical solution in 100 mL 0.9% NaCl); day 3 — intravenous administration of 500 mL of positively charged amino acids with a simultaneous infusion of 500 mL of Ringer's fluid — a continuous infusion of 4 hours; day 4 — serum albumin, ALT, AST, bilirubin, post-therapeutic scintigraphy, and patient's discharge. Follow-up tests (clinical and laboratory) were performed during a one-day hospitalization. The biochemical tests were performed in the Department of Laboratory Diagnostics of the Military Institute of Medicine using an automatic biochemical analyzer (Cobas C 501, Roche Diagnostics).

Statistical methods

Statistical analyzes were performed with the use of the IBM SPSS Statistics 25. It was used to analyze basic descriptive statistics with the Shapiro-Wilk test, two-factor analysis of variance in a mixed schema, and Mann-Whitney U tests. The classical threshold $\alpha = 0.05$ was considered the level of significance. Acute complications were assessed during the 1st and 4th course. Long-term complications were evaluated based on comparing the results obtained before the 1st course, before the 4th course, and during the follow-up examination. Data were also analyzed depending on the type of the applied therapy, sex, age, BMI,

comorbidities (chronic kidney disease, diabetes, hypercholesterolemia, hypertension), NEN point of origin, and the history of chemotherapy.

Results

The study group consisted of 36 patients, including 16 women (44.5%) and 20 men (55.5%). Details are presented in Table 1. The mean age was 58.1 ± 13.1 . Twenty-seven patients received [^{177}Lu] Lu-DOTATATE with an activity of 7.4 GBq (200 mCi), and nine patients received the tandem treatment [^{90}Y]Y-DOTATATE + [^{177}Lu] Lu-DOTATATE with an activity of 3.7 GBq (50 mCi + 50 mCi). Thirty patients completed full treatment (6 dropouts: 2 — disease progression, 1 — myelosuppression, 1 — the death of unknown cause, 2 — withdrawals). Long-term follow-up was not performed in 11 patients because of the Covid-19 pandemic.

The mean body mass index (BMI) was 24.9 kg/m^2 , and 50% of patients had normal BMI values. The most common comorbidities were arterial hypertension (41.66%) and diabetes (27.8%). Their frequency was significantly higher in the studied group than in the general population (41.66% vs 31.5% in the case of hypertension and 27.8% vs 9.1% in the case of diabetes). Pancreatic NENs (13/36) and small intestine NENs (11/36) were the most frequent. The percentage of patients with G1 and G2 stages was similar (47.2% vs 52.8%). The median time from disease diagnosis to initiation of radioisotope treatment was 3.4 years (range 0–15 years).

Most patients had liver metastases (91,7%). The three remaining cases had metastases only to lymph nodes and bone, including pulmonary NENs, paraganglioma, and one case with an unknown point of origin. Before PRRT therapy, 6 patients received chemotherapy for: NEN (1 patient — doxorubicin with etoposide, 2nd patient — everolimus, 3rd — capecitabine with temozolomide), breast cancer (1 patient, drug unknown), and colorectal adenocarcinoma (2 patients, unknown drugs). Before PRRT 77,8% of patients had primary NEN lesions surgically removed. Only in 8 cases, the primary tumor was not removed (1 patient did not consent to surgical treatment of a pancreatic tumor, in 6 patients, the lesions were unresectable at the time of diagnosis, one person could not be operated on due to anesthetic contraindications). Additionally, hemihepatectomy was performed in 2 patients, thermoablation — in 2 patients, and liver embolization in — 1 patient.

Acute complications after the 1st course

During the 1st course of PRRT, a slight but statistically significant decrease in the mean serum albumin concentration ($p < 0.001$) and ALT activity ($p = 0.002$), as well as an increase in the mean bilirubin concentration ($p = 0.003$), was observed (Tab. 2). However, these changes remained within the normal ranges. The type of therapy used, age, sex, BMI of the subjects, comorbidities, and the NEN point of origin did not affect the observed changes in hepatic parameters. It was only noted that in patients with a history of prior chemotherapy, the mean

Table 1. Characteristics of the study population

Characteristics	Value
Age (years)	
Mean	58.1 ± 13.1
Range	23–76
Sex	
Women	19
Men	23
Place of residence	
Village	12
Town < 100,000 citizens	10
City > 100,000 citizens	20
BMI (kg/m²)	
Mean	24.9 ± 5.2
Range	16.4–41.3
< 18.5	3 (7.1%)
18.5–24.9	21 (50%)
25.0–29.9	12 (28.6%)
≥ 30.0	6 (14.3%)
Comorbidities	
Chronic kidney disease G3	6 (14.3%)
Arterial hypertension	18 (42.9%)
Diabetes mellitus	12 (28.6%)
Hypercholesterolemia	6 (14.3%)
Primary NENs point of origin	
Pancreas	15 (35.6%)
Jejunum	13 (30.9%)
Colon	5 (12%)
Others	5 (12%) (2 × ovary, 1 × stomach, 1 × paraganglioma, 1 × lung)
Unknown	4 (9.5%)
Grading	
G1	20 (48%)
G2	22 (52%)
G3	0

BMI — body mass index

concentration of bilirubin slightly decreased after the first administration of radioisotopes ($p < 0.001$).

Acute complications after the 4th course

The biochemical parameters assessing liver function obtained during the 4th course are presented in Table 3. There was a slight, statistically significant decrease in serum albumin concentration ($p < 0.001$); however, it remained within the normal limits. There was no correlation between changes in albumin concentration and age, sex, and BMI of the subjects, the presence of chronic diseases, the NEN point of origin, and the type of therapy used. There were also no other significant changes in the parameters of hepatocyte injury.

Table 2. Changes in hepatic parameters during the first peptide receptor radionuclide therapy (PRRT) course

Parameter	Before the 1 st course (n = 36)		After the 1 st course (n = 36)		p	[¹⁷⁷ Lu]Lu-DO-TATATE (n = 27)		[⁹⁰ Y]/[¹⁷⁷ Lu]Lu-DOTATATE (n = 9)		p	Pancreas (n = 13)		Other locations (n = 23)		p
	M	SD	M	SD		Δ	SD	Δ	SD		Δ	SD	Δ	SD	
Serum albumin [mg/dL]	4.52	0.51	4.28	0.53	< 0.001	-0.30	0.34	-0.17	0.23	0.275	-0.26	0.40	-0.27	0.28	0.945
AST [IU/L]	25.48	10.97	23.33	9.92	0.086	-2.66	8.52	-0.82	5.12	0.509	-1.23	5.36	-2.59	8.69	0.608
ALT [IU/L]	25.80	18.20	22.20	14.88	0.002	-2.76	8.12	-6.00	4.47	0.220	-4.64	9.11	-3.12	6.42	0.540
Bilirubin [mg/dL]	0.65	0.42	0.76	0.45	0.003	0.09	0.20	0.15	0.25	0.463	0.13	0.23	0.09	0.20	0.611

AST — aspartate aminotransferase; ALT — alanine aminotransferase; M — mean, Δ — change; SD — standard deviation; p — the level of significance

Table 3. Changes in hepatic parameters during the 4th peptide receptor radionuclide therapy (PRRT) course

Parameter	Before the 4 th course (n = 30)		After the 4 th course (n = 30)		p	[¹⁷⁷ Lu]Lu-DO-TATATE (n = 23)		[⁹⁰ Y]/[¹⁷⁷ Lu]Lu-DOTATATE (n = 7)		p	Pancreas (n = 11)		Other locations (n = 19)		p
	M	SD	M	SD		Δ	SD	Δ	SD		Δ	SD	Δ	SD	
Serum albumin [mg/dL]	4.57	0.33	4.37	0.33	< 0.001	-0.20	0.26	-0.21	0.22	0.922	-0.16	0.25	-0.23	0.26	0.433
AST [IU/L]	24.34	9.05	22.71	7.71	0.106	-2.22	5.74	0.38	5.90	0.272	-1.91	4.74	-1.50	6.31	0.850
ALT [IU/L]	23.42	12.82	21.56	11.47	0.382	-2.50	5.22	0.43	8.96	0.434	-2.46	7.16	-1.59	5.53	0.690
Bilirubin [mg/dL]	0.62	0.40	0.71	0.48	0.110	0.04	0.14	0.29	1.05	0.557	-0.05	0.28	0.17	0.54	0.196

AST — aspartate aminotransferase; ALT — alanine aminotransferase; M — mean, Δ — change, SD — standard deviation, p — the level of significance

Table 4. Changes in hepatic parameters before treatment initiation and before the 4th peptide receptor radionuclide therapy (PRRT) course

Parameter	Before the 1 st course (n = 30)		Before the 4 th course (n = 30)		p	[¹⁷⁷ Lu]Lu-DO-TATATE (n = 23)		[⁹⁰ Y]/[¹⁷⁷ Lu]Lu-DOTATATE (n = 7)		p	Pancreas (n = 11)		Other locations (n = 19)		p
	M	SD	M	SD		Δ	SD	Δ	SD		Δ	SD	Δ	SD	
Serum albumin [mg/dL]	4.61	0.39	4.58	0.33	0.564	-0.09	0.32	0.17	0.38	0.075	-0.05	0.35	-0.02	0.35	0.810
AST [IU/L]	24.82	10.54	24.56	9.09	0.858	-0.69	9.41	1.13	5.38	0.608	0.10	8.06	-0.42	8.96	0.876
ALT [IU/L]	25.91	19.14	23.60	12.96	0.756	-3.41	16.43	1.71	15.87	0.465	-2.00	21.75	-2.57	12.25	0.922
Bilirubin [mg/dL]	0.64	0.43	0.63	0.40	0.685	-0.05	0.29	0.13	0.31	0.159	-0.02	0.36	-0.01	0.27	0.992

AST — aspartate aminotransferase; ALT — alanine aminotransferase; M — mean, Δ — change, SD — standard deviation, p — the level of significance

Chronic complications

1st course vs 4th course — the first assessment of chronic hepatic complications

Before the 4th course, as compared to the tests performed before the 1st course (i.e., after approx. eight months from the start of PRRT), no biochemical features of hepatocyte damage or disturbances in the synthetic function of the liver were found (Tab. 4).

4th course vs follow-up visit — the 2nd assessment of chronic hepatic complications

In the second long-term evaluation, in the control tests compared to the tests before the 4th course (approximately ten months after the end of PRRT), a slight statistically significant (p = 0.007) increase in

ALT, remaining within the reference range, was found. This increase was statistically significantly higher in the group of patients receiving tandem therapy (p = 0.010) and in the group of patients with the NEN point of origin in the pancreas (p = 0.049). The increase in ALT was also higher in men (p = 0.015) and patients with diabetes (p = 0.024). However, no disturbances in the synthetic function of the liver were found. Detailed results are presented in Table 5.

1st course vs follow-up visit — the long-term assessment of hepatic complications

In the follow-up at 18 months after the start of treatment, compared to the baseline lab tests before the first course of therapy, in the entire group of patients, no biochemical features of hepatocyte injury or disturbances in the synthetic function of the liver were

Table 5. Changes in hepatic parameters before the 4th peptide receptor radionuclide therapy (PRRT) course and the follow-up

Parameter	Before the 4 th course (n = 19)		Follow-up (n = 19)		p	[¹⁷⁷ Lu]Lu-DO-TATATE (n = 16)		[⁹⁰ Y]Y/[¹⁷⁷ Lu]Lu-DOTATATE (n = 3)		p	Pancreas (n = 7)		Other locations (n = 12)		p
	M	SD	M	SD		Δ	SD	Δ	SD		Δ	SD	Δ	SD	
Serum albumin [mg/dL]	4.60	0.42	4.51	0.40	0.172	-0.06	0.40	-0.30	0.36	0.343	0.09	0.37	-0.20	0.39	0.133
AST [IU/L]	29.42	16.68	25.42	10.00	0.402	5.25	20.51	17.67	11.02	0.329	6.71	8.88	7.50	24.24	0.936
ALT [IU/L]	23.95	14.18	26.95	20.82	0.007	0.44	8.81	16.67	9.29	0.010	9.14	10.75	-0.58	9.00	0.049
Bilirubin [mg/dL]	0.70	0.46	0.64	0.35	0.309	-0.03	0.20	0.17	0.06	0.118	0.06	0.21	-0.03	0.19	0.356

AST — aspartate aminotransferase, ALT — alanine aminotransferase, M — mean, Δ — change, SD — standard deviation, p — the level of significance

Table 6. Changes in hepatic parameters before the initiation of therapy and in the follow-up visit

Parameter	Before the 1 st course (n = 19)		Follow-up (n = 19)		p	[¹⁷⁷ Lu]Lu-DO-TATATE (n = 16)		[⁹⁰ Y]Y/[¹⁷⁷ Lu]Lu-DOTATATE (n = 3)		p	Pancreas (n = 7)		Other locations (n = 12)		p
	M	SD	M	SD		Δ	SD	Δ	SD		Δ	SD	Δ	SD	
Serum albumin [mg/dL]	4.61	0.43	4.51	0.40	0.712	0.19	0.48	0.17	0.25	0.927	0.26	0.44	0.15	0.47	0.629
AST [IU/L]	29.33	17.16	26.11	10.17	0.545	4.69	19.41	17.00	9.54	0.306	4.00	10.52	8.17	22.31	0.651
ALT [IU/L]	26.11	23.70	26.95	20.82	0.232	-0.13	13.58	23.33	22.50	0.023	5.57	22.55	2.42	13.73	0.707
Bilirubin [mg/dL]	0.68	0.36	0.64	0.35	0.505	-0.19	0.36	-0.13	0.55	0.807	-0.33	0.36	-0.10	0.38	0.212

AST — aspartate aminotransferase, ALT — alanine aminotransferase, M — mean, Δ — change, SD — standard deviation, p — the level of significance

found. However, it was noticed that in the group of patients treated with [⁹⁰Y]Y/[¹⁷⁷Lu]Lu-DOTATATE, there was a statistically significant increase in ALT (p = 0.023), and in the group of patients receiving chemotherapy in the past, a slight increase in bilirubin concentration, but within the reference range (p = 0.017) was observed. Detailed results are presented in Table 6.

Hepatic complications of PRRT according to CTCAE version 5.0

According to the Common Terminology Criteria for Adverse Events (CTCAE v 5.0) of the US National Cancer Institute, early and late hepatic complications are presented in Tables 7 and 8. Grade 3 and 4 (G3, G4) hepatic complications were not observed after the first administration of radioisotopes. On the other hand, a slight decrease in albumin concentration was found, which caused an increase in adverse event grade 1 and 2 groups. After the first PRRT course, an increase in bilirubin concentration was also noticed, as a result of which an increase in G1 and G2 groups was also found (Tab. 7). In the evaluation of long-term complications, no grade 2, 3, or 4 (G2, G3, G4) hepatic complications were found (Tab. 8).

Discussion

In the presented study, no hepatotoxicity of the applied radioisotope treatment was found in both short and long-term follow-up. The presence of metastatic lesions in the liver, which occurred in

91.7% of the patients, prior chemotherapy and previous locoregional treatment aimed at metastatic lesions in the liver also did not affect the deterioration of liver parameters. The slight increase in ALT activity was associated with tandem therapy, the location of the NENs primary origin in the pancreas, and the diagnosis of diabetes at the follow-up visit.

In the available literature, hepatotoxicity is also a rare complication of PRRT. It has been most frequently reported in patients with large and extensive hepatic metastases (size > 5 cm) [21, 22]. In the NETTER-1 study, the elevation of AST activity of grade 3 or 4 according to CTCAE v 5.0 was found in 4.5%, ALT — in 3.6%, and bilirubin concentration — in 1.8% of patients [23]. Brabander et al. [24], in a study assessing long-term efficacy, survival, and safety of [¹⁷⁷Lu]Lu-DOTATATE, noticed the elevated activity of AST and/or ALT (grades 3 or 4 CTCAE v 4.0) only in 3% of patients.

In the literature, patients with NENs with little or no hepatic metastases showed no evidence of significant liver injury [25–27]. However, severe liver damage may occur in a group of patients with extensive liver metastases and/or abnormal liver function. In other words, the safety of using PRRT in a patient with 25% liver involvement is not the same as the safety of treating a patient with 50%, or even 75%, organ involvement. They should also be considered in the case of preexisting liver disease or conditions affecting liver function. Then it is important to choose the right radioisotope and its activity. In such cases, Lutetium-177 labeled peptides are recommended, and the reported activity should be appropriately

Table 7. Early complications according to the Common Terminology Criteria for Adverse Events (CTCAE v 5.0) classification

	Before the 1 st course		After the 1 st course			In total before the 1 st course (%)	In total after the 1 st course (%)
	G1 (%)	G2 (%)	G1 (%)	G2 (%)	G3 (%)		
Serum albumin [mg/dL]	2 (5.6)	1 (2.8)	3 (7.7)	2 (5.1)	0	3/36 (8.4)	5/36 (12.8)
AST [IU/L]	5 (13.9)	0	2 (5)	0	0	5/36 (13.9)	2/36 (5)
ALT [IU/L]	6 (16.7)	0	4 (10)	0	0	6/36 (16.7)	4/36 (10)
Bilirubin [mg/dL]	1 (2.8)	1 (2.8)	3 (7.5)	2 (5)	0	2/36 (5.6)	5/36 (12.5)

AST — aspartate aminotransferase, ALT — alanine aminotransferase

Table 8. Long-term complications according to the Common Terminology Criteria for Adverse Events (CTCAE v 5.0) classification

	Before the 1 st course		Follow-up			In total before the 1 st course (%)	In total at follow-up (%)
	G1 (%)	G2 (%)	G1 (%)	G2 (%)	G3 (%)		
Serum albumin [mg/dL]	2 (5.6)	1 (2.8)	1 (5.3)	0	0	3/36 (8.4)	1/19 (5.3)
AST [IU/L]	5 (13.9)	0	5 (26.3)	0	0	5/36 (13.9)	5/19 (26.3)
ALT [IU/L]	6 (16.7)	0	3 (15.8)	0	0	6/36 (16.7)	3/19 (15.8)
Bilirubin [mg/dL]	1 (2.8)	1 (2.8)	1 (5.3)	0	0	2/36 (5.6)	1/19 (5.3)

AST — aspartate aminotransferase, ALT — alanine aminotransferase

reduced. In 2015 there were published the results of a retrospective study in which 17 patients from the United States of America (USA) were treated with a radioisotope in a Swiss center in Basel. The study evaluated 93 patients with confirmed NENs with liver metastases. Seventeen subjects (18%), after confirming disease progression despite using other traditional therapies available in the USA at that time, were qualified for PRRT treatment in various regimens using various radioisotopes: Yttrium-90, Lutetium-177, Indium-111, or tandem therapy (Lutetium-177 with Yttrium-90). The two study groups (treated or not with PRRT) did not differ in sex, age, baseline laboratory parameters, prior exposure to treatment, or disease duration. In the group not subjected to PRRT, 23 of 76 (30%) patients had increased liver injury markers associated with the use of traditional GEP NET therapy (surgery, chemoembolization, treatment [¹³¹I]-meta-iodobenzylguanidine). In 10 of 17 (59%) patients treated with PRRT, biochemical features of liver injury were found, while ascites occurred in 41% of patients in this group, compared with 6.5% in the second cohort. The higher incidence of hepatotoxicity in that group treated with radioisotope therapy, significantly higher than the one reported so far, could result from the delayed duration of PRRT use (this therapy was not available in the USA at that time) and the previous use of locoregional therapy (surgical treatment, chemoembolization or thermoablation of focal lesions in the liver, [¹³¹I]-MIBG treatment), causing more radiation damage to the liver [28].

In the study published in 2020 by Spanish researchers, one patient (out of a total of 36 treated with [¹⁷⁷Lu]Lu-DOTATATE) with extensive liver metastases present had a significant degree of liver injury. Liver parameters deteriorated within weeks after the first administration of the radioisotope, and the patient died of liver failure five weeks later. In the remaining 35 subjects, however, no signs of liver injury were observed [29]. Therefore, there are concerns regarding the safety of radioisotope therapy in patients with high liver involvement by metastatic lesions due to the possibility

of radiation hepatitis. However, data published in 2020 from the NETTER-1 study did not support this hypothesis. The increase in liver injury markers was rare and did not appear to correlate with the extent of the neoplastic disease [30]. In the NETTER-1 study, the subgroup of patients with extreme liver parenchymal involvement (> 90%) was not defined; therefore, no detailed safety analysis could be made in this subgroup.

In many patients, NENs are detected when the disease is already advanced. Often, however, it is limited to the liver only, where it is metastasizing from the intestines. In some cases, it is suggested to combine selective internal radiotherapy and PRRT by administering a somatostatin analog conjugated with Lutetium-177 or Yttrium-90 directly through the hepatic artery [31]. Theoretically, this ensures the delivery of higher radioisotope activity to the tumor itself (improving the effectiveness of treatment) while reducing its activity in the systemic circulation (reducing side effects). Initial results of such therapy show that it can be successfully used [31]. Moreover, radioembolization of metastatic lesions in the liver after systemic radionuclide treatment was also shown to be safe, and liver damage induced by this procedure was shown to be rare [32]. However, studies directly comparing these forms of therapy with systemic PRRT administration have not been conducted so far [33].

In our study, we did not observe any significant deterioration of liver parameters. This is most likely since PRRT has been used in Poland for almost 20 years and is a therapeutic option started in the early stages of NEN progression when there is no significant involvement of the liver parenchyma by metastatic lesions. In the presented study, five patients underwent prior locoregional treatment (hemihepatectomy — 2 patients, thermal ablation — 2 patients, or embolization of liver lesions — 1 patient) before starting PRRT, which may have somewhat reduced the adverse events of PRRT on liver function in our study. Furthermore, both in our study and the available literature, the type of radioisotope therapy used did not deteriorate liver parameters and function.

Study limitations

The presented paper, although preliminary, is one of the few prospective studies; however, it has some limitations. First, the study was conducted on a relatively small number of patients. Despite almost two years of recruitment, and in the center with a large number of isotope therapies per year, and the low incidence of neuroendocrine neoplasms, it was impossible to collect the larger group. The COVID-19 pandemic also played a significant role in this regard, due to which some patients did not survive to the end of the study or follow-up visit. Nevertheless, the presented group allowed obtaining many important and interesting results that undoubtedly require further research.

Conclusions

Our study showed that radioisotope treatment and its type did not affect the liver parameters in both early and long-term follow-up. Regarding liver function, treatment of NENs using Lutetium-177 or Yttrium-90/Lutetium-177 isotopes appeared to be safe.

Conflict of interest

None declared.

References

- Modlin IM, Lye KD, Kidd M. A 5-decade analysis of 13,715 carcinoid tumors. *Cancer*. 2003; 97(4): 934–959, doi: [10.1002/ncr.11105](https://doi.org/10.1002/ncr.11105), indexed in Pubmed: [12569593](https://pubmed.ncbi.nlm.nih.gov/12569593/).
- Chamberlain R, Canes D, Brown K, et al. Hepatic neuroendocrine metastases: does intervention alter outcomes? *J Am Coll Surg*. 2000; 190(4): 432–445, doi: [10.1016/s1072-7515\(00\)00222-2](https://doi.org/10.1016/s1072-7515(00)00222-2).
- Yao JC, Hassan M, Phan A, et al. One hundred years after "carcinoid": epidemiology of and prognostic factors for neuroendocrine tumors in 35,825 cases in the United States. *J Clin Oncol*. 2008; 26(18): 3063–3072, doi: [10.1200/JCO.2007.15.4377](https://doi.org/10.1200/JCO.2007.15.4377), indexed in Pubmed: [18565894](https://pubmed.ncbi.nlm.nih.gov/18565894/).
- Niederle B, Pape UF, Costa F, et al. ENETS Consensus Guidelines Update for Neuroendocrine Neoplasms of the Jejunum and Ileum. *Neuroendocrinology*. 2016; 103(2): 125–138, doi: [10.1159/000443170](https://doi.org/10.1159/000443170), indexed in Pubmed: [26758972](https://pubmed.ncbi.nlm.nih.gov/26758972/).
- Bednarczuk T, Bolanowski M, Zemczak A, et al. Neuroendocrine neoplasms of the small intestine and appendix - management guidelines (recommended by the Polish Network of Neuroendocrine Tumours). *Endokrynol Pol*. 2017; 68(2): 223–236, doi: [10.5603/EP.2017.0018](https://doi.org/10.5603/EP.2017.0018), indexed in Pubmed: [28540974](https://pubmed.ncbi.nlm.nih.gov/28540974/).
- Plöckinger U, Rindi G, Arnold R, et al. European Neuroendocrine Tumour Society. Guidelines for the diagnosis and treatment of neuroendocrine gastrointestinal tumours. A consensus statement on behalf of the European Neuroendocrine Tumour Society (ENETS). *Neuroendocrinology*. 2004; 80(6): 394–424, doi: [10.1159/000085237](https://doi.org/10.1159/000085237), indexed in Pubmed: [15838182](https://pubmed.ncbi.nlm.nih.gov/15838182/).
- Oberg K, Knigge U, Kwekkeboom D, et al. ESMO Guidelines Working Group. Neuroendocrine gastro-entero-pancreatic tumors: ESMO Clinical Practice Guidelines for diagnosis, treatment and follow-up. *Ann Oncol*. 2012; 23 Suppl 7: vii124–vii130, doi: [10.1093/annonc/mds295](https://doi.org/10.1093/annonc/mds295), indexed in Pubmed: [22997445](https://pubmed.ncbi.nlm.nih.gov/22997445/).
- Kos-Kudła B, Rosiek V, Borowska M, et al. Pancreatic neuroendocrine neoplasms - management guidelines (recommended by the Polish Network of Neuroendocrine Tumours). *Endokrynol Pol*. 2017; 68(2): 169–197, doi: [10.5603/EP.2017.2016](https://doi.org/10.5603/EP.2017.2016), indexed in Pubmed: [28540973](https://pubmed.ncbi.nlm.nih.gov/28540973/).
- Kos-Kudła B, Blicharz-Dorniak J, Strzelczyk J, et al. Diagnostic and therapeutic guidelines for gastro-entero-pancreatic neuroendocrine neoplasms (recommended by the Polish Network of Neuroendocrine Tumours). *Endokrynol Pol*. 2017; 68(2): 79–110, doi: [10.5603/EP.2017.0015](https://doi.org/10.5603/EP.2017.0015), indexed in Pubmed: [28597909](https://pubmed.ncbi.nlm.nih.gov/28597909/).
- Kulke MH, Siu LL, Tepper JE, et al. Future directions in the treatment of neuroendocrine tumors: consensus report of the National Cancer Institute Neuroendocrine Tumor clinical trials planning meeting. *J Clin Oncol*. 2011; 29(7): 934–943, doi: [10.1200/JCO.2010.33.2056](https://doi.org/10.1200/JCO.2010.33.2056), indexed in Pubmed: [21263089](https://pubmed.ncbi.nlm.nih.gov/21263089/).
- Ito T, Hijioka S, Masui T, et al. Advances in the diagnosis and treatment of pancreatic neuroendocrine neoplasms in Japan. *J Gastroenterol*. 2017; 52(1): 9–18, doi: [10.1007/s00535-016-1250-9](https://doi.org/10.1007/s00535-016-1250-9), indexed in Pubmed: [27539256](https://pubmed.ncbi.nlm.nih.gov/27539256/).
- Alonso-Gordoa T, Capdevila J, Grande E. GEP-NETs update: Biotherapy for neuroendocrine tumours. *Eur J Endocrinol*. 2015; 172(1): R31–R46, doi: [10.1530/EJE-14-0354](https://doi.org/10.1530/EJE-14-0354), indexed in Pubmed: [25430657](https://pubmed.ncbi.nlm.nih.gov/25430657/).
- Kolasińska-Ćwikła A, Łowczak A, Maciejewicz KM, et al. Peptide Receptor Radionuclide Therapy for Advanced Gastroenteropancreatic Neuroendocrine Tumors - from oncology perspective. *Nucl Med Rev Cent East Eur*. 2018; 21(2), doi: [10.5603/NMR.2018.0019](https://doi.org/10.5603/NMR.2018.0019), indexed in Pubmed: [29741203](https://pubmed.ncbi.nlm.nih.gov/29741203/).
- Navalkisoor S, Grossman A. Targeted Alpha Particle Therapy for Neuroendocrine Tumours: The Next Generation of Peptide Receptor Radionuclide Therapy. *Neuroendocrinology*. 2019; 108(3): 256–264, doi: [10.1159/000494760](https://doi.org/10.1159/000494760), indexed in Pubmed: [30352433](https://pubmed.ncbi.nlm.nih.gov/30352433/).
- Kunikowska J, Pawlak D, Bąk MI, et al. Long-term results and tolerability of tandem peptide receptor radionuclide therapy with Y/Lu-DOTATATE in neuroendocrine tumors with respect to the primary location: a 10-year study. *Ann Nucl Med*. 2017; 31(5): 347–356, doi: [10.1007/s12149-017-1163-6](https://doi.org/10.1007/s12149-017-1163-6), indexed in Pubmed: [28316066](https://pubmed.ncbi.nlm.nih.gov/28316066/).
- Bodei L, Ferone D, Grana CM, et al. Peptide receptor therapies in neuroendocrine tumors. *J Endocrinol Invest*. 2009; 32(4): 360–369, doi: [10.1007/BF03345728](https://doi.org/10.1007/BF03345728), indexed in Pubmed: [19636207](https://pubmed.ncbi.nlm.nih.gov/19636207/).
- Imhof A, Brunner P, Marincek N, et al. Response, survival, and long-term toxicity after therapy with the radiolabeled somatostatin analogue [90Y-DOTA]-TOC in metastasized neuroendocrine cancers. *J Clin Oncol*. 2011; 29(17): 2416–2423, doi: [10.1200/JCO.2010.33.7873](https://doi.org/10.1200/JCO.2010.33.7873), indexed in Pubmed: [21555692](https://pubmed.ncbi.nlm.nih.gov/21555692/).
- Pfeifer AK, Gregersen T, Grønbaek H, et al. Peptide receptor radionuclide therapy with Y-DOTATOC and (177)Lu-DOTATOC in advanced neuroendocrine tumors: results from a Danish cohort treated in Switzerland. *Neuroendocrinology*. 2011; 93(3): 189–196, doi: [10.1159/000324096](https://doi.org/10.1159/000324096), indexed in Pubmed: [21335949](https://pubmed.ncbi.nlm.nih.gov/21335949/).
- Waldherr C, Pless M, Maecke HR, et al. Tumor response and clinical benefit in neuroendocrine tumors after 7.4 GBq (90Y)-DOTATOC. *J Nucl Med*. 2002; 43(5): 610–616, indexed in Pubmed: [11994522](https://pubmed.ncbi.nlm.nih.gov/11994522/).
- Sabet A, Ezziddin K, Pape UF, et al. Accurate assessment of long-term nephrotoxicity after peptide receptor radionuclide therapy with (177)Lu-octreotate. *Eur J Nucl Med Mol Imaging*. 2014; 41(3): 505–510, doi: [10.1007/s00259-013-2601-x](https://doi.org/10.1007/s00259-013-2601-x), indexed in Pubmed: [24196919](https://pubmed.ncbi.nlm.nih.gov/24196919/).
- Kendi AT, Halfdanarson TR, Packard A, et al. Therapy With Lu-DOTATATE: Clinical Implementation and Impact on Care of Patients With Neuroendocrine Tumors. *AJR Am J Roentgenol*. 2019; 213(2): 309–317, doi: [10.2214/AJR.19.21123](https://doi.org/10.2214/AJR.19.21123), indexed in Pubmed: [31039017](https://pubmed.ncbi.nlm.nih.gov/31039017/).
- Frilling A, Li J, Malamutmann E, et al. Treatment of liver metastases from neuroendocrine tumours in relation to the extent of hepatic disease. *Br J Surg*. 2009; 96(2): 175–184, doi: [10.1002/bjs.6468](https://doi.org/10.1002/bjs.6468), indexed in Pubmed: [19160361](https://pubmed.ncbi.nlm.nih.gov/19160361/).
- Strosberg J, El-Haddad G, Wolin E, et al. NETTER-1 Trial Investigators. Phase 3 Trial of Lu-Dotatate for Midgut Neuroendocrine Tumors. *N Engl J Med*. 2017; 376(2): 125–135, doi: [10.1056/NEJMoa1607427](https://doi.org/10.1056/NEJMoa1607427), indexed in Pubmed: [28076709](https://pubmed.ncbi.nlm.nih.gov/28076709/).
- Brabander T, van der Zwan WA, Teunissen JJM, et al. Long-Term Efficacy, Survival, and Safety of [Lu-DOTA,Tyr]octreotate in Patients with Gastroen-

- teropancreatic and Bronchial Neuroendocrine Tumors. *Clin Cancer Res.* 2017; 23(16): 4617–4624, doi: [10.1158/1078-0432.CCR-16-2743](https://doi.org/10.1158/1078-0432.CCR-16-2743), indexed in Pubmed: [28428192](https://pubmed.ncbi.nlm.nih.gov/28428192/).
25. Kunikowska J, Zemczak A, Kolodziej M, et al. Tandem peptide receptor radionuclide therapy using Y/Lu-DOTATATE for neuroendocrine tumors efficacy and side-effects — polish multicenter experience. *Eur J Nucl Med Mol Imaging.* 2020; 47(4): 922–933, doi: [10.1007/s00259-020-04690-5](https://doi.org/10.1007/s00259-020-04690-5), indexed in Pubmed: [31980909](https://pubmed.ncbi.nlm.nih.gov/31980909/).
 26. Zhang J, Kulkarni HR, Singh A, et al. Peptide Receptor Radionuclide Therapy in Grade 3 Neuroendocrine Neoplasms: Safety and Survival Analysis in 69 Patients. *J Nucl Med.* 2019; 60(3): 377–385, doi: [10.2967/jnumed.118.215848](https://doi.org/10.2967/jnumed.118.215848), indexed in Pubmed: [30115686](https://pubmed.ncbi.nlm.nih.gov/30115686/).
 27. Zemczak A, Gut P, Pawlak D, et al. The Safety and Efficacy of the Repeated PRRT with [Y]Y/[Lu]Lu-DOTATATE in Patients with NET. *Int J Endocrinol.* 2021; 2021: 6615511, doi: [10.1155/2021/6615511](https://doi.org/10.1155/2021/6615511), indexed in Pubmed: [33552155](https://pubmed.ncbi.nlm.nih.gov/33552155/).
 28. Riff BP, Yang YX, Soulen MC, et al. Peptide Receptor Radionuclide Therapy-Induced Hepatotoxicity in Patients With Metastatic Neuroendocrine Tumors. *Clin Nucl Med.* 2015; 40(11): 845–850, doi: [10.1097/RLU.0000000000000935](https://doi.org/10.1097/RLU.0000000000000935), indexed in Pubmed: [26284763](https://pubmed.ncbi.nlm.nih.gov/26284763/).
 29. Abou Jokh Casas E, Pubul Núñez V, Anido-Herranz U, et al. Evaluation of Lu-Dotatate treatment in patients with metastatic neuroendocrine tumors and prognostic factors. *World J Gastroenterol.* 2020; 26(13): 1513–1524, doi: [10.3748/wjg.v26.i13.1513](https://doi.org/10.3748/wjg.v26.i13.1513), indexed in Pubmed: [32308351](https://pubmed.ncbi.nlm.nih.gov/32308351/).
 30. Strosberg J, Kunz PL, Hendifar A, et al. Impact of liver tumour burden, alkaline phosphatase elevation, and target lesion size on treatment outcomes with Lu-Dotatate: an analysis of the NETTER-1 study. *Eur J Nucl Med Mol Imaging.* 2020; 47(10): 2372–2382, doi: [10.1007/s00259-020-04709-x](https://doi.org/10.1007/s00259-020-04709-x), indexed in Pubmed: [32123969](https://pubmed.ncbi.nlm.nih.gov/32123969/).
 31. Kratochwil C, López-Benítez R, Mier W, et al. Hepatic arterial infusion enhances DOTATOC radiolabeled peptide therapy in patients with neuroendocrine liver metastases. *Endocr Relat Cancer.* 2011; 18(5): 595–602, doi: [10.1530/ERC-11-0144](https://doi.org/10.1530/ERC-11-0144), indexed in Pubmed: [21791571](https://pubmed.ncbi.nlm.nih.gov/21791571/).
 32. Braat AJ, Ahmadzadehfar H, Kappadath SC, et al. Radioembolization with Y Resin Microspheres of Neuroendocrine Liver Metastases After Initial Peptide Receptor Radionuclide Therapy. *Cardiovasc Intervent Radiol.* 2020; 43(2): 246–253, doi: [10.1007/s00270-019-02350-2](https://doi.org/10.1007/s00270-019-02350-2), indexed in Pubmed: [31646375](https://pubmed.ncbi.nlm.nih.gov/31646375/).
 33. Mitra ES. Neuroendocrine Tumor Therapy: Lu-DOTATATE. *AJR Am J Roentgenol.* 2018; 211(2): 278–285, doi: [10.2214/AJR.18.19953](https://doi.org/10.2214/AJR.18.19953), indexed in Pubmed: [29949416](https://pubmed.ncbi.nlm.nih.gov/29949416/).

Efficacy of long-term ultrasonography in follow-up of patients with papillary thyroid carcinoma: a case of neck metastasis developed 19 years following primary treatment

Vlatka Jozanovic¹, Sanja Kusacic Kuna^{2, 3}, Marija Despot², Tatjana Samardzic², Drazen Huic^{2, 3}

¹Department of Nuclear Medicine, Clinical Hospital Centre Dubrava, Croatia

²Clinical Department of Nuclear Medicine and Radiation Protection, University Hospital Centre Zagreb, Croatia

³The University of Zagreb School of Medicine, Zagreb, Croatia

[Received 01 IV 2021; Accepted 07 VII 2021]

Abstract

The cases of relapse in papillary thyroid cancer patients who were initially considered low-risk and for many years were without signs of the disease are extremely rare, but exist. This is supported by the clinical case of a patient who underwent a total thyroidectomy due to papillary thyroid cancer and 19 years later metastasis with extracapsular spreading in a presumed thyroid place was revealed. Due to such cases, the importance of long-term ultrasound monitoring is emphasized.

KEY words: papillary thyroid carcinoma; neck metastases; follow-up

Nucl Med Rev 2022; 25, 1: 62–63

Introduction

The metastases of papillary thyroid cancer usually occur during the first few years after the initial procedure and generally develop in patients with a higher risk of persistent or recurrent disease such as the presence of local invasion and metastases. Ultrasound is the best method for detection of those lesions in the neck, it provides reliable information regarding the lesion size, shape, internal architecture, and vascularity and is recommended during regular intervals throughout life. The aim of this report is to present the occurrence of cystic metastasis in the neck 19 years after total thyroidectomy in a patient who was considered low-risk and did not have any recurrence of the disease at regular follow-up for many years.

Correspondence to: Sanja Kusacic Kuna, Clinical Department of Nuclear Medicine and Radiation Protection, University Hospital Centre Zagreb, Kispaticeva 12, 10 000 Zagreb, Croatia, tel.: 00385 98 238315, fax number: +385 1 2376 040
e-mail: sanja.kusackikuna@gmail.com

Case report

A 27-years old female patient underwent total thyroidectomy and radioiodine ablation in 2000 due to accidental ultrasound finding of small papillary thyroid cancer in the left lobe that was confirmed cytologically and then histologically. During regular follow-up, the patient was free of disease with a normal thyroglobulin level and completely normal neck ultrasound. But, at regularly scheduled examination at the end of 2019 ultrasound revealed a newly formed hypoechoic, avascular cystic formation in the right thyroid bed measuring 0.7 × 0.8 × 0.7 cm (Fig. 1). Ultrasound-guided FNAB indicated a suspicious cystic change with atypia of thyrocytes and elevated thyroglobulin level in the punctate content that amounted to 71.50 µg/L. The patient was referred for paratracheal dissection during which the formation was extirpated. The result of pathohistological analysis proved it was a metastasis of papillary thyroid carcinoma, in a nodule of 0.6 cm in diameter with extracapsular spreading that penetrates the capsule of the affected lymph node. Due to the extracapsular spreading patient was treated with a therapeutic dose of 3700 MBq (100 mCi) of iodine-I31. Post-therapeutic

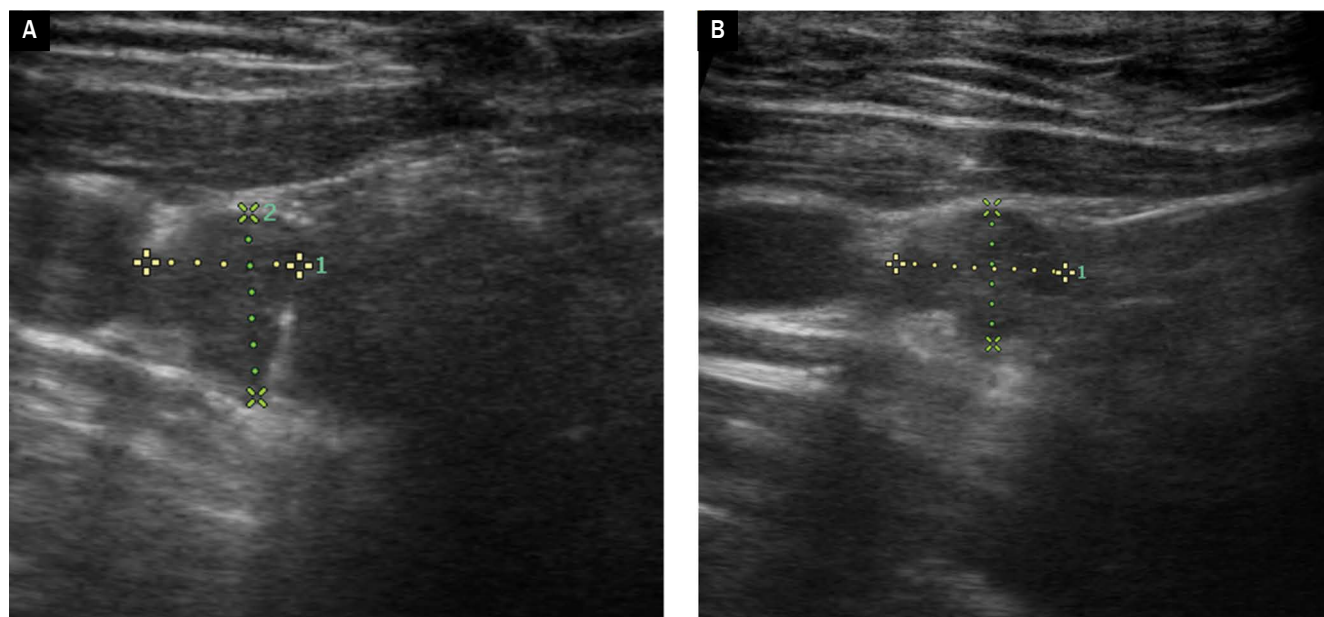


Figure 1A–B. Echographic presentation of surgically resected and histologically proven cystic metastasis in right thyroid bed

whole-body scan verified pathological accumulation of low intensity in the medial line of the neck. Postoperative ultrasound of the neck did not reveal any residual formation in the thyroid bed as well as elsewhere in the neck, and thyroglobulin level was within the reference ranges expected in thyroidectomized patients ($< 0.30 \mu\text{g/L}$). At the regular follow-up performed ten months after the surgery, the patient had no signs of recurrence of the disease. This case of

metastasis occurred almost 20 years after initial treatment reports in a favor of lifelong ultrasonographic follow-up of patients with papillary thyroid cancer.

Conflict of interest

The authors declare that they have no conflict of interest.

Different glucose metabolism behavior relating to histotypes in synchronous breast cancers evaluated by [¹⁸F]FDG PET-CT

Pietro Bellini¹, Domenico Albano¹, Francesco Dondi¹, Francesco Bertagna¹, Raffaele Giubbini¹

Nuclear Medicine, University of Brescia and ASST Spedali Civili Brescia, Brescia, Italy

[Received 07 IV 2021; Accepted 12 X 2021]

Abstract

Glucose metabolism is increased in most aggressive tumors and it is commonly evaluated by positron emission tomography-computed tomography (PET-CT) with ¹⁸F-fluorodeoxyglucose ([¹⁸F]FDG), measuring the Maximum Standardized Uptake Value (SUVmax) for the assessment. Particularly, it is known that breast cancer expresses different glucose metabolism in relation to estrogen receptor (ER), progesterone receptor (PR), Ki67 score, tumor grading, tumor size, and Human Epidermal Growth Factor Receptor 2 (HER2). We present an interesting case of a woman with two different, synchronous breast cancers characterized by different glucose metabolism, according to literature knowledge.

KEY words: breast cancer; [¹⁸F]FDG; PET; histotype; glucose metabolism

Nucl Med Rev 2022; 25, 1: 64–65

During breast cancer screening performed with ultrasonography and mammography, in a 91-years-old woman two bilateral breast nodules were found and both nodules appeared oncologically suspicious. Trucut biopsy was subsequently performed on both lesions, with the confirmation of their malignancy.

The left lesion was diagnosed as invasive breast cancer, no special histotype, grading stage G3 with a 33% Ki67 expression, positive for estrogen receptor (ER), negative for progesterone receptor (PR), and positive for Human Epidermal Growth Factor Receptor 2 (HER2).

In contrast, the right lesion was diagnosed as invasive breast cancer, however with unclear histotype, suspicious for lobular carcinoma, grading stage G2 with a 20% Ki67 expression, positive for ER and PR, and without HER2 expression.

Then ¹⁸F-fluorodeoxyglucose positron emission tomography-computed tomography ([¹⁸F]FDG PET-CT) was performed for staging purposes.

The tumor size of the right lesion was 23 mm × 19 mm × 19 mm and FDG uptake was moderate with a Maximum Standardized Uptake Value (SUVmax) of 5.82 and a Metabolic Tumor Volume (MTV) of 7.1 cm³ (Fig. 1).

The tumor size of the left lesion was 25 mm × 19 mm × 20 mm, with MTV of 7.6 cm³ and SUVmax of 16.05 (Fig. 2).

The two breast lesions had similar tumor size and MTV values (MTV ratio between the two was 1.07), but a significantly different FDG uptake, expressed as SUVmax (SUVmax ratio between the two was 2.76).

Due to the age of the patient, no surgery was performed and Letrozole therapy was started.

It is known that SUVmax in breast cancer lesions has a positive correlation with Ki67 expression [1, 2] and the grading of the lesion [1]. A similar positive correlation with nodule size [1], presence of HER2 [1], and absence of PR [1, 2] was also suggested by other studies, however without shared consensus.

Correspondence to: Pietro Bellini, Nuclear Medicine, Spedali Civili di Brescia, P.le Spedali Civili, 1 25123 Brescia Italy, tel.: +39-30-3995461, fax: +39-30-3995420 e-mail: bellini.pietro@outlook.it

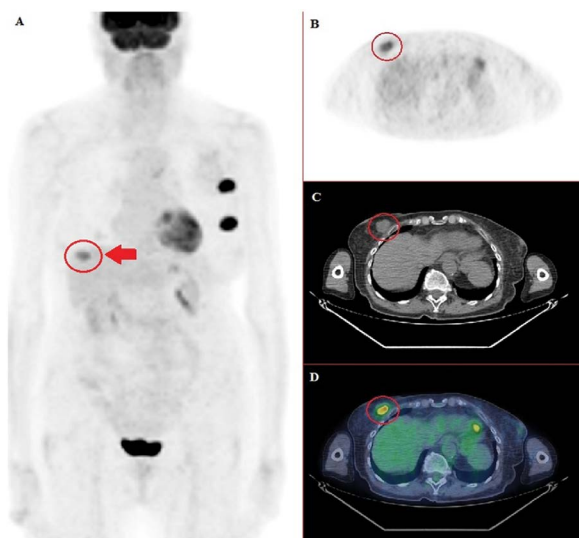


Figure 1. Maximum Intensity Projection (MIP) (A), axial PET (B), axial CT (C) and fused PET-CT in FRENCH color (D) images of a PET-CT scan reporting bilateral breast lesions (right lesion labeled by red circle and arrow) and left axillary metastasis

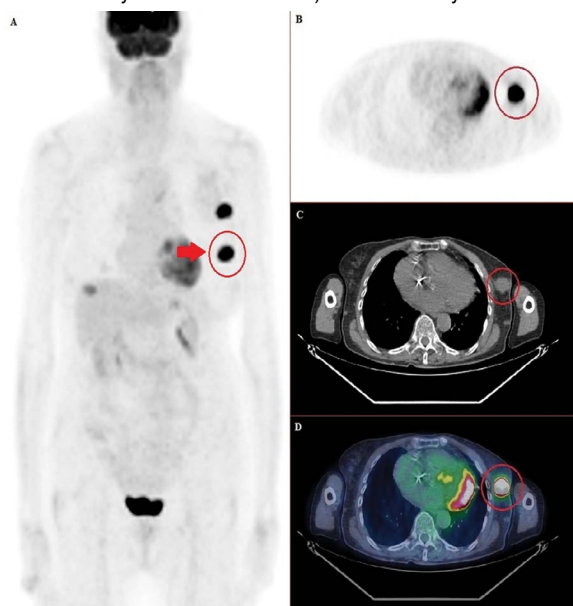


Figure 2. MIP (A), axial PET (B), axial CT (C) and fused PET-CT in FRENCH color (D) images of the same PET-CT scan (left lesion labeled by red circle and arrow)

According to the literature, our case report underlines two metabolic patterns related to different biological and genetic characteristics of the breast lesions with similar size in the same patient, in particular without the presence of confounding volume difference.

Bilateral breast cancer is an uncommon finding [3], even more, if presented with different metabolic behavior as reported and clearly showed by [^{18}F]FDG PET-CT.

Conflict of interest

The authors declare that they have no conflict of interest.

References

1. Cerci SM, Bozkurt KK, Eroglu HE, et al. Evaluation of the association between HIF-1 and HER-2 expression, hormone receptor status, Ki-67 expression, histology and tumor FDG uptake in breast cancer. *Oncol Lett.* 2016; 12(5): 3889–3895, doi: [10.3892/ol.2016.5199](https://doi.org/10.3892/ol.2016.5199), indexed in Pubmed: [27895745](https://pubmed.ncbi.nlm.nih.gov/27895745/).
2. Qu YH, Long N, Ran C, et al. The correlation of F-FDG PET/CT metabolic parameters, clinicopathological factors, and prognosis in breast cancer. *Clin Transl Oncol.* 2021; 23(3): 620–627, doi: [10.1007/s12094-020-02457-w](https://doi.org/10.1007/s12094-020-02457-w), indexed in Pubmed: [32683540](https://pubmed.ncbi.nlm.nih.gov/32683540/).
3. Albano D, Bertoli M, Morassi ML, et al. Incidental 18F-FDG PET/CT bilateral breast uptake due to carcinoma. *Nucl Med Rev Cent East Eur.* 2016; 19(B): 14–16, doi: [10.5603/NMR.2016.0028](https://doi.org/10.5603/NMR.2016.0028), indexed in Pubmed: [27900755](https://pubmed.ncbi.nlm.nih.gov/27900755/).

Incidental detection of breast cancer by ^{18}F -fluorocholine PET/CT performed for primary hyperparathyroidism

Vlatka Jozanovic¹, Drazen Huic^{1,2}

¹Clinical Department of Nuclear Medicine and Radiation Protection, University Hospital Centre Zagreb

²The University of Zagreb School of Medicine, Zagreb, Croatia

[Received 30 VIII 2021; Accepted 30 XI 2021]

Abstract

We present a case report of incidental detection of breast cancer in a female patient referred for ^{18}F -fluorocholine (FCH) positron emission tomography/computed tomography (PET/CT) due to primary hyperparathyroidism. This imaging method was recently shown as more sensitive for the detection of metabolically hyperactive parathyroid glands than neck ultrasound and (2-metoksyizobutyloizonitryl labeled with technetium-99m) [$^{99\text{m}}\text{Tc}$]MIBI. Increased accumulation of FCH was found in the hyperactive parathyroid gland and unexpectedly in the right breast lesion. The surgery confirmed parathyroid adenoma. One month later right upper medial quadrantectomy confirmed breast carcinoma — a combination of invasive ductal carcinoma and intracystic papillary breast carcinoma. To the best of our knowledge, this is the first reporting of simultaneous detection of parathyroid adenoma and breast cancer by using ^{18}F -fluorocholine PET/CT.

KEY words: ^{18}F -fluorocholine PET/CT; breast cancer; primary hyperparathyroidism

Nucl Med Rev 2022; 25, 1: 66–67

We report a case of a 75-year old female patient with accidentally diagnosed breast cancer using ^{18}F -fluorocholine PET/CT indicated due to primary hyperparathyroidism. Elevated serum parathyroid hormone (PTH) and calcium levels stood out from the other laboratory parameters. Neck ultrasound examination showed a hypochoic zone along the upper edge of the right thyroid lobe. Cytological analysis of the punctate verified only thyroid cells without elevated PTH values in the punctate. ^{18}F -fluorocholine (FCH) PET/CT was performed to localize small and hard-to-reach hyperfunctional parathyroid glands. Abnormal cell proliferation and upregulation of choline kinase activity are thought to enhance the accumulation of fluorocholine and increase the efficiency of detecting such abnormalities. Thanks to these features of this radiopharmaceutical, the detection of enhanced cell proliferation, which is typical for

neoplasms, has become more frequent. Imaging of neck and thoracic regions was performed 20 minutes after intravenous administration of 119 MBq (3.2 mCi) of [^{18}F]FCH. Increased metabolic activity was found in the parathyroid gland with axial dimensions of 0.9 × 1.0 cm localized behind the upper third of the right thyroid lobe (Fig. 1). In addition, a metabolically active isodense lesion with irregular edges measuring 1.4 × 1.0 cm located in the upper medial quadrant of the right breast highly suspicious of the neoplasm was verified (Fig. 2). Resection of the described hyperfunctional parathyroid gland was performed and the pathohistological diagnosis corresponded to the adenoma. Postoperative calcium values returned to normal, while PTH levels were slightly elevated. Shortly afterwards, the patient underwent upper medial quadrantectomy of the right breast. The final pathohistological diagnosis confirmed the findings of cytological puncture and percutaneous biopsy that it was combination of invasive ductal carcinoma and intracystic papillary breast carcinoma. Since the diagnostic potential of ^{18}F -fluorocholine has already been investigated in cancers of stomach, prostate, breast as well as melanoma or lymphoma, the possibility of concomitant neoplasms should always be considered when imaging with [^{18}F]FCH.

Correspondence to: Vlatka Jozanovic, Clinical Department of Nuclear Medicine and Radiation Protection, University Hospital Centre Zagreb, Kispaticeva 12, 10 000 Zagreb, Croatia, tel.: 0038 5981807705, e-mail: vlatka.jozanovic@gmail.com

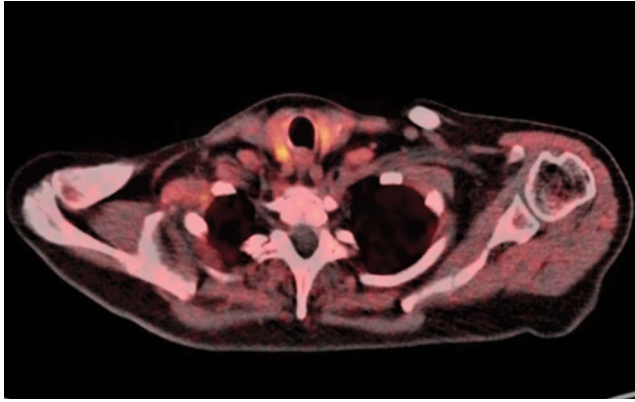


Figure 1. [^{18}F]FCH PET/CT showed increased uptake in the parathyroid gland localized behind the right thyroid lobe

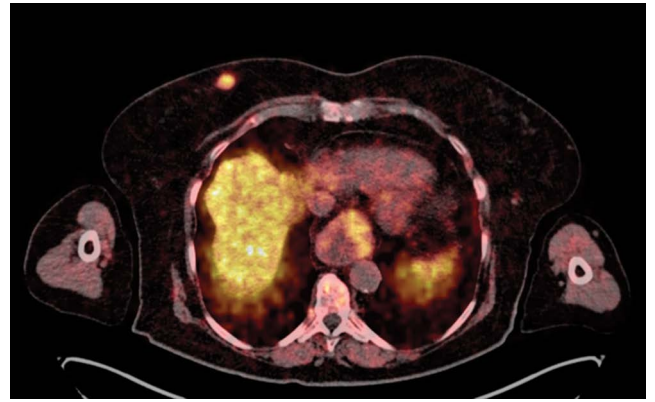


Figure 2. A metabolically active lesion in the right breast highly suspicious of the neoplasm

Rare osteoarticular complications on [18F]FDG-PET/CT — following intravesical BCG immunotherapy for bladder cancer

Jan-Henning Schierz¹, Anke McLeod², Farzana Ali³

¹Department of Radiology, Municipal Hospital and Academic Teaching Hospital of the Technical University Dresden, Germany

²Department of Nuclear Medicine, University of Leipzig, Germany

³Department of Biomedical Engineering, Stony Brook University, NY, USA

[Received 1 IX 2021; Accepted 30 XI 2021]

Abstract

This case illustrates rare osteoarticular complications of Bacillus Calmette-Guérin (BCG) immunotherapy in a 55-year-old male with high-risk non-muscle-invasive bladder cancer (NMIBC). The patient was referred for ¹⁸F-fluorodeoxyglucose ([¹⁸F]FDG) positron emission tomography/computed tomography (PET/CT) to rule out bone metastases suspected on prior post-gadolinium magnetic resonance imaging (MRI). Although metastases were excluded, nearly symmetrical uptakes were detected in the costovertebral and costotransverse joints. Medical history revealed that the patient had been receiving intravesical instillations of BCG, the first-line therapy for high-risk NMIBC. The patient was diagnosed with reactive arthritis (ReA), a rare autoimmune complication of BCG, that was successfully treated with a nonsteroidal anti-inflammatory drug (NSAID).

KEY words: oncology treatment; NMIBC therapy; BCG side effects; reactive arthritis; metastasis

Nucl Med Rev 2022; 25, 1: 68–69

A 55-year-old male with high-risk non-muscle invasive (superficial) bladder cancer (NMIBC), associated with a greater risk for progression, was referred for [¹⁸F]FDG-PET/CT after post-gadolinium MRI raised suspicion for bone metastases. A review of the [¹⁸F]FDG-PET/CT imaging excluded bone (and other) metastases. However, remarkable, almost symmetrical uptakes were noted in the costovertebral and costotransverse joints. The fused volume-rendered coronal view showed multifocal enhancement along the thoracic spine (Fig. 1A). The transaxial fused volume rendering technique VRT (Fig. 1B) and the correlated initial T1W FS post-gadolinium MRI (Fig. 1C) showed intense uptakes in the right costovertebral (yellow arrow) and left costotransverse (red arrow) joints at T5, that were not characteristic of metastases.

These imaging findings clinically correlated with the patient's history of spinal pain in the thoracic region at night for over a year. Medical history further revealed that the patient had been receiving intravesical instillations of Bacillus Calmette-Guérin (BCG), the first-line therapy for high-risk (CIS/Tis, high grade/G3, T1, or low-grade with multiple, recurrent, Ta tumors measuring > 3 cm) NMIBC, that contains a live strain of *Mycobacterium Bovis* in an attenuated (weakened) state. Yet, it can result in local complications through contamination of urine or systematic complications from dissemination in the bloodstream.

Review of the [¹⁸F]FDG-PET/CT findings and correlated clinical history in this patient led to the suspicion of inflammation due to reactive arthritis (ReA), a rare autoimmune complication of BCG that is commonly associated with HLA-B27. The diagnosis was clinically confirmed, and the patient was successfully treated with NSAID (Ibuprofen).

This is the first case to provide visual evidence of ReA following BCG therapy on [¹⁸F]FDG-PET/CT. This case highlights the rare autoimmune side effects of BCG (and other immunotherapy) that necessitate a thorough consideration of the clinical history and initial tumor stage to avoid potential upstaging and unnecessary treatment.

Correspondence to: Jan-Henning Schierz, MD, Department of Radiology, Municipal Hospital Dresden, Friedrichstraße 41, 01067 Dresden, Germany. phone: (+49) 0351 480 1197; fax: (+49) 0351 480 3198, e-mail: JHS@klinikum-dresden.de

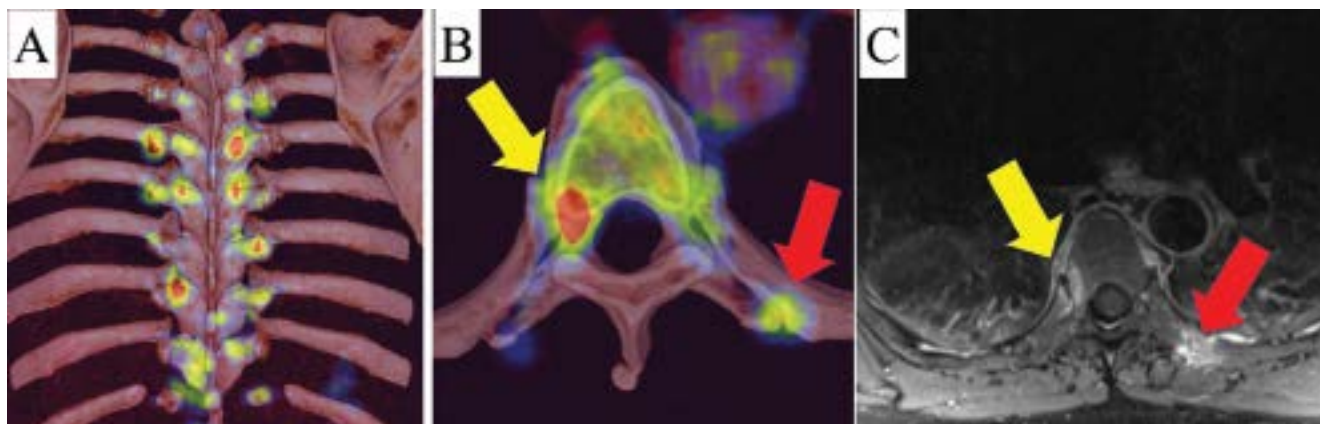


Figure 1. Coronal volume rendering technique (VRT) of the fused ¹⁸F-fluorodeoxyglucose ([¹⁸F]FDG) positron emission tomography/computed tomography ([¹⁸F]FDG-PET/CT) images of the patient demonstrated multifocal enhancement along the thoracic spine (A). The volume-rendered transaxial view of the fused [¹⁸F]FDG-PET/CT at the level of the T5 vertebra showed intense uptakes in the right costovertebral (yellow arrow) and left costotransverse (red arrow) joints (B). These findings correlated with the initial T1-weighted fat saturation (FS) post-gadolinium magnetic resonance imaging (MRI) (C)

Funding

The authors did not receive any specific funding for this work.

Ethical approval

The submitted work does not contain any studies with human participants performed by any of the authors.

Informed consent

Informed consent was obtained from the individual patient for the data and images included in this report.

Conflict of interest

All three authors declare that they have no conflict of interest that is directly or indirectly related to the work submitted for publication.

Hybrid bone SPECT/CT reveals spleen calcification in sickle cell mutation and beta-thalassemia

Konstantinos Sakellariou, Sofia Charalampidou, Andreas Fotopoulos[✉], Chrissa Sioka[✉]
Department of Nuclear Medicine, Medical School, University Hospital of Ioannina, Greece

[Received 8 IX 2021; Accepted 30 XI 2021]

Abstract

We present a case of a 65 years-old male with sickle cell mutation and beta-thalassemia (Hb S/ β -Thal), who had whole-body bone scan evaluation for osteomyelitis. The examination revealed high radiopharmaceutical uptake in the left abdomen. Further evaluation with hybrid single photon emission computed tomography/computed tomography (SPECT/CT) showed calcification of approximately the entire spleen, in the context of sickle cell anemia. This report highlights the role of SPECT/CT in such cases.

KEY words: sickle cell anemia; whole-body bone scan; SPECT/CT; spleen calcification

Nucl Med Rev 2022; 25, 1: 70–71

Introduction

Thalassemias denote a mixed grouping of genetic disorders that result from a decreased synthesis of alpha or beta chains of hemoglobin (Hb). Depending on the alpha or beta hemoglobin deletion, the abnormality is called alpha or beta-thalassemia [1, 2]. Sickle cell anemia results from a mutation in the beta-globin gene that creates the abnormal Hb S hemoglobin. Approximately 20 million people around the world are diagnosed with sickle cell anemia (SCA). In some countries, the diagnosis of sickle cell disease is performed immediately after birth, which leads to early management and relative reduction of morbidity and mortality [3]. Combination of sickle cell mutation and beta-thalassemia (Hb S/ β -Thal) exhibits similar clinical manifestations like sickle cell disease [4].

Whole-body bone scintigraphy (BS) with Technetium-99m-methylene bisphosphonate (MDP) is a very sensitive imaging method for various reasons and in various diseases to assess bone metabolism and bone remodeling, including SCA or variant patients [5–11]. When BS demonstrates abdominal uptake in SCA patients [11], then further imaging with SPECT/CT is recommended for anatomical verification and further evaluation of the extra-osseous finding [6].

In this report, we present a case of a patient with Hb S/ β -Thal who underwent BS to rule out osteomyelitis, during which an extra-osseous radiotracer uptake was imaged in the left abdominal area, most likely representing spleen uptake. A subsequent SPECT/CT verified the spleen uptake which was due to spleen calcification.

Case report

A 65-year-old patient with known Hb S/ β -Thal and the sub-acute onset of pain in the left mandibular area was referred to Nuclear Medicine Laboratory, for a three-phase BS, to rule out possible mandibular osteomyelitis. The patient was injected with intravenous 740 MBq (20 mCi) of MDP, followed by three phases of BS. During the first phase, serial scans were obtained during the first 2–5 seconds post-injection; The second phase included scans acquired 5 min post-injection that evaluated the inflammatory nature of the lesion; the third phase obtained after 3 hours assessed the bone turnover of the lesion [12]. The mandibular BS was unremarkable, since all three phases were negative, and thus, the diagnosis of osteomyelitis was ruled out. From the evaluation of the rest of the skeleton, it was observed extra-osseous mixed (moderate and high) radiotracer uptake in the left upper abdomen consisted with possible spleen uptake (Fig. 1). A hybrid SPECT/CT imaging was followed that revealed a completely calcified spleen (Fig. 2). Thus, the radiotracer uptake seen in the spleen during the BS was due to its calcification in the context of sickle cell anemia.

Correspondence to: Andreas Fotopoulos
Department of Nuclear Medicine, Medical School,
University Hospital of Ioannina, Greece
e-mail: professor.fotopoulos@yahoo.com

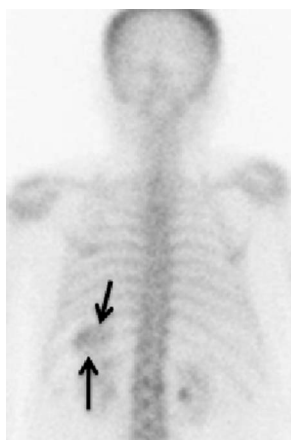


Figure 1. Posterior view in bone scintigraphy showing extra-osseous radiotracer uptake in the left upper abdomen (arrows)

Discussion

The BS is a very accurate imaging study to rule out osteomyelitis in patients with SCA or Hb S/ β -Thal exhibiting bone pain [13, 14]. Increased spleen uptake of ^{99m}Tc -methylene diphosphonate on a BS may occur because of various conditions [11]. In patients with SCA or Hb S/ β -Thal, BS may show increased osteoblastic activity in the skeleton due to bone marrow hyperplasia. Increased splenic uptake in patients with SCA or Hb S/ β -Thal, as in our case, may be due to splenic infarction followed by calcifications [10]. In such cases, further imaging with SPECT/CT improves the diagnostic accuracy and provides anatomical information [6].

In conclusion, in adult patients with SCA or Hb S/ β -Thal, MDP BS and SPECT/CT can identify spleen calcification possibly related to previous splenic infarction. Furthermore, in cases of not known disease, if BS reveals unusual extra-osseous radiotracer uptake, SPECT/CT should be performed, so a combination of anatomical and functional information may determine the accurate diagnosis.

Conflict of interest

None declared.

References

1. Bajwa H, Basit H. *Thalassemia*. Treasure Island (FL): StatPearls Publishing. 2021, indexed in Pubmed: [31424735](#).
2. Needs T, Gonzalez-Mosquera LF, Lynch DT. *Beta-Thalassemia*. Treasure Island (FL): StatPearls Publishing. 2021, indexed in Pubmed: [30285376](#).
3. Ashorobi D, Bhatt R. *Bone marrow transplantation in sickle cell disease*. Treasure Island (FL): StatPearls Publishing. 2021, indexed in Pubmed: [30860750](#).
4. Figueiredo MS. The compound state: Hb S/beta-thalassemia. *Rev Bras Hematol Hemoter*. 2015; 37(3): 150–152, doi: [10.1016/j.bjhh.2015.02.008](#), indexed in Pubmed: [26041415](#).
5. Sioka C, Konstanti E, Papadopoulos A, et al. Heterotopic ossification in patients previously hospitalized in an intensive care unit. *Nucl Med Rev Cent East Eur*. 2018; 21(2): 100–103, doi: [10.5603/NMR.2018.0027](#), indexed in Pubmed: [30070350](#).
6. Niccoli Asabella A, Altini C, Nappi AG, et al. Sickle cell diseases: What can nuclear medicine offer? *Hell J Nucl Med*. 2019; 22(1): 2–3, doi: [10.1967/s002449910950](#), indexed in Pubmed: [30843001](#).
7. Sioka C, Sakellariou K, Papoudou-Bai A, et al. Osteoblastic Solitary Plasmacytoma of Bone. *Turk J Haematol*. 2019; 36(2): 117–119, doi: [10.4274/tjh.galenos.2019.2018.0419](#), indexed in Pubmed: [30820260](#).
8. Fotopoulos A, Sioka C, Papadimitropoulos K, et al. Radiotherapy for breast cancer induced long-term diminished accumulation of radiotracer on bone scan of the irradiated ribs. *Nucl Med Rev Cent East Eur*. 2019; 22(2): 85–87, doi: [10.5603/NMR.2019.0020](#), indexed in Pubmed: [31482562](#).
9. Sioka C, Gkika E, Paliouras A, et al. Huge Abdominal Photopenic Area Due to Kidney Cyst Imaged by Bone Scintigraphy in a Prostate Cancer Patient. *Clin Nucl Med*. 2018; 43(11): 850–851, doi: [10.1097/RLU.0000000000002282](#), indexed in Pubmed: [30222683](#).
10. Goy W, Crowe WJ. Splenic accumulation of ^{99m}Tc -diphosphonate in a patient with sickle cell disease: case report. *J Nucl Med*. 1976; 17(2): 108–109, indexed in Pubmed: [1245869](#).
11. Kaur H, Muhleman M, Balon HR. Spleen Uptake on a Bone Scan. *J Nucl Med Technol*. 2017; 45(3): 245–246, doi: [10.2967/jnmt.117.192427](#), indexed in Pubmed: [28611233](#).
12. Mavrogenis AF, Soucacos PN, Papagelopoulos PJ. Heterotopic ossification revisited. *Orthopedics*. 2011; 34(3): 177, doi: [10.3928/01477447-20110124-08](#), indexed in Pubmed: [21410128](#).
13. Sutter CW, Shelton DK. Three-phase bone scan in osteomyelitis and other musculoskeletal disorders. *Am Fam Physician*. 1996; 54(5): 1639–1647, indexed in Pubmed: [8857786](#).
14. Skaggs DL, Kim SK, Greene NW, et al. Differentiation between bone infarction and acute osteomyelitis in children with sickle-cell disease with use of sequential radionuclide bone-marrow and bone scans. *J Bone Joint Surg Am*. 2001; 83(12): 1810–1813, doi: [10.2106/0004623-200112000-00007](#), indexed in Pubmed: [11741059](#).

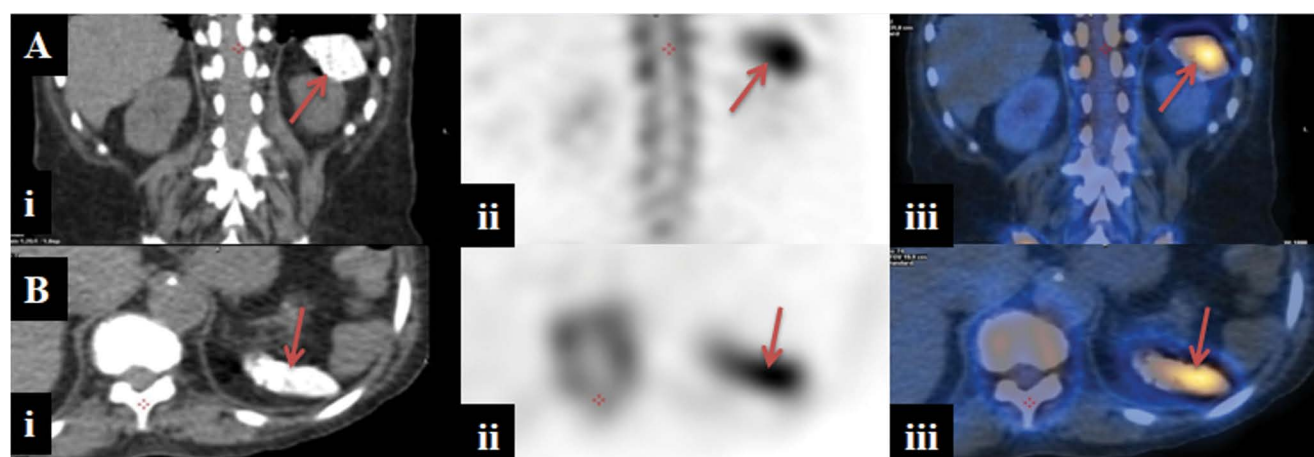


Figure 2. (A) Coronal images; (B) axial images; (i) computed tomography (CT); (ii) single photon emission computed tomography (SPECT); (iii) (SPECT/CT). Single photon emission computed tomography/computed tomography (SPECT/CT) exam confirms the radiotracer activity seen in bone scintigraphy in the left upper abdomen area showing splenic uptake (arrows)

